Selective inhibition of NFAT in mouse and human T cells by CRISPR/Cas9 to ameliorate acute Graft-versus-Host Disease while preserving Graft-versus-Leukemia effect

Selektive Hemmung von NFAT in murinen und humanen T-Zellen durch CRISPR/Cas9 zur Linderung der akuten Graft-versus-Host-Erkrankung bei gleichzeitigem Erhaltdes Graft-versus-Leukemia-Effekts

Doctoral thesis for a doctoral degree
at the Graduate School of Life Sciences,
Julius-Maximilians-Universität Würzburg,
Section Infection and Immunity

submitted by

Snigdha Majumder

from

Kolkata, India

Würzburg 2022

Submitted on: ……..……..

Office stamp

Members of the Thesis Committee

Chairperson: ……....

Primary Supervisor: PD. Dr. Friederike Berberich-Siebelt

Supervisor (Second): PD. Dr. med. Niklas Beyersdorf

Supervisor (Third): Dr. Martin Väth

Supervisor (Fourth): Prof. Dr. Thomas Winkler

Date of Public Defence: ……..……

Date of Receipt of Certificates: ……..

Acknowledgement

First and foremost, I would like to express my sincere gratitude to my first supervisor, PD. Dr. Friederike Berberich-Siebelt for giving me the opportunity to become a member of her wonderful group, and for supporting me personally and professionally during all the steps of my Ph.D. journey. Her patience, guidance, advice, and encouragement have enormously helped me in the completion of this thesis.

My heartfelt thanks go to PD. Dr. Niklas Beyersdorf, for his significant scientific advice and constructive criticism of my work. This has greatly helped me to learn a lot and pay attention to small important details.

I would like to sincerely thank Dr. Martin Väth, for constantly being the go-to person, each time being enthusiastically available for long scientific discussions, for giving immensely valuable suggestions, and promptly bringing solutions to many scientific problems.

I am grateful to Prof. Dr. Thomas Winkler, for sharing his vast knowledge of mouse genetics, during our TRR221 meetings. I am forever thankful to him for taking out time and traveling to Würzburg for attending my long annual thesis committee meetings. His positive attitude, invaluable scientific ideas, and immense support have been a major asset in the past three years.

I am forever grateful to TRR221, DFG for funding my research, organizing exciting scientific workshops and conferences as well as introducing me to the vast exhilarating field of allogeneic-cell transplantation. Special thanks to mentors of Integrated Research Training Group (IRTG), Prof. Dr. Mathias Edinger, and PD. Dr. Petra Hoffman for their scientific exchange and career advice.

I would like to thank the Graduate School of Life Sciences (GSLS), for their support throughout my Ph.D. studies, for improving my soft skills, and also for guiding me on future career prospects.

The long hours of lab-life were enjoyable, due to the company of my wonderful colleagues, Nadine Hundhausen, Cristina Chiarolla, Rishav Seal, Yin Xiao, Sabrina Giampaolo, Muhammad Azeem, and Salvador Sampere. We have learned from each other, celebrated each other's success, and supported each other during difficult times. Our scientific discussions, as well as the social time together, made the last three years unforgettable. I would also like to thank Benjamin Lunz for being a constant help in completing all the research work. My sincere thanks to my other colleagues, Dr. Anika König, Dr. Stefan Klein Heßling, Dr. Andris Avots, and Prof. Dr. Edgar Serfling for sharing their extensive knowledge in the field of immunology and the fruitful discussions during our weekly meetings. I thank my students Isabelle Jugovic, Larissa Roth, Oliver Maier, and Svenja Bee for sincerely working along with me.

A special thanks to the director of the Institute of Pathology, Prof. Dr. Andreas Rosenwald for financially supporting me during the last few months of my Ph.D. studies.

I would like to acknowledge my collaborators, because of whom this work has been completed. I thank, Prof. Dr. Andreas Beilhack for allowing me to work in his laboratory, and the GvHD team, especially Dr. Musga Qureischi for introducing me to the technical aspects of GvHD experiments. My sincere thanks to Prof. Dr. Michele Hudecek and his team, particularly Dr. Razieh Monjezi and Dr. Hardik Kumar Jetani for introducing me to the technical aspects of CAR-T cell therapy. I am thankful to Prof. Dr. Dimitrios Mougiakakos (FAU, Erlangen) and Domenica Saul for supporting me with their expertise in metabolism studies. I am also grateful to Prof. Dr. Ingolf Berberich for his extensive help during the first year of my doctoral studies.

My deepest gratitude goes to my lovely parents, for all their sacrifices and constant support. They have encouraged me to work harder and become resilient. I extend my heartfelt thankfulness to my parents-in-law for their love, care, support, and positive energy throughout my Ph.D. studies.

Last, but not least, I am indebted to my amazing husband, Saiveer, for being the greatest support throughout these years. I thank him for his sacrifices, for discussing and asking questions eagerly about my research, for always believing in my capabilities, and for being there during the difficult times.

Table of Contents

1 Affidavit/Declaration

I hereby confirm that my thesis entitled “Selective inhibition of NFAT in mouse and human T cells by CRISPR/Cas9 to ameliorate acute Graft-versus-Host Disease while preserving Graft-versus-Leukemia effect” is the result of my own work. I did not receive any help or support from commercial consultants.
All sources and/or materials applied are listed and specified in the thesis.

Furthermore, I confirm that this thesis has not yet been submitted as part of another examination process neither in identical nor in similar form.

Place, Date Signature

Eidesstattliche Erklärung

Hiermit erkläre ich an Eides statt, die Dissertation „Selektive Hemmung von NFAT in murinen und humanen T-Zellen durch CRISPR/Cas9 zur Linderung der akuten Graft-versus-Host-Erkrankung bei gleichzeitigem Erhaltdes Graft-versus-Leukemia-Effekts“ eigenständig, d.h. insbesondere selbständig und ohne Hilfe eines kommerziellen Promotionsberaters, angefertigt und keine anderen als die von mir angegebenen Quellen und Hilfsmittel verwendet zu haben.

Ich erkläre außerdem, dass die Dissertation weder in gleicher noch in ähnlicher Form bereits in einem anderen Prüfungsverfahren vorgelegen hat.

Ort, Datum Unterschrift

2 List of Figures

3 List of Tables

4 Abstract

Allogenic hematopoietic stem cell transplantation (allo-HCT) is a curative therapy for the treatment of malignant and non-malignant bone marrow diseases. The major complication of this treatment is a highly inflammatory reaction known as Graft-versus-Host Disease (GvHD). Cyclosporin A (CsA) and tacrolimus are used to treat GvHD which limits inflammation but also interferes with the anticipated Graft-versus-Leukemia (GvL) effect. These drugs repress conventional T cells (Tcon) along with regulatory T cells (Treg), which are important for both limiting GvHD and supporting GvL. Both of these drugs inhibit calcineurin (CN), which dephosphorylates and activates the nuclear factor of activated T-cells (NFAT) family of transcription factors. Here, we make use of our *Cd4cre.*Cas9^{+} mice and developed a highly efficient non-viral CRISPR/Cas9 gene editing method by gRNA-only nucleofection. Utilizing this technique, we demonstrated that unstimulated mouse T cells upon NFATc1 or NFATc2 ablation ameliorated GvHD in a major mismatch mouse model. However, *in vitro* pre-stimulated mouse T cells could not achieve long-term protection from GvHD upon NFAT single-deficiency. This highlights the necessity of gene editing and transferring unstimulated human T cells during allo-HCT. Indeed, we established a highly efficient ribonucleoprotein (RNP)-mediated CRISPR/Cas9 gene editing for NFATC1 and/or NFATC2 in pre-stimulated as well as unstimulated primary human T cells. In contrast to mouse T cells, not NFATC1 but NFATC2 deficiency in human T cells predominantly affected proinflammatory cytokine production. However, either NFAT single-knockout kept cytotoxicity of human CD3^{+} T cells untouched against tumor cells *in vitro*. Furthermore, mouse and human Treg were unaffected upon the loss of a single NFAT member. Lastly, NFATC1 or NFATC2-deficient anti-CD19 CAR T cells, generated with our non-viral 'one-step nucleofection' method validated our observations in mouse and human T cells. Proinflammatory cytokine production was majorly dependent on NFATC2 expression, whereas, *in vitro* cytotoxicity against CD19^{+} tumor cells was undisturbed in the absence of either of the NFAT members. Our findings emphasize that NFAT single-deficiency in donor T cells is superior to CN-inhibitors as therapy during allo-HCT to prevent GvHD while preserving GvL in patients.

5 Zusammenfassung

Die allogene hämatopoetische Stammzelltransplantation (allo-HCT) ist eine kurative Therapie zur Behandlung bösartiger und nicht bösartiger Knochenmarkerkrankungen. Die Hauptkomplikation dieser Behandlung ist eine hochgradige Entzündungsreaktion, die als Graft-versus-Host-Disease (GvHD) bekannt ist. Zur Behandlung der GvHD werden Cyclosporin A (CsA) und Tacrolimus eingesetzt, die die Entzündung eindämmen, aber auch den gewünschten Graft-versus-Leukämie-Effekt (GvL) beeinträchtigen. Diese Medikamente unterdrücken sowohl konventionelle T-Zellen (Tcon) als auch regulatorische T-Zellen (Treg), die sowohl für die Begrenzung der GvHD, als auch für die Unterstützung der GvL wichtig sind. Beide Medikamente hemmen Calcineurin (CN), das die Transkriptionsfaktoren der Familie der Nuclear Factor of Activated T-Cells (NFAT) dephosphoryliert und aktiviert. Hier nutzten wir unsere *Cd4cre.Cas9*$^{+}$-Mäuse und entwickelten eine hocheffiziente, nicht-virale CRISPR/Cas9-Geneditierungsmethode mittels reiner gRNA-Nukleofektion. Mithilfe dieser Technik konnten wir zeigen, dass unstimulierte T-Zellen der Maus nach Ablation von NFATc1 oder NFATc2 die GvHD in einem Major-Mismatch-Mausmodell mildern. *In vitro* vorstimulierte T-Zellen von Mäusen konnten jedoch keinen langfristigen Schutz vor GvHD bei NFAT-Einzeldefizienz erreichen. Dies unterstreicht die Notwendigkeit der Gen-Editierung und des Transfers unstimulierter menschlicher T-Zellen während einer allo-HCT. In der Tat konnten wir ein hocheffizientes Ribonukleoprotein (RNP)-vermitteltes CRISPR/Cas9 *gene-editing* für NFATC1 und/oder NFATC2 nicht nur in vorstimulierten, sondern auch in unstimulierten primären menschlichen T-Zellen etablieren. Im Gegensatz zu T-Zellen von Mäusen wirkte sich der Mangel an NFATC2, nicht aber so sehr an NFATC1, in menschlichen T-Zellen überwiegend auf die Produktion proinflammatorischer Zytokine aus. Bei beiden NFAT-Single-Knockouts blieb jedoch die Zytotoxizität menschlicher CD3^{+} T-Zellen gegen Tumorzellen *in vitro* unangetastet. Darüber hinaus wurden die Treg von Maus und Mensch durch den Verlust eines einzelnen NFAT-Mitglieds nicht beeinträchtigt. Schließlich bestätigten NFATC1- oder NFATC2-defiziente Anti-CD19-CAR-T-Zellen, die mit unserer nicht-viralen "Ein-Schritt-Nukleofektionsmethode" erzeugt wurden, unsere Beobachtungen zu T-Zellen von Maus und Mensch. Die Produktion proinflammatorischer Zytokine hing hauptsächlich von der NFATC2-Expression ab, während die *In-vitro*-Zytotoxizität gegen CD19^{+}-Tumorzellen in Abwesenheit eines der beiden NFAT-

Mitglieder ungestört war. Unsere Ergebnisse unterstreichen, dass der Mangel eines einzelnen NFAT-Mitglieds in Spender-T-Zellen einer Therapie mit CN-Inhibitoren während einer allo-HCT überlegen ist. Hier könnten wir eine GvHD verhindern und gleichzeitig den GvL-Effekt in allo-HCT-Patienten erhalten.

6 Introduction

6.1 The Immune System

The human body is protected from the pathogen-caused damage by a variety of cells and molecules that together build the immune system. Most immune cells are derived from pluripotent hematopoietic stem cells (HSC) in the bone marrow. Mature immune cells circulate in the blood, lymphatic system or reside in peripheral tissue. The immune system in vertebrates consists of innate and adaptive immunity. Innate immunity is rapid and an early defense mechanism that comprises neutrophils, macrophages, dendritic cells (DC), natural killer cells (NK), and innate lymphoid cells (ILC). Adaptive immunity is antigen-specific and consists of T and B lymphocytes (T cells and B cells). It can generate immunological memory which protects from subsequent exposure to a foreign pathogen[1]. Furthermore, over the past decade, studies demonstrate the evidence of memory in lymphocytes of innate immunity (NK and ILCs)[2].

6.2 T lymphocytes (T cells)

Common lymphoid progenitors (CLP) which are originated from HSCs in the bone marrow give rise to all the lymphocytes including T cells, B cells, and NK cells. T cells express antigen-specific receptors known as T-cell receptors (TCR). TCRs are remarkably diverse due to RAG-1/RAG-2 protein directed V(D)J (V-variable, D-diversity, J-joining) recombination. T cells can only recognize an antigen when it's presented as a peptide via a specialized cell-surface glycoprotein named major histocompatibility complex (MHC). T cells that haven't yet encountered a specific antigen by their TCR in the periphery are called naïve T cells. They appear as rather small cells with few cytoplasmic organelles and condensed chromatin. Naïve T cells rapidly proliferate and differentiate into effector T cells (T_{EFF}) after activation by TCR-peptide-MHC (pMHC) interaction. Following neutralization of the antigen, few T cells become long-lasting memory cells (T_M), which can get more rapidly activated upon repeated antigen encounter[3]. The development of T cells occurs in a primary lymphoid organ called the thymus, in which T-lymphoid progenitors migrate from bone marrow. The majority of developing progenitors within the thymus (thymocytes) give rise to $\alpha\beta$ T cells (bearing $\alpha\beta$ TCR). The early developing thymocytes lack expression of the co-receptors CD4 and CD8, hence termed as

double-negative (DN) cells. DN thymocyte population can be subdivided into four stages (DN1 to DN4) based on the expression of an adhesion molecule CD44 and interleukin-2 (IL-2) receptor α chain, CD25 (DN1, $CD44^{+}CD25^{-}$; DN2, $CD44^{+}CD25^{+}$; DN3, $CD44^{-}CD25^{+}$ and DN4, $CD44^{-}CD25^{-}$). DN3 cells, which have undergone successful TCR-β chain rearrangement, are selected for the pairing of a β chain to pre-TCR-α, producing the pre-TCR. A pre-TCR then forms a complex with CD3 molecules and the pre-TCR signaling leads to the survival of these cells along with co-expression of CD4 and CD8. These cells are termed double-positive (DP) thymocytes. The TCR-α chain rearrangement happens in DP cells to produce a mature $\alpha\beta$-TCR, after which they undergo positive selection in the cortex. DP cells that can interact with an appropriate affinity of their $\alpha\beta$-TCR to self-antigen-bound MHC class I or class II molecule complexes, presented primarily by cortical thymic epithelial cells or cTECs, survive. However, in a phenomenon known as death by neglect, those cells that interact with too weak affinity or not at all, die by apoptosis. After positive selection, thymocytes migrate into the medulla to undergo negative selection. Here, medullary thymic epithelial cells (mTECs) expressing autoimmune regulator (AIRE), and thus presenting a wide variety of self-antigens are crucial in inducing thymic negative selection. According to the current model, very strong TCR-self-antigen-MHC interactions lead to induction of apoptosis, while a strong, but comparatively weaker affinity induces thymus-derived natural regulatory T cell (abbreviated either as nTreg or tTreg) generation. This mechanism creates central tolerance against self-antigens. Intermediate TCR-signal strength mediates survival of the cell generating conventional T cells (Tcon). Successful interaction with either MHC-I or MHC-II downregulates either co-receptor generating $CD4^{+}$ or $CD8^{+}$ T cells (single positive, SP) respectively. After selection, SP cells exit the thymus (2-4% of total lymphocytes in the thymus) and circulate in the periphery[1, 3, 4, 5].

6.3 T-cell activation, differentiation, and function

Due to the thymic selection processes and the presence of Treg, Tcon should not respond to MHC-bound self-peptide in the periphery. However, in a pathological condition, the MHC-I and MHC-II start presenting foreign peptides to $CD4^{+}$ or $CD8^{+}$ naïve T cells, respectively, leading to activation, proliferation, and differentiation. Three signals are necessary for the activation of T cells. The first is an interaction of the TCR complex ($\alpha\beta$-TCR and CD3) with pMHC. This primary signal initiates a signaling cascade with the help of the antigen-

independent interaction between coreceptor CD4/CD8 and MHC. Src-family kinase, Lck, which is constitutively associated with cytoplasmic domains of CD4 and CD8, phosphorylates the immunoreceptor tyrosine-based activation motifs (ITAM) present in the cytoplasmic domains of the CD3 chains γ, δ, and ε as well as the ζ-chains. Phosphorylated ITAMs recruit and bind to ZAP70 (another tyrosine kinase) through its SH2 domains, enabling phosphorylation and activation of ZAP70 by Lck. ZAP-70 activation leads to phosphorylation of scaffold protein LAT and adaptor protein SLP-76 as well as recruits these proteins to the TCR complex. An adaptor protein, Gads, holds the tyrosine-phosphorylated LAT and SLP-76 together forming a three-protein complex. With rapid activation of the PI3-kinase (PI3K), another early event following TCR-pMHC engagement, these phosphorylated scaffolds recruit and activate multiple signaling proteins including phospholipase C-γ (PLC-γ), ADAP, Vav, and Akt. PLC-γ is recruited to the plasma membrane (PM) by the binding with PIP3, generated by the phosphorylation of PIP2 by PI3K. Itk, another protein recruited by the LAT:Gads:SLP-76 complex, activates PLC-γ by phosphorylation. Activated PLC-γ then breaks down membrane lipid PIP2 into the membrane lipid diacylglycerol (DAG) and the second messenger inositol 1,4,5-triphosphate (IP3). IP3 binds to and opens IP3 receptor channels situated in the endoplasmic reticulum (ER). These are Ca^{2+} channels, which upon opening, release Ca^{2+} stored in the ER into the cytoplasm, resulting in a decrease in Ca^{2+} level in the ER. Dissociation of Ca^{2+} from ER-luminal EF-hand domains of stromal interaction molecule 1 (STIM1) and STIM2 proteins prompts their translocation to ER–plasma membrane (ER–PM) junctions, where they bind to and activate Ca^{2+} release-activated Ca^{2+} (CRAC) channels formed by ORAI1 and ORAI2 proteins. This results in subsequent Ca^{2+} influx known as store-operated Ca^{2+} entry (SOCE). The Ca^{2+} influx activates further signaling pathways and replenishes ER Ca^{2+} stores. Ca^{2+} entry eventually activates the nuclear factor of activated T-cell (NFAT) pathway. DAG recruits protein kinase C-θ (PKC) (activated by PLC-γ) and activates the small G protein Ras. Ras/MAPK pathway further induces expression of the transcription factor activator protein 1 (AP-1) and PKC induces nuclear factor kappa B (NF-κB). The transcription factors NFAT, AP-1, and NF-κB together induce the cytokine IL-2, facilitating proliferation and differentiation of T cells. The detailed description of NFAT signaling is demonstrated in Section. 6.8 and 6.9. Moreover, LAT:Gads:SLP-76 complex is involved in activation of the serine/threonine kinase Akt, which affects metabolism, the recruitment of the adaptor protein ADAP that upregulates cell adhesion, and the activation of the protein Vav, which begins actin polymerization. In

summary, these signaling pathways together, enhance survival, metabolic activity, adhesiveness, and cytoskeletal reorganization of T cells[1]. Of note, the first / TCR signal is not on its own sufficient to activate a naive T cell.

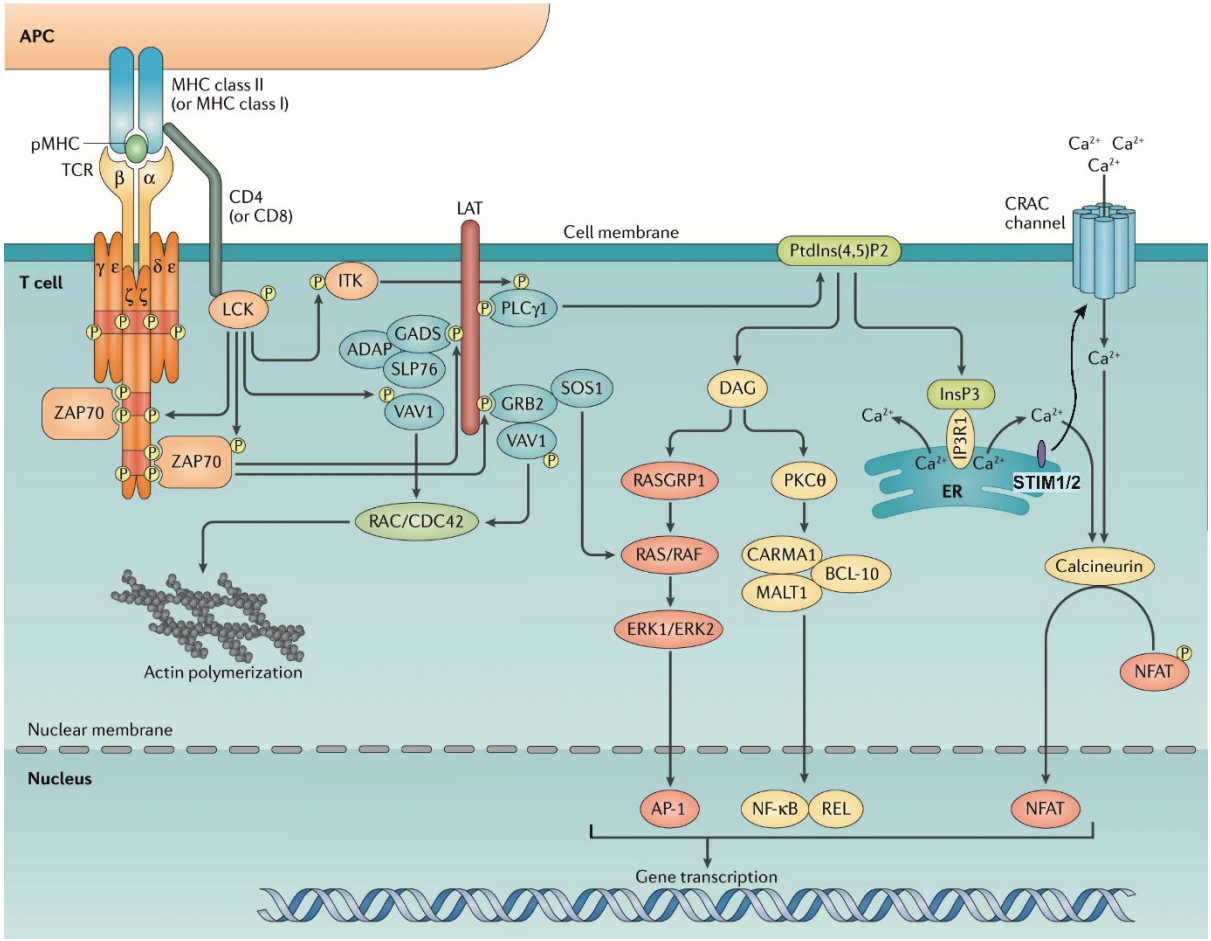

Figure 1: ***Overview of the major TCR signaling pathways.***

TCR signal transduction is triggered by TCR-pMHC engagement. LAT signalosome results in signal propagation and activates transcription factors NFAT, NF-κB, and AP-1. The concerted activity of these transcription factors in the presence of costimulation results in T-cell proliferation, migration, and effector function[6].

The second signal is costimulation, which is additionally required for naïve T-cell activation. The most prominent costimulatory signal is provided by the interaction between the constitutively expressed CD28 on T cells with its ligands CD80 (B7-1) or CD86 (B7-2), expressed on antigen-presenting cells. CD28 becomes tyrosine phosphorylated by Lck in its cytoplasmic domain, recruits other proteins, and enhances activation of PI3-kinase to generate PIP3, which in turn facilitates activation of Akt, PLC-γ, and Vav. Maximal activation of PLC-γ amplifies the expression of AP-1 and NF-κB, which are not sufficiently induced by TCR-pMHC signals alone. Costimulation by CD28 amplifies most of the downstream pathways of TCR

signaling. Indirectly, it also ensures the presence of antigen in the body, since its ligands CD80/86 are only upregulated on APCs upon infection and inflammation. With this, amplification of the primary signal by costimulation is a safeguard mechanism to avoid T-cell activation in a sterile surrounding. Additional costimulatory molecules upregulated upon T-cell activation are OX40, 4-1BB, CD30, and CD27. Apart from this, certain coinhibitory molecules are also upregulated such as CTLA4, TIM3, PD1, and LAG3. The latter mostly contain immunoreceptor tyrosine-based inhibitory motifs (ITIM) which inhibit T-cell activation, thus limiting an immune response[1].

The third signal is given by cytokines which initiate lineage-specific transcriptional programs that differentiate T cells into subtypes. $CD4^+$ Tcons are differentiated into different helper and regulatory subtypes, which include Th1, Th2, *in vitro* induced regulatory T cells (iTreg) or *in vivo* induced peripheral Treg (pTreg), Th9, Tfh or Th17 lineage (Fig. 1). Th1 cells are induced by sequential interferon (IFN)-γ and IL-12-mediated JAK1/2 and STAT1/4 pathway activation to stimulate T-bet, the 'master regulator' of Th1 cells. This subtype predominantly produces IFN-γ which activates macrophages and thus helps in protecting against intracellular infection by viruses and bacteria. IFN-γ supports B-cell class switch to produce IgG, such as IgG2a in mice and fights against cancerous cells. IL-4 triggers JAK1/3 and STAT6 to activate the transcription factor GATA-3 resulting in Th2 cells[7]. These cells are characterized by IL-4, IL-5, and IL-13 production, activate B cells to fight parasitic infections which are susceptible to IL-4-switched IgE production, IL-5 induced eosinophilia and IL3, IL-4-stimulated mast cell proliferation and degranulation[7]. In mice, activated naïve $CD4^+$ T cells differentiate into Th17 upon encounter of IL-6, IL-21, IL-23, and transforming growth factor-β (TGF-β). TGF-β leads to SMAD activation, which along with IL-6-induced STAT3, NFAT and others lead to the transactivation of the key transcription factor RORγt[8, 9]. Th17 cells produce IL-17, IL-22 and are important in tissue inflammation and combating extracellular bacteria by recruiting neutrophils via stimulating stromal cell-mediated GCSF production[1]. In the absence of IL-6-mediated STAT3 activation, but IL-2-mediated STAT5 phosphorylation, TGF-β-facilitated Smad3 cooperates with NFAT for FoxP3 expression[10], favouring the development of pTreg.

In general, Treg cells are defined as $CD4^+CD25^+FoxP3^{+}$[11], can produce anti-inflammatory IL-10 and TGF-β, and are involved in limiting the immune response and preventing autoimmunity[1, 7]. They constitutively express high levels of CTLA-4 which binds to CD80/CD86. Due to higher

affinity to CD80/86 than CD28, it competes with CD28 and deprives Tcons of their costimulation. Tregs inhibit activated DCs via CTLA4-mediated downregulation of CD80/86 expression and induction of indoleamine 2,3-dioxygenase (IDO) expression on DCs. IDO catalyzes tryptophan into kynurenines, which are toxic to DC-neighboring T cells. Activated Treg can also inhibit the survival of macrophages by the Fas/FasL pathway and B cells by granzyme/perforin release[12, 13, 14]. Additionally, since Treg constitutively express a high level of CD25 and very much depend on IL-2, which they cannot produce themselves, they can compete with Tcon for IL-2 acting as a so-called IL-2 sink. Thereby, Treg indirectly downregulate proliferation and mediate apoptosis of Tcons[15, 16].

Similar to T-helper subsets, $CD8^+$ T cells can also be differentiated into Tc1, Tc2, Tc9, Tc17, and $CD8^+$ Treg. Their cytokine profiles and transcription factors involved are similar to the respective Th cells. Among them, Tc1 cells are best characterized. They are cytotoxic, clear out intracellular pathogens and tumor cells by releasing granzymes, perforin, and cytokines, such as IFN-γ and tumor necrosis factor (TNF)-α[17, 18, 19]. Moreover, $CD8^+$ T cells, traditionally known as cytotoxic T lymphocytes (CTL), can also induce apoptosis of target cells by Fas-L/Fas interaction[18], as well as recruit and activate macrophages[20]. Apart from these different types of T_{EFF} cells which die after the elimination of pathogens, naïve T cells can generate long-lived memory cells. The memory population is very heterogeneous, containing stem cell memory (T_{SCM}, $CD45RO^-CD45RA^+CCR7^+CD95^+CD122^+CD62L^{hi}$), central memory ($T_{CM}$, $CD45RO^+CD45RA^-CCR7^+CD62L^{hi}$), effector memory ($T_{EM}$, $CD45RO^+CD45RA^-CCR7^-CD62L^{lo}$) and terminally differentiated $CD45RA^+$ T_{EM} cells (T_{EMRA}) [21, 22, 23].

T cells can also reach a hyporesponsive state when stimulated via the TCR signal but in absence of co-stimulation or the presence of co-inhibitory signals. This state is called T-cell anergy. In cancer or chronic viral infection, i.e. constant and unresolved antigen presentation, $CD8^+$ T cells reach another hyporesponsive state called “exhaustion”. Exhausted $CD8^+$ T cells (T_{EX}) display a transcriptional program distinct from effector or memory T cells, characterized by reduced proliferation and cytokine production along with expression of co-inhibitory surface molecules, such as PD-1, LAG-3, TIM-3, TIGIT, and CTLA-4[24, 25]. Here, pre-exhausted T_{PEX} defines a transitional state, in which the CTLs can still be reactivated to generate T_{EFF} in response to immune checkpoint blockade, while true T_{EX} is in a state of no return[26].

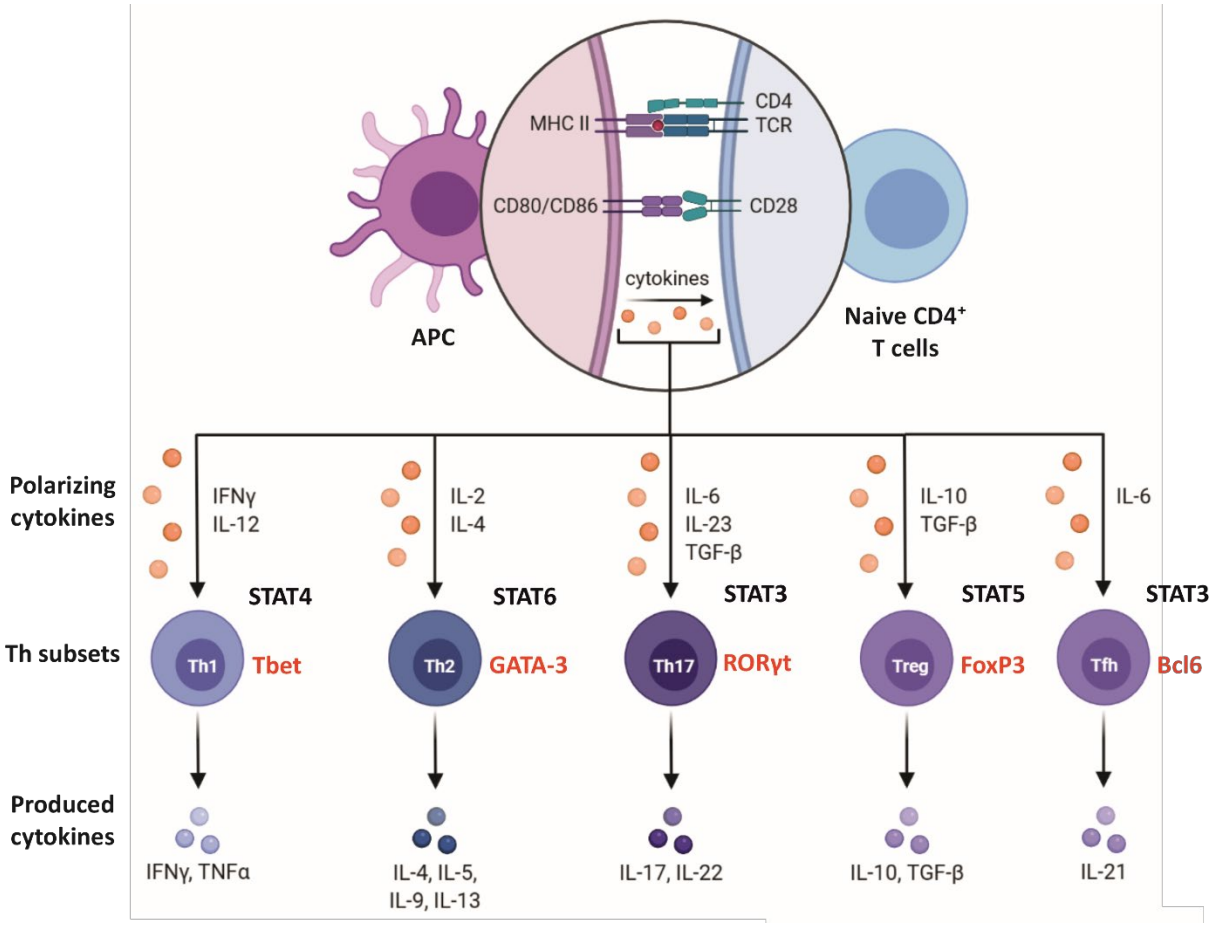

Figure 2: **T cell activation and differentiation**.

Signal 1 (binding of the T-cell receptor (TCR) to the peptide-MHCII complex on the antigen-presenting cell (APC) surface) and signal 2 (binding of the T-cell costimulatory receptor CD28 to CD80/CD86 on the APC surface) are required for T-cell activation. The binding of polarizing cytokines to their respective receptors on the T-cell surface represents signal 3. Different combinations of these cytokines influence T-cell differentiation into distinct T_{EFF} cell subtypes that produce signature cytokines. The lineage-specific transcription factors for each type of subsets are mentioned in red, cytokine-induced transcription factors (STAT) in black[27, 28]. Created by Biorender.com

6.4 Hematopoietic cell transplantation (HCT)

Hematopoietic stem cells (HSC) are multipotent cells with self-renewal capacity that reside in the bone marrow and can develop into all types of blood cells[29]. HSC transplantation (HCT) is a procedure where donor HSCs are transplanted to a recipient to replenish or replace the hematopoietic system[30]. Depending on the source of stem cells, HCT can be autologous (from the same patient) or allogeneic (allo-HCT), where the source of stem cells is an HLA-matched unrelated or related healthy donor[31]. HCT is a well-established treatment option for hematological malignancies (leukemia, lymphoma, myeloma, or myelodysplastic syndrome), non-malignant diseases like acquired severe aplastic anemia, and other inherited blood disorders[30, 32]. The first successful allo-HCT was performed by E. D. Thomas in 1959[33] after an

initial attempt in 1957[34] and he was awarded the Nobel prize in Medicine in 1990[35, 36]. According to a survey, 19,630 patients underwent allo-HCT in Europe in 2018[37] and 55,000 patients annually worldwide[38]. Before performing an allo-HCT, a conditioning regimen (chemotherapy or total body irradiation) is used for tumor eradication, removing the recipient immune system to decrease the risk of rejection of donor cells, and also to create space for engraftment of donor cells in the bone marrow[39]. Allo-HCT is associated with lower rates of malignant relapse due to tumor surveillance by the transplanted immune system, an effect more commonly known as graft-versus-tumor (GvT) or graft-versus-leukemia (GvL) effect[40]. However, immune cells of the graft recognize the recipient's antigens as 'allo' and mount an immune response against them. This causes the major complication of allo-HCT known graft-versus-host disease (GvHD). The other risk factors include infections, engraftment failure, and tumor relapse. In allo-HCT, matched related donors (MRD) or matched unrelated donors (MUD) are preferred to ensure donor human leukocyte antigen (HLA, name of human MHC) allele type match with the recipient. Although ensuring the best possible HLA match by this, minor histocompatibility-antigens (miHAgs) are often mismatched between donor and recipient, still resulting in GvHD[41]. When MRD and MUD are unavailable, patients undergo haplo-identical transplantation (Haplo), like parental donors, would be for their children. However, this increases post-transplantation complications and mortality[42].

6.5 Acute Graft-versus-Host Disease (aGvHD)

Acute and chronic GvHD are among the leading non-relapse complications of allo-HCT which still cause substantial morbidity and mortality[43]. GvHD is an immunological disorder affecting many organs, including the gastrointestinal tract (GIT), skin, lungs, and liver, primarily triggered by donor lymphocytes interacting with host allo-antigens (due to MHC mismatch and miHAgs mismatch) promoting inflammation[44, 45]. About 40-60% of patients undergoing allo-HCT develop acute or chronic GvHD[46, 47, 48]. By definition, acute-GvHD (aGvHD) occurs in the initial 100 days post-transplantation and develops in three phases[49] (Fig. 2). In the first phase, conditioning before transplantation triggers host-tissue damage with the subsequent production of inflammatory cytokines such as TNF-α, IL-6, and IL-1. The release of bacteria and changes in the gut microbiome is caused by damage of intestinal epithelium and lead to the propagation of pro-inflammatory immune responses. Damage-associated molecular patterns (DAMPs) and pathogen-associated molecular patterns (PAMPs) exaggerate

inflammatory responses by activating monocytes and neutrophils which then cause local tissue damage mediated by reactive oxygen species (ROS). This consequential cytokine storm activates host APCs (dendritic cells, Langerhans cells, B cells, and non-hematopoietic cells) enhancing host (allo-) antigens recognition by donor T cells. In the next phase, donor $CD4^+$ and $CD8^+$ T cells are activated in secondary lymphoid organs (SLOs) by TCR-antigen-bound MHC signal and co-stimulation. Upon activation, donor T cells proliferate, differentiate into Th1/Tc1, Th17/Tc17 subtypes, and migrate to the host tissues. In the final phase, cytotoxic T_{EFF} cells reach target organs (skin, GIT, liver, lung) and cause apoptosis of target cells by TNF-α, IFN-γ, granzyme, perforin, and Fas ligand. Homing of T cells to the target organs is facilitated by integrins (heterodimeric transmembrane proteins containing α and β subunits) and selectins. α4β7 integrin expressed on T cells upon activation binds to its ligand, MAdCAM-1 on endothelial cells and helps in homing to the intestine[50]. In addition, mononuclear phagocytes are activated by bacteria-derived lipopolysaccharide (LPS) during tissue damage causing a feedback loop augmenting aGvHD response[43, 48, 49, 51].

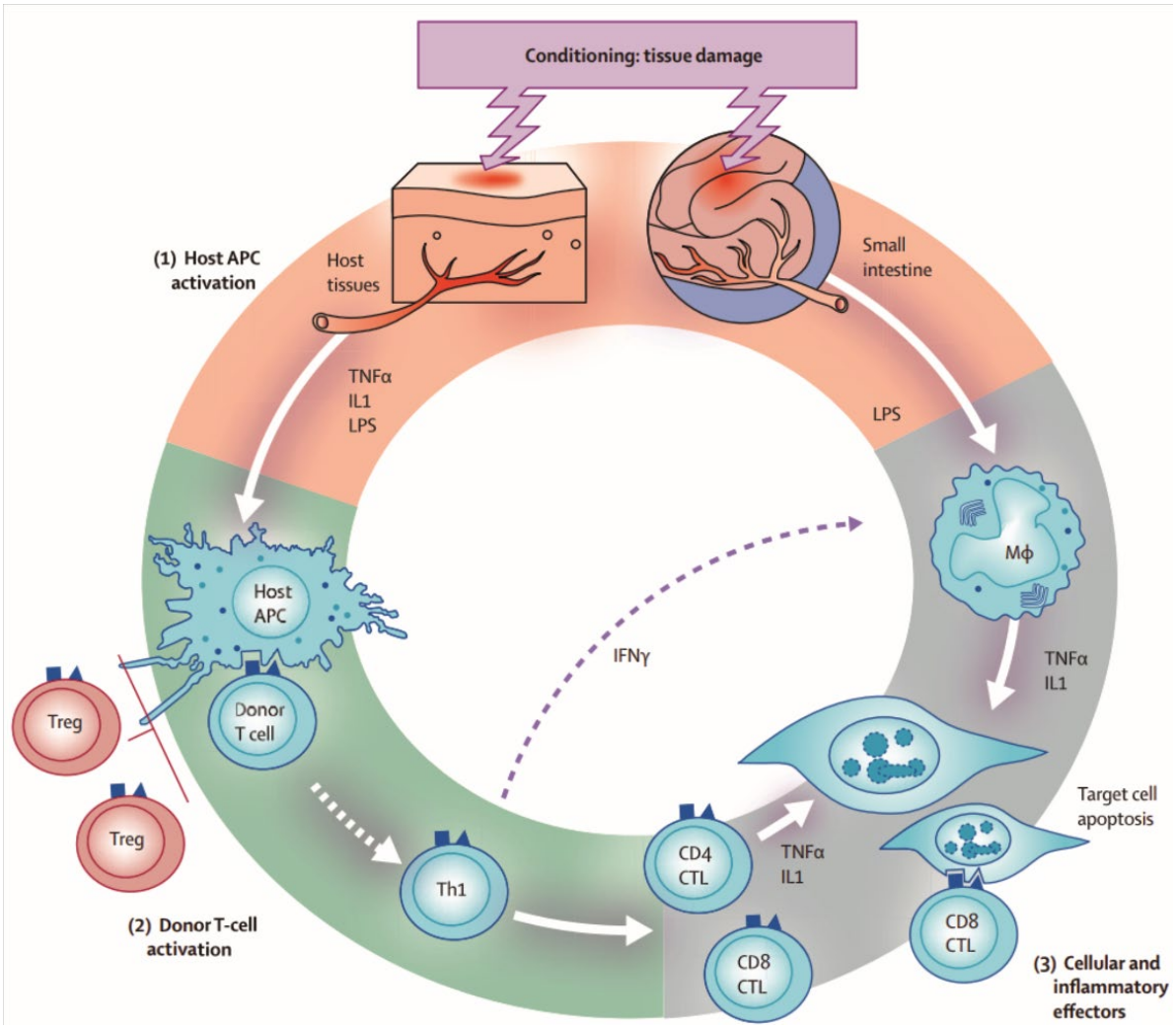

Figure 3: **GvHD pathophysiology**

GvHD development can be divided into three distinct phases: In phase I, the conditioning regimen damages host tissues and induces the release of inflammatory cytokines which leads to host antigen-presenting cells (APCs)-induced tissue damage. In phase II, the donor T cells are activated by host APCs, proliferate, and differentiate into Th1 and Th17 subtypes. In phase III, the alloreactive cytotoxic effector T cells (CTL) and innate cells attack the host tissue. This damage is further supported by lipopolysaccharide (LPS) that has originated from intestinal mucosa damage which recruits myeloid cells to produce proinflammatory cytokines thus increasing the cytokine storm[45].

6.6 Clinical manifestations and disease management of GvHD

GvHD causes the death of 20-40% of patients undergoing allo-HCT[52]. Signs of disease are seen as skin rashes showing cutaneous GvHD, anorexia, nausea, and diarrhea showing GIT involvement and increased serum bilirubin level indicating liver damage. The severity of GvHD is graded in four categories (I, II, III, and IV) and is often diagnosed by histological analysis of organ biopsies[49]. Corticosteroids and calcineurin (CN) inhibitors (CNI) are commonly used as primary treatment options for patients suffering from GvHD. However, corticosteroids only work in 50% of the patients and CNIs (Cyclosporin-A and tacrolimus/FK506) interfere with GvL

efficacy causing an increase in relapse-related mortality[53,46,54]. Some of the secondary therapy options are other immunosuppressants (e.g. Methotrexate, Mycophenolate mofetil), phototherapy (UVA and UVB), and mTOR inhibitors (Rapamycin). These therapies suppress overall the immune system of the patient, hence they increase chances of CMV reactivation and further opportunistic infections as well as tumor relapse[48]. Several emerging therapies have shown exciting outcomes in preclinical models and clinical trials, including mesenchymal stromal cell (MSCs)[55] and Treg therapy. Normally, the production of IL-2 by Th1 cells would support the generation and maintenance of Treg, whereas IL-2 production is inhibited by CNIs. Treg can suppress proliferation, migration of alloreactive Tcons, arrest maturation and impair the function of dendritic cells[56, 57]. It has been demonstrated that Treg can ameliorate aGvHD in mouse models and humans[45, 58, 59] and, importantly, preserve GvL effects in mice[60]. Yet, to date, it is challenging to generate and expand enough stable Treg *in vitro* for therapeutic application[61]. Additionally, targeting signaling pathways like JAK/STAT (Ruxolitinib), PKCα and PKCθ, MEK, NFAT, ITK, toll-like receptor/myeloid differentiation factor 88, DR3 signaling might provide strategies to lessen GvHD, without compromising GvL effects[62, 63, 64].

6.7 Experimental aGvHD

GvHD and GvL often co-occur, hence the focus is on understanding the cellular and molecular basis of GvHD and GvL to successfully promote GvL while avoiding or limiting the toxicity of GvHD. Experimental aGvHD murine mouse models are crucial and an ideal platform in studying donor T-cell activation and migration pattern *in vivo* and to assess promising therapeutic ideas. There are several well-established mouse models used for this purpose[65]. To induce aGvHD in mice, a major mismatch mouse model (mismatch in MHC-I, MHC-II, and miHAgs) is often applied. Although not reflecting the exact clinical situation, the onset and phenotype of aGvHD very much resemble the clinical picture. For a GvHD experiment, recipient mice are conditioned by X-ray irradiation before transplantation. Most commonly, C57BL/6 mouse T cells (B6; H-2^b) are transplanted with T-cell depleted bone marrow (or even from *Rag1*$^{-/-}$ mice; also H-2^b) into BALB/c (H-2^d) recipient mice. In this mouse model, both $CD4^+$ and $CD8^+$ T cells contribute to the phenotype and, lethal disease is established within one week of transplantation. Luciferase-expressing donor T cells could be used to measure GvHD by tracking proliferation and target organ infiltration by *in-vivo* bioluminescence

imaging[63, 66, 67, 68]. To visualize the GvL effect, on the other hand, luciferase$^+$ (luc$^+$) tumor cells can be transfused[63, 69, 70].

6.8 Nuclear factor of activated T-cells (NFAT)

The nuclear factor of activated T-cells (NFAT) is a transcription factor family which was first discovered in nuclear extracts of activated T cells binding to the *Il2* promoter. NFATs are also expressed in several other immune cells and even in non-lymphoid tissues such as the heart, muscles, brain, cartilages, and fat. There are 5 known members of this family, NFATc1 (alias NFAT2 or NFATc), NFATc2 (NFAT1 or NFATp), NFATc3 (NFAT4 or NFATx), NFATc4 (NFAT3), and NFAT5. NFATc1-4 are regulated by Ca^{2+}/calcineurin signaling and NFAT5 by osmotic stress. Thus in T cells, TCR signals leading to heightened intracellular Ca^{2+} levels enable NFAT activation. Calcineurin (CN) dephosphorylates N-terminal regulatory domains of NFAT members, which leads to the exposure of a nuclear localization signal (NLS) on NFAT proteins and translocation into the nucleus. The CNIs, CsA, and FK506, used in the treatment of GvHD or organ transplantation block the phosphatase activity of CN by binding with immunophilins[71], thereby inhibiting NFAT translocation to the nucleus and subsequently T-cell function[72, 73]. NFAT proteins consist of N- and C-terminal transactivating domains (TAD), a less conserved N-terminal regulatory domain (also known as NFAT homology region or NHR), and a conserved core DNA-binding Rel-homology domain or Rel-similarity domain (RHD or RSD)[74]. The NHR contains a CN-binding site, the NLS, and a serine-rich domain (SRD), which are targets of phosphorylation and dephosphorylation. The RHD domain harbors an AP-1 (i.e. heterodimers of members of the Jun and Fos family) interaction site and another NLS (Fig. 4). In addition, alternative splicing and usage of different promoters give rise to several isoforms of each NFAT family member (Fig. 4), which have different as well as redundant functions. As mentioned, apart from T cells NFAT also regulates other immune cells including functions of B cells, DCs, NK cells[75, 76, 77, 78, 79].

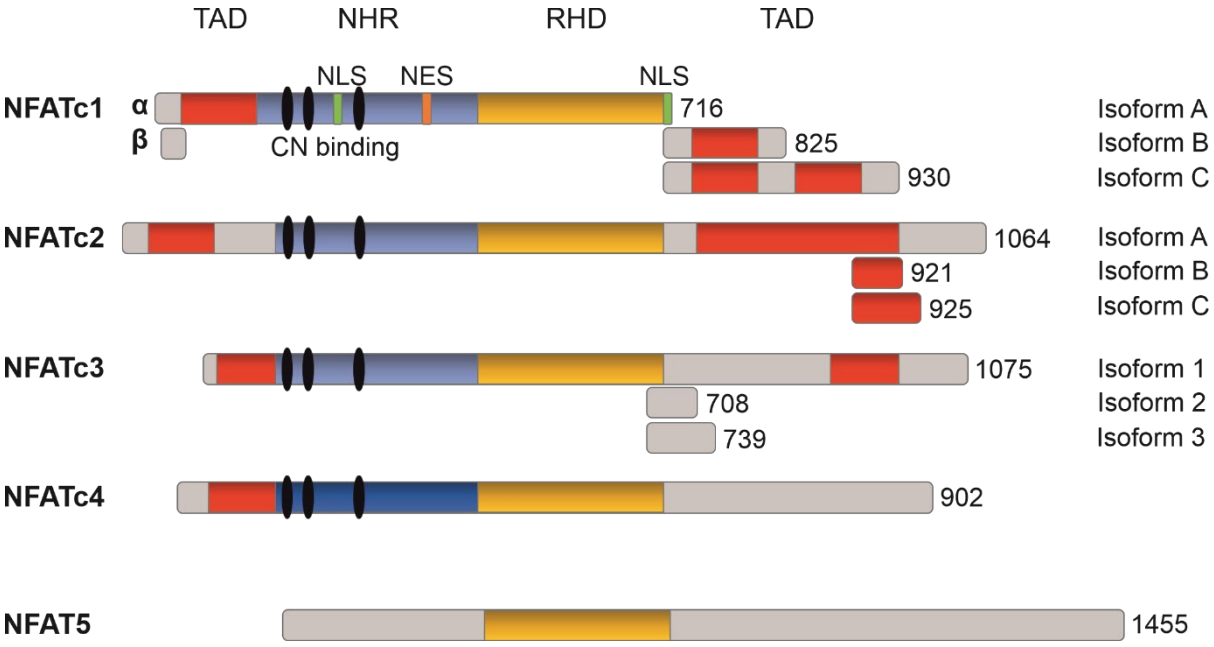

Figure 4: **Schematic diagram of the NFAT transcription factor family members.**

The five NFAT family members are mentioned on the left with the amino acid length on the right. NFATc1-4 consist of N-terminal and C-terminal trans-activating domains (TAD in red), NFAT homology region (NHR in blue), the regulatory domain, and Rel homology domain (RHD in yellow) or the DNA-binding domain. The NHR contains a CN-binding site, nuclear localization signal (NLS), nuclear export signal (NES), and multiple phosphorylation sites (in black). The RHD domain contains AP1-binding sites and another NLS. NFATc1, c2, and c3 have several isoforms indicated on the right. By the usage of the inducible P1 *vs* the constitutive P2 promoter, NFATc1 can give rise to α and β isoforms indicated on the left.

6.9 Role of NFAT in T-cell function

TCR-pMHC interaction leads to SOCE, which increases Ca^{2+} level in the cytoplasm of T cells. Calmodulin binds to the free cytosolic Ca^{2+} and activates the serine/threonine phosphatase CN. CN dephosphorylates multiple serine and threonine residues in the regulatory domain of NFAT, which results in a conformational change, exposure of the NLS, and translocation of NFAT into the nucleus. Once in the nucleus, NFAT binds to the DNA in conjunction with other transcription factors and regulates the transcription of several other genes. Nuclear kinases re-phosphorylate and thereby export NFAT to the cytoplasm, where maintenance kinases help in keeping NFAT in the cytoplasm. Several other post-translational modifications regulate NFAT activation including acetylation, proteolytic cleavage by Caspase 3, and SUMOylation facilitated by the attachment of small ubiquitin-like modifier (SUMO)[80]. Additionally, NFATc1 is transcriptionally regulated by NFATc1 protein expression itself. The *Nfatc1* gene in mice and humans consists of 11 exons, while the usage of two promoters (P1 & P2) and poly-A sites, as well as different splicing events give rise to 6 isoforms. Within hours of TCR stimulation,

NFATc1 can bind to its P1 promoter and via this auto-regulatory loop induces the short isoform NFATc1/αA, which lacks the C-terminal domain also present in other NFAT proteins (Fig. 4). Thus, NFATc1/αA acts in a positive auto-regulatory loop to induce T-cell activation and NFAT target gene expression[81]. This isoform is expressed in T_{EFF} cells, but not in circulating Treg. The constitutive P2 promoter leads to exon2-encoded β-peptide expression and therefore NFATc1/βB and NFATc1/βC. NFATc1 and NFATc2 are predominantly expressed in peripheral T cells and control their effector function, such as cytokine expressions like IL-2, IL-4, IL-5, IL-13, IFN-γ, IL-17, TNFα, granulocyte/macrophage colony-stimulation factor (GM-CSF), surface molecules like CD40 ligand (CD40L) and CD25. In sum, NFAT proteins take part in the control of cell proliferation and cell cycle, differentiation, exhaustion/anergy, apoptosis, and metabolism[73, 79]. NFAT often binds composed response elements with AP1 and also interacts on protein level with AP1 to regulate effector gene expression. In absence of AP1, NFAT leads to T-cell anergy and exhaustion[24, 82]. The role of NFAT in differentiation has been elucidated by NFAT-deficient mice. Here, the overall loss of NFATc2 promotes a mild bias towards Th2 cell differentiation characterized by an increase in IL-4, IL-5, and IL-13, but a decrease in IFN-γ production. In *Nfatc2/Nfatc3* double-knockout (DKO) mice Th2 differentiation was further increased suggesting that NFATc2 and NFATc3 are positive regulators of Th1 responses. In contrast, NFATc1-deficient mice (BM chimera with fetal liver cells and T cell-specific knockout, whereas total NFATc1 knockout in embryonic lethal due to cardiac valve development defect) show impaired Th2 cytokine production and reduced IgG1 and IgE levels. Several other studies indicated NFATc1 to positively regulate Th2 differentiation with a possible reciprocal relationship with NFATc2 and NFATc3[83]. We and others have demonstrated that *Nfatc1$^{fl/fl}$.Cd4cre* mice exhibit lower RORγt levels and reduced IL-17, IFN-γ, GM-CSF[84], and IL-21[85] production and thus being protected from severe experimental autoimmune encephalomyelitis (EAE)[84, 85]. Whereas NFATc2-deficient mice also showed decreased EAE pathogenicity, this was due to non-pathogenic Th17 differentiation (expressing IL-17 along with IL-4 and IL-10)[84].

Our group has also demonstrated earlier that for Treg individual NFAT members make less difference than for Tcon. Nfatc1/2/3 single or Nfatc1/2 and Nfatc2/3 double-deficiency diminished iTreg and pTreg induction, but not their suppressive function. Thymic nTreg differentiation, their frequency in the periphery, and their suppressive function appeared

NFAT-independent[10]. This dichotomy of NFAT dependency for differentiation of pTreg vs nTreg is based on the Foxp3 enhancer element CNS3, which is accessible during thymic development and regulated by NF-κB[86], contrasting iTreg-essential and NFAT-regulated CNS1[10, 87]. NFATs and predominantly NFATc1/αA are also expressed in $CD4^+$ T follicular helper (Tfh) and interestingly in T follicular regulatory (Tfr) cells and are critical for shaping humoral immunity[73, 88].

The role of NFAT in CTLs is still underexplored. Recent studies in an LCMV mouse model showed that NFATc1 is required for promoting memory $CD8^+$ T cells in a cell-intrinsic manner and that NFATc2 is required for IFN-γ production by $CD8^+$ T_{EFF} cell. However, they did not observe increased viral load in single-deficient mice, whereas the DKO T cells were unable to control the virus efficiently *in vivo*[89]. Another study showed *Nfatc1*$^{-/-}$ but not *Nfatc2*$^{-/-}$ CTLs to have defective cytoskeleton organization and recruitment of cytosolic organelles to immunological synapses. *Nfatc1*$^{-/-}$ CTLs exhibit defective *in vitro* killing of MOPC 315 plasmacytoma cells, diminished RNA level of *Gzmb* (but increased protein level), *Tbx21*, cytokine, and chemokines. In this study, *Nfatc1*$^{fl/fl}$*.Cd4cre* mice also revealed defective control of *Listeria monocytogenes* infection[90]. Previous work from our group documented that T cells from NFATc1 or NFATc2 single or NFATc1/c2 double-deficient mice when transplanted in major mismatch allo-HCT mouse model (B6, H-2^b into BALB/c, H-2^d), proliferated less, homed less to target tissue, and had an impaired function. In contrast, the frequency of NFAT-deficient Treg was increased. They were still functional as they protected the mice from severe aGvHD and prolonged survival. In line with the presence of functional Treg, the GvL activity of donor T cells was preserved as demonstrated in two different mouse models of B-cell lymphoma. No difference in granzyme B and perforin expression could be detected in comparison to wildtype (WT) donor T cells 6 d after allo-HCT. However, in DKO T-cell recipient mice, aGvHD was so limited that survival was ensured despite a mild tumor relapse[63]. Taken together, these studies showed that loss of a single NFAT member can lessen aGvHD and still confer GvL during allo-HCT in mice.

Recently, our group has also shown that sumoylation sites mutated in NFATc1 long C-terminus create NFATc1/A-like isoforms. Such T cells (NFATc1/ΔS), when adoptively transferred in mice, ameliorated aGvHD and EAE. This was firstly due to the enhanced IL-2 production by NFATc1/ΔS Tcons which supported Treg expansion. Secondly, NFATc1/ΔS Tcons produced

decreased proinflammatory cytokines IFN-γ and IL17A, thereby limiting autoreactive and alloreactive immune responses[67]. With this, even the deletion of solely the long isoforms of NFATc1 might be a therapeutic option for autoimmunity like multiple sclerosis and allo-responses in aGvHD.

6.10 T-cell genome editing using CRISPR/Cas9

Until today, immunological studies depend on mouse models, which provide a manipulable systemic approach. Hence, to understand, the cause and consequence of gene function in health and disease, multiple transgenic mice have been created. For allo-HCT, mouse models of T-cell transfer serve translational purposes. Prominent examples are experimental GvHD mouse models. To circumvent the creation of transgenic animals for such experiments, one could envisage an *in vitro* manipulation of primary T cells. However, in that case, efficient gene targeting is mandatory. Primary lymphocytes are difficult to transfect, which proves almost impossible for primary mouse T cells[91]. For any success with electroporation or viral infection, usually activation is necessary. Yet, pre-activation directs the T cells towards a certain status before the transgene is expressed or an endogenous gene is inhibited and, importantly, before the T cells face the *in vivo* situation. Thus, the possibility for gene targeting in naive murine T cells is desirable, especially, when one wants to study genes involved in T-cell activation and differentiation. This, however, should be so effective that one can transfer the transgenic T cells without any further selection, enrichment, or expansion. This is tedious, although modern Clustered Regularly Interspaced Short Palindromic Repeats-associated nuclease 9 (CRISPR/Cas9)-mediated techniques have improved the procedure enormously. CRISPR is a microbial adaptive immune system that uses RNA-guided nucleases to cleave foreign genetic elements, identified across a broad range of bacterial and archaeal hosts. CRISPR/Cas9, the type II CRISPR system, consists of an RNA-guided cluster of CRISPR-associated 9 (Cas9) nuclease, a CRISPR RNA (crRNA) array, and a transactivating crRNA (tracrRNA). crRNA array consists of repetitive elements (direct repeats), interspaced by short variable sequences originating from exogenous DNA targets known as protospacers. Within the DNA target, each protospacer is always associated with a protospacer adjacent motif (PAM). In the CRISPR/Cas9 system derived from *Streptococcus pyogenes,* which is used in this study, the PAM sequence is 5'-NGG (N can be any nucleotide). The tracrRNA facilitates the processing of crRNA into distinct units and crRNA are 20 nucleotides (nt) long and are

complementary to the target DNA (20nt long). In eukaryotic cells, such as lymphocytes, the crRNA and tracrRNA (together called guide RNA or gRNA), bound to the Cas9 endonuclease form a ribonucleoprotein (RNP) complex. This RNP complex then binds to the complementary DNA target adjacent to a PAM and makes double-stranded breaks in the DNA. Upon cleavage, DNA damage repair system, the error-prone non-homologous end-joining (NHEJ), or the high fidelity homology-directed repair (HDR) pathway attempts to repair the DNA. In the absence of a repair template, NHEJ re-ligates the DNA leaving insertion/deletion (indel) mutations. This error causes frame-shift mutations in the coding sequence and leads to premature stop codons and the knockout of a gene[92] (Fig. 5). CRISPR/Cas9 has become a very popular tool in the field of adoptive T-cell therapy and chimeric antigen receptor (CAR) T-cell therapy, wherein human T cells are genetically modified to delete a gene (such as PD1) using RNP nucleofection, Cas9 mRNA/gRNA nucleofection or virus-mediated Cas9/gRNA delivery to enhance the function of T cells to combat cancer more efficiently[93, 94]. However, non-viral gene modification by CRISPR/Cas9 in mouse and human T cells is still being studied to provide a safe, easy, cost-effective, and efficient method of generating gene-edited T cells for translational research and clinical application.

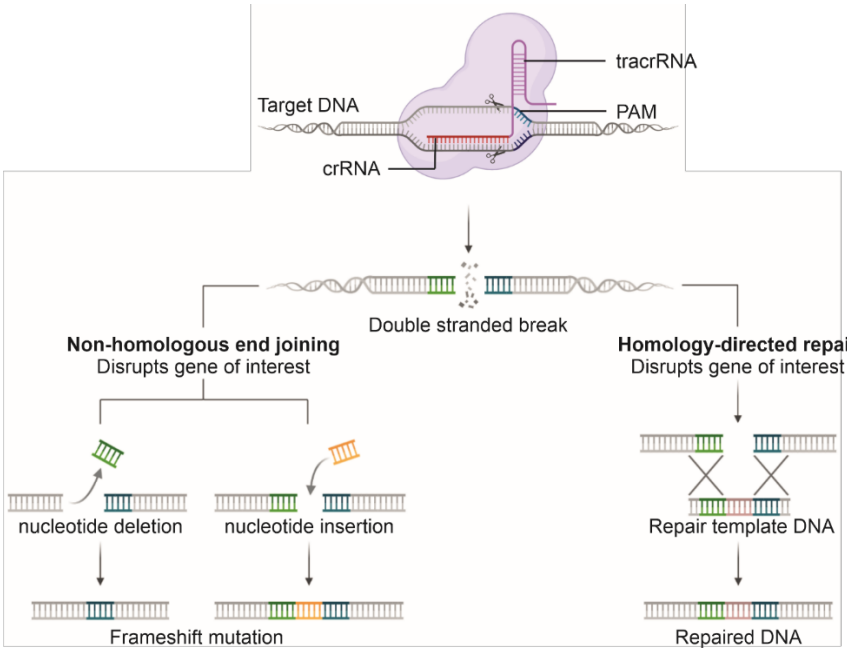

Figure 5. **CRISPR/Cas9 gene editing.**

The Cas9 complex with crRNA (in red) and tracrRNA (in purple) recognizes a specific sequence, the protospacer. This is only possible if this sequence is followed by a Protospacer Adjacent Motif (PAM). When Cas9 binds, a dsDNA break is generated. Repair pathway Non-homologous end-joining (NHEJ) leads to a frameshift mutation and premature stop codon resulting in gene knockout. Homology-directed repair (HDR) can occur when a repair template is available, leading to repair or precise editing of the gene. Created by Biorender.com.

6.11 CAR T-cell therapy

Chimeric antigen receptor (CAR) T-cell therapy represents a major step forward in treating hematological malignancies. Patients with relapsed/refractory B-cell acute lymphoblastic leukemia (B-ALL) are treated with anti-CD19-CAR T cells (also known as CD19-CAR) as approved by the U.S. Food and Drug Administration (FDA). In CAR T-cell therapy a patient's own T cells are isolated from peripheral blood, genetically manipulated, expanded *ex vivo*, and then infused back into the same patients (Fig. 6A). CAR are synthetic receptors that comprise an extracellular domain derived from a single-chain variable fragment (scFv) of an antigen-specific mAb and a transmembrane (TM) as well as intracellular domains containing the signaling modules of TCR and co-stimulation molecules. The intracellular domain contains a part of the CD3ζ chain and one or more co-stimulatory domains of CD28 or 4-1BB (Fig. 6B). In contrast to endogenous TCRs, CARs provide distinct characteristics in antigen binding and tumor recognition. CD19-CARs can specifically bind to CD19-expressing tumor cells and also normal $CD19^+$ B cells. In this study, we used second-generation CD19-CAR. The extracellular domain scFv was derived from FMC63 mAb, which is linked to the intracellular CD3ζ and 4-1BB co-stimulatory domain by IgG4-hinge as a spacer domain, which provides flexibility and reaches for antigen binding[95]. This CD19-CAR has been successfully used in clinical trials of follicular lymphoma[96], non-Hodgkin lymphoma[97], and B-ALL[98, 99]. The CAR transgene is fused with a truncated human epidermal growth factor receptor (EGFRt) by a T2A ribosomal skip sequence. EGFRt is lacking extracellular N-terminal ligand binding domains and intracellular receptor tyrosine kinase activity but retains the native amino acid sequence, type I transmembrane cell surface localization, and a conformationally intact binding epitope for anti-EGFR monoclonal antibody[100]. The EGFRt serves as a successful CAR delivery/expression marker and can be used to enrich CAR-expressing T cells. Moreover, it can be used to deplete CAR T cells *in vivo* by EGFR-specific antibodies (Fig. 6C)[100, 101, 102]. 4-1BB is a member of the TNF receptor superfamily (TNFRSF), which interacts with the 4-1BB ligand expressed on APCs. 4-1BB cytoplasmic signaling domain associates with TNFR-associated factor (TRAF) adaptor molecules to provide costimulatory signal and synergizes with TCR-signaling to promote cell cycle progression, effector function, and T-cell survival[103, 104]. 4-1BB costimulation in CD19-CAR T cell has shown more efficient overall survival and less cytokine release syndrome (CRS) compared to CD28 costimulation in preclinical mouse models[105]. T-cell exhaustion induced by

persistent CAR signaling is lessened in 4-1BB costimulation compared to CD28 costimulation[106, 107].

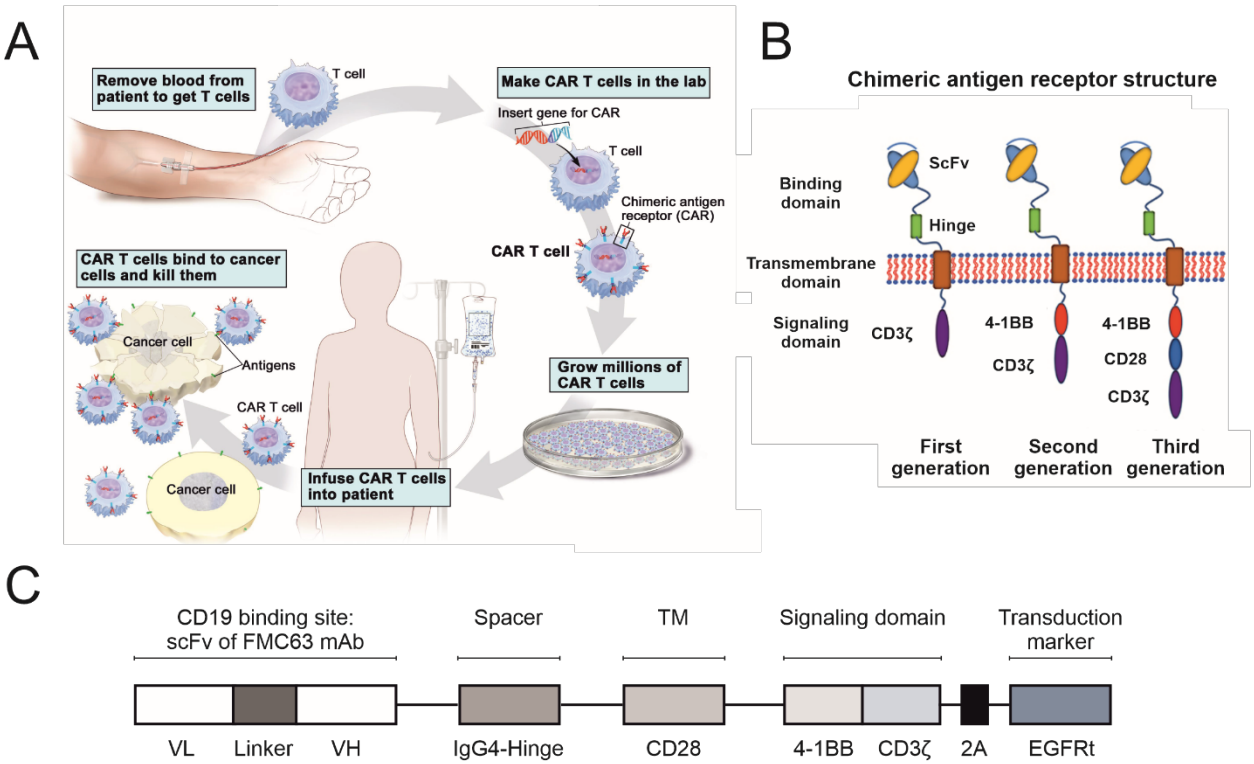

Figure 6. **CAR T-cell therapy.**

A. Procedure of CAR T-cell treatment in patients with hematological malignancies (credit: National Cancer Institute[108]) T cells are isolated from peripheral blood drawn from patients and CAR constructs are inserted in the genome of T cells by viral transduction or a non-viral method. CAR$^+$ T cells are selected and expanded *in vitro* before infusing back to the patients. In the patient body, the antigen-specific cytotoxic CAR T cells can recognize tumor cells and eradicate them. **B.** Structure of CAR receptors of different generations[109]. **C.** Structure of CD19-CAR construct used in this study[102].

7 Objective of the work

CsA or FK506 are routinely used to prevent and/or treat patients with acute GvHD. These drugs reduce inflammation and allo-reactivity, but also interfere with the anticipated GvL activity. Both drugs inhibit CN, which at first dephosphorylates and activates members of the NFAT family of transcription factors by binding to their conserved PxIxIT and LxVP motifs. Independent of NFAT suppression and NF-κB pathway inhibition[110, 111], CNIs cause severe side effects due to overall CN phosphatase inhibition as well as their interaction with immunophilins. GvL efficacy is compromised due to direct and indirect inhibition of $CD4^+FoxP3^+$ Treg as well as by limiting the cytotoxic function of $CD8^+$ T cells. Regimes to block aGvHD by the direct and exclusive hindrance of NFAT activation seemed advantageous. Our previous study shows the absence of one or two NFAT transcription factors in T cells prevents harmful aGvHD by reducing the effector function of allogeneic T cells and increasing the frequency of still functional Treg. Yet lack of only one member fully preserved the beneficial GvL effect[63]. We, therefore, propose here to develop and evaluate treatment regimens that avoid broad immune suppression and instead specifically target NFAT during allo-HCT.

- The first objective of this study was a proof of concept to investigate whether NFAT-ablated donor T cells by the CRISPR/Cas9 method also ameliorated aGvHD in mice like T cells from NFAT-deficient transgenic mice. For this, we aimed to optimize a highly efficient CRISPR/Cas9 gene editing method to ablate individual NFAT members in primary mouse T cells.
- Next, we optimized a non-viral CRISPR/Cas9 gene editing method to ablate NFAT members in primary human $CD3^+$ T cells. By using this method we aimed to analyse the potential of NFAT-deficient human $CD3^+$ T cells to ameliorate GvHD and to confer anti-tumor efficacy. We asked whether NFAT single or double-knockout affects Treg and other T-cell subpopulations.
- Lastly, we aimed to optimize a highly efficient, non-viral, CRISPR/Cas9-mediated gene-modified, CD19-CAR T-cell generation method. Using this method we sought to investigate the role of NFATC1 and NFATC2 in the anti-tumor efficacy of $CD8^+$ CD19-CAR T cells *in vitro.*

8 Material and Methods

8.1 Material

8.1.1 Media/Cell culture supplements

Name	Cat. No.	Source
DMEM	323430-100	Gibco
Fetal bovine serum (FBS)	10500-064	Gibco
RPMI1640	21875-059	Gibco
Penicillin/Streptomycin	15140-122	Gibco
Sodium Pyruvate	11360-39	Gibco
Non-essential amino acids	11140-035	Gibco
L-glutamine	25030-024	Gibco
HEPES	15630-56	Gibco
2-mercaptoethanol	31350-010	Gibco
XF Base Medium		Agilent Technologies
DMEM for Mitochondrial Stress Test		Sigma-Aldrich

8.1.2 Consumables

Name	Source
Ingenio 100ul cuvettes	Mirus
Well plates (6, 12, 24, 96-well)	GBO
Syringes (1 ml, 5 ml, 10 ml)	BD Pharmigen™, Braun
Sterile filter (0,2 and 0,45 µm)	Rotilabo ROTH
Serological pipettes (5, 10, 25 ml)	GBO
ROTI®-Nylon plus membrane	ROTH
Reaction tubes 1,5 and 2 ml	Eppendorf
Petri dishes (10 cm diameter)	GBO
LS-colums	Miltenyi Biotech
Centrifuge tubes 15 ml and 50 ml	GBO
Blotting paper	Laborhaus Scheller
70 µm Nylon filter	Falcon
5 ml round-bottom tubes	Falcon
Nuclease free PCR tubes	Eppendorf
Micropipette tips	Laborhaus Scheller
Seahorse XFe96 culture plates	Agilent/Seahorse Bioscience
Corning™ Cell-Tak Cell and Tissue Adhesive	BD
Seahorse XFe96 cartridge	Agilent/Seahorse Bioscience

8.1.3 Equipment

Name	Cat. No./Source
MojoSort™ Magnetic Cell Separation System	480019, BioLegend
Autoclave systec DX-45	Systec
Autoclave systec V-75	Systec
Balance KERN PFB	Kern und Sohn
BD FACSCANTO™ II	BD

Centrifuge Eppendorf 5415C	Eppendorf
Centrifuge Eppendorf 5424	Eppendorf
Cell counting chamber (Neubauer)	ZK03 Hartenstein
X-ray irradiation source	CP-160 Faxitron
ABI Prism Genetic Analyzer	Applied Biosciences
Centrifuge Rotina 420R	Hettich Laborapparate
Freezer -20 °C	Liebherr, Privileg
Freezer -70 °C	Siemens
Refrigerator 4 °C	Liebherr, Privileg
Gel electrophoresis system Mini-PROTEAN System	Biorad
Heating Block Liebisch 2099-DA	Liebisch
Ice machine Scotsmen AF100	Genheimer
37°C CO_2 Incubator	Thermo Fisher Scientific
Light microscope LEICA DMIL	Leica
Magnetic stirrer	Heidolph
Microliter pipettes	Brand
Microplate reader Fluostar Omega	BMG Labtech
Orbital shaker KS10 DIGI	Edmund Bühler
pH meter	WTW
Photometer nanodrop	PeqLab
Powerpack 2009	Biorad
Laminar hood	Heraeus
Vortexer Reamix 2789	Hartenstein Laborversand
Nucleofector 4D	Lonza
Nucleofector IIb/2b	Lonza
Water bath RM6 Lauda	Hartenstein
ABI Prism 770 light cycler	Roche
IVIS Spectrum Imaging system	Caliper Life Sciences
Muse® Cell Analyzer	Luminex Corp.

8.1.4 Solution and Buffers

Name	**Composition/Source**
Blotting buffer	0.025 M Tris 0.192 M Glycine 20% (v/v) methanol, pH 8,3
D-Luciferin	5 g D-luciferin 165 ml water for injection
Erythrocyte lysis buffer	89.9 g NH4Cl 10 g KHCO3 0.37 g EDTA in 1 L deionized water
Laemmly Buffer (SDS-Page, 4x)	8% (w/v) SDS 10% β- mercaptoethanol 40% Glycerol 0.2 M Tris 0.04% Bromophenol blue
LB	Roth
LB Agar	2g LB 1.3% (w/v) Agar Agar in deionized water
Phosphate Buffered Saline (PBS)	0.02 M Natrium-Phosphat 0.7% (w/v) Sodium chloride pH 7.2

	Institut für Virologie und Immunbiologie, Universität Würzburg
T cell isolation buffer or FACS buffer	0.1% BSA in PBS
	Institut für Virologie und Immunbiologie, Universität Würzburg
BSS/BSA	Institut für Virologie und Immunbiologie, Universität Würzburg
Running gel buffer (SDS-PAGE)	1,5 M Tris 0,015 M SDS pH 8,8
Stacking gel buffer (SDS-PAGE)	0,5 M Tris 0,015 M SDS pH 6,8
TBS (Tris buffered saline)	0,02 M Tris 8% (w/v) Sodium chloride pH 7,6
TBST	1 x TBS 0.05% (v/v) Tween-20
TBST in Milk	5% (w/v) milk powder in TBST
XF Calibrant solution	Agilent/Seahorse Bioscience
Nuclease-free H_2O	Thermo Fisher Scientific

8.1.5 Plasmids

Name	Cat. No.	Source/Reference
FgH1tUTG-BFP	Modified from Addgene #70183	Marco Harold[112]/Ingolf Berberich
FgH1tUTG-CFP	Modified from Addgene #70183	Marco Harold[112]/Ingolf Berberich
VSV-G	Addgene #12259	Ingolf Berberich
pMDL		Ingolf Berberich
pRSV-Rev		Ingolf Berberich
FUCas9mcherry	Addgene #70182	Marco Harold[112]/Ingolf Berberich
HA-NFATc2		AG FBS[113]
Flag-IRF4		AG FBS
SB100x MC		AG Hudececk
CD19-CAR MC		AG Hudececk

8.1.6 gRNA cloning primer sequences

Name	Sequence 5‘ to 3‘	Target domain	Target exon
m*Nfatc1*_1.f	TCCCCCAGAGTGCTATCGGTGGTC	NHR	3
m*Nfatc1*_1.r	AAACGACCACCGATAGCACTCTGG	NHR	3
m*Nfatc1*_2.f	TCCCCACAGCCCCTCCGTAACTGG	NHR	3
m*Nfatc1*_2.r	AAACCCAGTTACGGAGGGGCTGTG	NHR	3
m*Nfatc1*_3.f	TCCCTACCCGGGGTGGACGTCTGG	NHR	3
m*Nfatc1*_3.r	AAACCCAGACGTCCACCCCGGGTA	NHR	3
m*Nfatc2*_1.f	TCCCGCTGACATCGAGCTGCGGAA	RSD	6
m*Nfatc2*_1.r	AAACTTCCGCAGCTCGATGTCAGC	RSD	6
m*Nfatc2*_2.f	TCCCGAACTTCACAGCGGAGTCCA	RSD	7
m*Nfatc2*_2.r	AAACTGGACTCCGCTGTGAAGTTC	RSD	7
m*Nfatc2*_3.f	TCCCGGACGTGCACGCGGAACACC	RSD	6
m*Nfatc2*_3.r	AAACGGTGTTCCGCGTGCACGTCC	RSD	6
ins_det_pri_FgH1t.f	AACGGATCGGCACTGCGT		
NFAT_Seq.f	TGTCGCTATGTGTTCTGGGA		
NFAT_Seq.r	TTAATTAAGGGTGCAGCGGC		

8.1.7 crRNA sequences

Table 1. **Designed crRNA sequences for CRISPR/Cas9 in primary mouse and human T cells**

Name	Sequence (5' to 3')	Target domain	Target exon
m*Nfatc1*_1	CCAGAGTGCTATCGGTGGTC	NHR	3
m*Nfatc1*_2	CACAGCCCCTCCGTAACTGG	NHR	3
m*Nfatc1*_3	TACCCGGGGTGGACGTCTGG	NHR	3
m*Nfatc1*_4	CCGTCTCATAGTGAGCCCTG	RSD	4
m*Nfatc1*_5	GATGCCATACCTGCACAATG	RSD	4
m*Nfatc1*_7	GTGACCGAAGATACCTGGCT	NHR	3
m*Nfatc1*_8	AGGAACAGCTGAGATACCCG	NHR	3
m*Nfatc1*_9	TTCGGTCACACTGACCCGAG	NHR	3
m*Nfatc2*_1	GAAGATCGTAGGCAACACCA	RSD	6
m*Nfatc2*_2	CCGCCACATCTACCCTACTG	NHR	3
m*Nfatc2*_3	CCACAGTAGGGTAGATGTGG	NHR	3
m*Cd8a*_1	ATCCCACAACAAGATAACGT		
m*Cd8a*_2	TGGGTGAGTCGATTATCCTG		
m*Cd8a*_3	TGAAGCCATATAGACAACGA		
m*Pd1*_1	ACAGCCCAAGTGAATGACCA		
m*Pd1*_2	TGAATGACCAGGGTACCTGC		
*mPd1*_3	AGTTGAGCTGGCAATCAGGG		
m*Cd4*_1	ACTCCTAGCTGTCACTCAA		
m*Cd4*_2	AAGGGAAGACGCTGGTGCT		
m*Cd4*_3	TAAGTTTATTGATGATGAG		
m*Cd90*_1	ATGGCGGCAGTCCAGGCGA		
m*Cd90*_2	CCTTGGTGTTATTCTCATGG		
m*Cd90*_3	GAGCAGGAGAGCGACGCTGA		
m*Irf4*_1	CCGCATCCCGTGGAAACACG		
m*Irf4*_2	CGCATCCCGTGGAAACACGC		
m*Irf4*_3	ACGCGTCATGAACTTGGAGA		
h*NFATC1*_gRNA_1	GCACACTGCTGGGTTCCCCG	NHR	3
h*NFATC1*_gRNA_2	CTTCTGCGACCAGTACCTGG	NHR	3
h*NFATC1*_gRNA_3	CCGTCTCGTAGTGGGCTCGG	RSD	4
h*NFATC2*_gRNA_1	CTAGCGGGGCTCAAGCAAAG	NHR	3
h*NFATC2*_gRNA_2	AAGTCCATACCTGAACCACA	RSD	4
h*NFATC2*_gRNA_3	TCCATACCTGAACCACAGGG	RSD	4
h*CXCR4*_gRNA_1	GAAGCGTGATGACAAAGAGG		
h*CXCR4*_gRNA_2	AGGGAAGCGTGATGACAAAG		
h*CXCR4*_gRNA_3	ACGGCATCAACTGCCCAGAA		

8.1.8 Primers for quantitative RT-PCR

Name	Sequence
Nfatc1 P1 product	5' GGGAGCGGAGAAACTTTGC 3' and 5' CAGGGTCGAGGTGACACTAGG 3'
Nfatc1 P2 product	5' GACCCGGAGTTCGACTTCGA and 5' CAGGGTCGAGGTGACACTAGG 3'
Nfatc2 product	5' GTCCCGGAGCCGCAGCCCGA and 5' AATCGAAGAGGATGGAAAAG 3'
Actb	5' GACGGCCAGGTCATCACTATTG and 5' AGGAAGGCTGGAAAAGAGCC 3'

8.1.9 Primers for indel detection

Gene	Primer sequence
Nfatc1	5' TGGCAAGCTATGACCACACA and 5' TTCATGAAGGACTCACTGGGACA 3'
Nfatc2	5' AGCATCCGTTTTAGAGGAGG and 5' GAAGGCTCTCTGATGCTGACA 3'

8.1.10 Human Materials

Human blood was collected from anonymous donors in the *Institut für Klinische Transfusionsmedizin und Hämotherapie*, UK Würzburg.

8.1.11 Mice

BALB/cAnNRj recipients for HCT experiments were purchased from Janvier Laboratories (France). All donor and recipient mice were sex- and age-matched for HCT experiments. The transgenic mice mentioned below were bred and kept in the "Zentrum für Experimentelle Molekulare Medizin" (ZEMM) in Wuerzburg. At the age of 4 weeks, the mice were genotyped. Animals of at least 6 weeks of age were used for the experiments. The HCT study was reviewed and approved by the Government of Lower Frankonia (Regierung von Unterfranken/55.2.2-2532-2-592).

Transgenic lines	**References**
Cd4cre.*Nfatc1*$^{fl/fl}$	63
Rag1$^{-/-}$	63
Rosa26-floxed STOP-*Cas9*	114
Cd4cre	115
L2G85.CD90.1	66
B6.*Cas9*.*Cd4cre*.*luc*.CD90.1 (H-2b CD90.1^{+})	This study[68]
Nfatc1^{caaA}	116
dLckcre	117

8.1.12 Cell lines

Name	**Source**
HEK 293T (Human Embryonic Kidney)	AG FBS
EL4 (Mouse T cell Lymphoma)	AG FBS
WEHI-231 (Mouse B cell Lymphoma)	AG FBS
MV4-11 luc^{+}	AG Hudececk
MOLM-13 luc^{+}	AG Hudececk
RPMI 8226 luc^{+}	AG Hudececk
TM-LCL	AG Hudececk

K562 luc$^+$	AG Hudececk
K562-CD19 luc$^+$	AG Hudececk
Raji luc$^+$	AG Hudececk

8.1.13 Chemicals, reagents, and kits

Name	Cat. No.	Source
T4 PNK	M0201S	NEB
T4 Ligase	M0202T	NEB
ATP	P0756S	NEB
BSA	B9000S	NEB
Esp3I	R0734S	NEB
DH5α Competent Cells	18263-012	Invitrogen
GenElute™ HP Plasmid Maxiprep Kit	NA0310	Sigma-Aldrich
PCR Master Mix (2X)	K0171	Thermo Fisher Scientific
Midori Green Advance	MG04	Nippon Genetics
Generuler 1Kb plus	SM1331	Thermo Fisher Scientific
Hi-Di™ Formamide	4311320	Applied Biosystems
GenJet™ Plus In Vitro Transfection Reagent	SL100499	SignaGen Laboratories
Lenti- X™ Concentrator	631231	Takara Bio
Polybrene	TR-1003-G	Sigma-Aldrich
Doxycycline	D9891-1G	Sigma-Aldrich
Interleukin-7	200-07	Peprotech
MojoSort™ mouse CD3 T Cell Isolation Kit	480024	BioLegend
MojoSort™ mouse CD4 T Cell Isolation Kit	480006	BioLegend
MojoSort™ mouse CD8 T Cell Isolation Kit	480008	BioLegend
TrueCut™ Cas9 Protein v2	A36499	Invitrogen
Human Interleukin-2	200-02	Peprotech
Ingenio Electroporation Solution	MIR 50112	Mirus
P4 Primary Cell 4D-Nucleofector™ X Kit S	V4XP-4032	Lonza
Alt-R CRISPR-Cas9 crRNA		IDT
Alt-R CRISPR-Cas9 tracrRNA	1072533	IDT
Dulbecco's PBS	D8537-500ML	Sigma Aldrich
D-luciferin firefly, potassium salt	L-8220	Biosynth
Ficoll-Paque	17-1440-02	GE Healthcare
MojoSort™ Human CD3 T Cell Isolation Kit	480022	BioLegend
MojoSort™ Human CD8 T Cell Isolation Kit	480012	BioLegend
TrueCut™ Cas9 Protein v2	A36499	Invitrogen
Alt-R Sp Cas9 Nuclease V3	1081059	IDT
P2 Primary Cell 4D-Nucleofector™ X Kit S	V4XP-2032	Lonza
P3 Primary Cell 4D-Nucleofector™ X Kit S	V4XP-3032	Lonza
Beetle-Juice Luciferase Assay Firefly	102510	PJK GmbH
Dynabeads Human T-Activator CD3/CD28	11131D	Thermo Fisher Scientific
Anti-biotin microbeads	130-090-485	Miltenyi Biotec
Recombinant Cas9	CP02	PNA Bio
Luciferin for cytotoxic assay		AG Hedececk, UK Würzburg
Trizol	15596026	Thermo Fisher Scientific
iScript II cDNA synthesis kit	1708891	Bio-rad
PMA	57716-89-9	Sigma
Ionomycin	56092-81-0	Merck Biosciences
Zombie Aqua™ Fixable Viability Kit	423101	Biolegend

Zombie NIR™ Fixable Viability Kit	423105	Biolegend
GolgiStop	554724	BD Biosciences
GolgiPlug	555029	BD Biosciences
Brefeldin	00-4506-51	eBioscience
Monensin	00-4505-51	eBioscience
IC Fixation Buffer kit	00-8222-49	eBioscience
Foxp3/Transcription Factor staining kit	00-5523-00	eBioscience
Omega E.Z.N.A DNA/RNA Isolation kit	R6731-01	Omega Bio-tek
TA cloning vector kit	A1360	Promega
Glucose		Agilent/Seahorse Bioscience
Oligomycin		Sigma Aldrich
2-deoxyglucose (2DG)		Sigma Aldrich
Trifluoromethoxy carbonylcyanide phenylhydrazone (FCCP)		Sigma Aldrich
antimycin A		Sigma Aldrich
Rotenone		Sigma Aldrich
$NaHCO_3$		Sigma Aldrich
DEAE Dextran	9013-34-7	Roth
NTC Nontargeting crRNA	1072544	IDT
NE-PER™ Nuclear and Cytoplasmic Extraction Reagents	78833	Thermo Fisher Scientific

8.1.14 Antibodies

Name	**Cat. No./Clone**	**Source**
Anti-mouse-CD3	BE0001/1	Bio-X-Cell
Anti-mouse-CD28	BE0015/1	Bio-X-Cell
Ultra-LEAF™ Purified anti-human CD3	OKT3/317326	Biolegend
Ultra-LEAF™ Purified anti-human CD28	CD28.2/302934	Biolegend
EGFRt biotin antibody		AG Hudececk, UK Würzburg
Anti-FcgRII/FcgRIII	2.4G2	BD Pharmingen
Anti-mouse-CD4-FITC	RM4-5	Biolegend
Anti-mouse-CD8α-FITC	53-6.7	Biolegend
Anti-mouse-CD90.1-FITC	OX-7	Biolegend
Anti-mouse/human-CD44-PECy7	IM7	Biolegend
Anti-mouse-α4β7-PE	LPAM-1, DATK32	Biolegend
Anti-mouse-CD4-PE	RM4-5	Biolegend
Anti-mouse-CD8α-PE	53-6.7	Biolegend
Anti-mouse-CD62L-PE	MEL-14	Biolegend
Anti-mouse/human-CD44-PE	IM7	Biolegend
Anti-mouse-CD25-PE	PC61	Biolegend
Anti-mouse-CD90.1-APC	OX-7	Biolegend
Anti-mouse-FoxP3-APC	FJK-16s	eBiosience
Anti-mouse/human-NFATc1-PE	7A6	Biolegend
Anti-mouse/human-NFATc2-FITC	611960	BD Biosciences
Anti-mouse/human-IRF4-Pacific Blue	3E4	Biolegend
Anti-mouse/human-IRF4-APC	3E4	Biolegend
Anti-mouse-IFN-γ-APC	XMG1.2	Biolegend
Anti-mouse-TNF-α-FITC	MP6-XT22	Biolegend
Anti-mouse-IL-2-PE	JES6-5H4	Biolegend
Anti-human-CD3-APC	HIT3a	Biolegend
Anti-human-CD4-BV510	OKT4	Biolegend

Anti-human-CD4-APC	RPA-T4	Biolegend
Anti-human-CD8α-PerCP	HIT8a	Biolegend
Anti-human-CD25-PE/Cy7	BC96	Biolegend
Anti-human-IL-2-PE	MQ1-17H12	Biolegend
Anti-human-IFN-γ-FITC	4S.B3	Biolegend
Anti-human-TNF-α-APC	Mab11	Biolegend
Anti-human-CD40L-Pacific blue	24-31	Biolegend
Anti-human-GranzymeB-Pacific blue	GB11	Biolegend
Anti-human-Perforin-PE-Cy7	B-D48	Biolegend
Anti-human-CCR7-PE	G043H7	Biolegend
Anti-human-CD45RA-APC	HI100	Biolegend
Anti-human-CD45RO-FITC	UCHL1	Biolegend
Anti-human-Egfrt-Alexa-fluor-647		AG Hudececk
Anti-human-CXCR4-APC	12G5	Biolegend
Anti-human-CD107a	H4A3	Biolegend
Mouse-IgG1,κ-isotype control-PE	MOPC-21	Biolegend
Anti-human-FoxP3-PE	206D	Biolegend
Anti-human-CD25-FITC	BC96	Biolegend
Rabbit anti-NFATc1/aA	IG-457	ImmunoGlobe
Goat anti-IRF4	sc-6059	Santa Cruz biotechnology
Mouse anti-β-actin	C-4	Santa Cruz biotechnology
Anti-mouse/human NFATc2	0112-02	immunoGlobe
Anti-mouse/human NFATc1	7A6	BD Biosciences
Goat anti-mouse IgG HRP	A2304	Invitrogen
Goat anti-rabbit IgG HRP		Invitrogen

8.1.15 Anaesthesia and antibiotics

Name	**Source**
Ketamine hydrochloride	Pfizer
Xylavet (20 mg/ml)	CP-pharma
Baytril	Bayer
Ampicillin	Sigma-Aldrich

Anesthesia was prepared as follows: 2 ml of Ketamine hydrochloride and 2 ml of Xylavet were added to 21 ml DPBS. 10 µl per g body weight were injected i.p. (end concentration Ketamin 80 mg/kg, Xylazin 16 mg/kg).

8.1.16 Cell Culture Media composition

T-cell media for mouse or human $CD3^+$ T cells:

RPMI-Medium, supplemented with 10% FCS (v/v), 2 mM L-Glutamine, 1X NEAA, 1 mM Sodium Pyruvate, 100 U/ml Penicillin/Streptomycin and 55 µM β-Mercaptoethanol.

Media for HEK-293T cells:

DMEM-Medium, supplemented with 10% FCS (v/v), 2 mM L-Glutamine, 1 mM Sodium Pyruvate, 100 U/ml Penicillin/Streptomycin.

CTL Media for human CAR T cells:

RPMI-Medium, supplemented with 10% Human Serum (v/v), 2 mM L-Glutamine, 100 U/ml Penicillin/Streptomycin, and 55 µM β-Mercaptoethanol.

Media for TMLCL/Raji/K562/MV4-11/RPMI 8226/MOLM-13/EL4/WEHI-231 cells:

RPMI-Medium, supplemented with 10% FCS (v/v), 2 mM L-Glutamine, 100 U/ml Penicillin/Streptomycin.

Media for MST:

XF Base Medium, 2 mM sodium pyruvate, 10 mM Glucose, 2 mM L- Glutamine, pH 7.4 +/- 0.05.

Media for GST:

DMEM, 2 mM L- Glutamine, pH 7.35 +/- 0.05.

8.1.17 Software and tools

Name	**Source**
Living Image 4.0	Caliper Life Sciences
FlowJo	Tree Star
Tracking of Indels by Decomposition (TIDE)	https://tide.nki.nl/
Deskgen	https://www.deskgen.com/landing/cloud.html
CHOPCHOP	http://chopchop.cbu.uib.no/
CrispRGold 1.1	https://crisprgold.mdc-berlin.de/
BD FACSDiva 5.0	BD
GraphPad Prism 5	Graphpad
CorelDRAW	Corel
XF Wave software	Agilent/ Seahorse Biosciences
Microsoft office	Microsoft

8.2 Methods

8.2.1 Molecular Biology techniques

8.2.1.1 Lentivirus mediated gRNA delivery

Guide RNA oligos were designed using CrispRGold 1.1 online tool. Standard vector (lentiCRISPRv2) was chosen as a cloning vector (for ready-to-order oligos set up). The top three gRNAs were chosen, forward and reverse primer sequences were obtained and oligos were ordered from Thermo Fisher Scientific.

8.2.1.2 Cloning of gRNA in FgH1tUTG plasmid

Phosphate group addition to oligo

Phosphate group was added to 5' end of each oligos using the following protocol:

gRNA oligo forward	2 µl of 100 µM stock
gRNA oligo reverse	2 µl of 100 µM stock
10X PNK Buffer	2 µl
10mM ATP	2 µl
T4 PNK	1 µl
H_2O	11 µl (up to 20 µl total volume)

To anneal the oligos, 20 µl of the above mix was incubated in a PCR machine with the following settings:

37℃	30 minutes (mins)
95℃	5 mins
RT	Until cool

The mixture was then diluted at 1:10 to a concentration of 1 µM with H_2O.

Ligation of oligos to FgH1tUTG plasmid:

FgH1tUTG BFP/CFP	1 µl (100 ng)
1 µM hybridized oligos	1 µl
10X Ligase Buffer	5 µl
Esp3I	2 µl
10 µM ATP	5 µl
20 mg/ml BSA	0.25 µl
T4 Ligase	1 µl
H_2O	34.75 µl (Up to 50 µl total volume)

Incubated in a PCR machine with the following settings:

37℃	5 mins
20℃	5 mins
20 cycles (Step 1-2)	
80℃	20 mins
4℃	∞

The ligated mix was stored at -20℃ until further use.

Transformation

Transformation was performed using DH5α competent cells according to the manufacturer's protocol. Briefly, 2 µl of ligation mix was added to 40 µl thawed competent cells and incubated on ice for 30 mins. Heat shock was given to the cells at 42℃ for 45 secs and cells were incubated on ice for 5 mins. SOC media (360 µl) was added to the transformed cells and incubated at 37℃ in a 225 rpm shaker for 60 mins. Cell suspension (200 µl) was plated on LB+Ampicillin plates and incubated at 37℃ overnight. The next day plates were examined for the presence of colonies.

Plasmid DNA isolation

Distinct colonies were picked and inoculated into 3 ml LB+Ampicillin medium for miniprep or into 150 ml LB+Ampicillin medium for maxiprep. The cultures were maintained for 12-16 hours (h) at 37°C on a 225 rpm shaker incubator. Then the DNA was extracted from the bacteria using the GenElute plasmid isolation kit according to the manufacturer's protocol. DNA concentration was measured using Nanodrop.

PCR confirmation of clones

Plasmid DNA was amplified with the following PCR conditions using a forward primer specific for FgH1tUTG and a reverse primer binding individual gRNA.

Plasmid DNA 100 ng	1 µl
PCR Mastermix	20 µl
Forward primer (100 µM stock)	0.2 µl
Reverse primer (100 µM stock)	0.2 µl
H_2O	8.6 µl (Up to 20 µl total volume)

Settings in PCR machine:

95℃	3 mins
95℃	30 secs
53℃	30 secs
72℃	30 secs
25 cycles (Step 2-4)	
72℃	10 mins
4℃	∞

The PCR product was run in 2% Agarose Gel with 2 µl Midori dye in parallel with the 1 Kb ladder. Positive clones gave a product size of 500 bp.

Sanger sequencing confirmation of clones

Positive clones were confirmed by Sanger sequencing in a mix prepared for each sample as follows:

Plasmid DNA 300-400 ng	1 µl
Sequencing Mastermix	4 µl
Primer (10-20 ng)	1 µl
H_2O	4 µl (Up to 10 µl total volume)

PCR program:

96℃	3 mins
94℃	25 secs
55℃	15 secs
60℃	3 mins
50 cycles (Step 2-4)	
8℃	∞

The PCR product (10 µl) was mixed with 10 µl H_2O and purified by centrifuging at 4000 rpm in the Sepharose column for 2 mins. To the purified PCR product 15 µl HiDi was added and sequenced in a Sanger sequencing machine.

8.2.1.3 Quantitative RT-PCR

RNA was extracted from cultured cells using Trizol followed by cDNA synthesis with the iScript II kit following the manufacturer's instructions. Quantitative RT-PCR was performed with an ABI Prism 770 light cycler with the appropriate primer pairs (Section 8.1.8).

8.2.1.4 Indel Detection

Genomic DNA was extracted from cultured cells using Omega E.Z.N.A DNA/RNA Isolation kit. PCR (initial denaturation 95°C, 3 min, denaturation 95°C, 15 sec, annealing 55°C, 30 sec, elongation 72°C, 2 min, 40 cycles, final elongation 72°C, 10 min) was performed to amplify gRNA target regions using specific forward and reverse primer. The amplified product was gel-purified and cloned in a TA-cloning vector kit and transformed in DH5α E.coli competent cells. Colonies were individually grown in LB media and plasmid DNA was isolated. The presence of insert was confirmed by PCR using indel detection primers (Section 8.1.9). Clones were sequenced by Sanger sequencing using Hi-Di and ABI Prism Genetic Analyzer from Applied Biosystems. For performing 'Tracking of Indels by Decomposition' (TIDE), amplified target regions were gel-purified and sequenced by Sanger sequencing. Sequencing files were uploaded to TIDE DESKGEN website along with the gRNA sequences and analysed using the TIDE tool.

8.2.1.5 crRNA design and gRNA assembly for non-viral genome editing

crRNAs were selected using DESKGEN or CHOPCHOP (*Irf4*) online platform. The target area was limited to the first ~40% of the coding sequence. From guides targeting common exons between isoforms with 40-80% GC-content, the ones with the highest on-target as well as off-target scores were selected. crRNAs were ordered from Integrated DNA Technologies in their proprietary Alt-R format. crRNA and Alt-R CRISPR/Cas9 tracrRNA were mixed in equimolar concentration (10 µl each) in nuclease-free PCR tubes, heated at 95°C for 5 mins, and then cooled to anneal at RT for 10 mins. This resulted in gRNA of concentration around 50 pmol/µl.

8.2.2 Cell Culture and Nucleofection

Cells were cultured at 37°C and 5% CO_2 incubator.

8.2.2.1 Lentivirus production and transduction of cells

Transfection:

For transfection $2x10^6$ HEK 293T cells were seeded in a 6 cm dish and cultured at 37℃ overnight until 80% confluent. Media was changed to fresh culture media 1 h before transfection. DNA (DMEM+ 1 µg pMDL+ 1 µg pRSV-Rev+ 1 µg VSV-G+ 5 µg plasmid up to 250 µl total volume) and Transfection reagent (DMEM+ 17.5 µl GenJet up to 250 µl total volume) were mixed, vortexed and incubated at RT for 10 mins. The mix was added to the cells carefully and dropwise, the plate was swirled and transferred into a 37℃ incubator. The next morning the media was changed to fresh media. The virus was collected 48 and 72 h post-transfection.

Transduction:

The virus was concentrated using Lenti-X concentrator according to the manufacturer's instruction and stored at -70℃ until further use. EL4 or WEHI-231 cells ($1x10^6$) were resuspended in a 15 ml tube with 1 ml of culture media containing virus with 1 µl Polybrene and centrifuged at 2200 rpm and 32℃ for 2.5 h. The supernatant was discarded and the cells were resuspended in 2 ml of fresh culture media and seeded in a 12-well plate. The next day, media was changed and the cells were cultured for a further 72 h.

Mouse $CD3^+$ T cells were pre-stimulated with 5 µg/ml plate-bound anti-CD3, 1 µg/ml anti-CD28 with 10 ng/ml IL-2 for 72 h and transduced like the cell lines.

Doxycycline treatment:

For gRNA induction, cells were treated with 1 µg/ml Doxycycline for 72 h. Knockout efficiency was checked using flow cytometry.

8.2.2.2 BM and T-cell isolation

BM cells were isolated by flushing femur and tibia bones of *Rag1*$^{-/-}$ mice with PBS containing 0.1% BSA and passed through a 70 µm cell strainer. Spleens and lymph nodes (LN) were passed through a 70 µm cell strainer, washed with PBS containing 0.1% BSA, and enriched with Mojosort Mouse CD3 T cell negative isolation kit according to the manufacturer's instructions. $CD4^+$ or $CD8^+$ T cells were isolated using a Mojosort negative isolation kit according to the manufacturer's instructions.

8.2.2.3 Mouse T-cell culture and stimulation

Purified T cells were cultured in T-cell media. T cells were stimulated with plate-bound 5 µg/ml anti-CD3, and soluble 1 µg/ml anti-CD28 and 10 ng/ml IL-2 for 72 h in 1 million cells per ml density. Naïve $CD3^+$ T cells were either cultured with 5 ng/ml IL-7 overnight before nucleofection or immediately nucleofected after purification.

8.2.2.4 Mouse T-cell nucleofection

T-cell culture media was pre-warmed in a 37°C incubator. T cells ($2.5x10^6$) were washed with Ca/Mg-free PBS to remove traces of FBS and resuspended in 100 µl of Ingenio Electroporation Solution. Cells were added on 3 µl (150 pmol) crRNA-tracrRNA duplex (gRNA) in a nuclease-free tube, mixed gently by pipetting, and incubated at RT for 2 min. When targeting two genes, 2 µl (100 pmol) of each gRNA was used. The cell-gRNA mix was then transferred into a cuvette and nucleofection was performed using Lonza Nucleofector™ IIb and X-001 pre-set program or using Lonza Nucleofector 4D and CM-137 (for stimulated cells) or DS137 (for naïve T cells). For the Nucleofector 4D, cells were nucleofected in 20 µl of P4 buffer (Lonza) or Ingenio electroporation solution. Post nucleofection, pre-warmed T-cell media was added to the cells slowly and cells were carefully transferred to a 12-well (IIb) or 96-well (4D) plate. Cells were incubated in the CO_2 incubator up to 3 d before allo-HCT into BALB/c mice.

8.2.2.5 Human T-cell isolation and stimulation

The human blood was collected in a 50 ml tube and mixed with PBS in a 1:1 ratio. One volume of Ficoll-Paque was taken in a 50 ml tube and overlaid carefully with the blood-and-PBS

mixture. The tube was centrifuged at 1600 rpm for 35 minutes at room temperature without brake or acceleration. After centrifugation, the plasma was removed and the buffy coat, containing the PBMCs was transferred into a fresh 50 ml tube. The PBMCs were resuspended in 50 ml cold PBS and washed at 1500 rpm for 5 minutes at 4°C. The supernatant was discarded and the washing step was repeated once. Subsequently, the pellet was resuspended and the number of PBMCs was determined using a hemocytometer.

$CD3^+$ or $CD8^+$ T cell isolation was performed through a negative selection, using the Mojosort human CD3 or CD8 T cell isolation kit and the Magnetic Cell Separation System, following the manufacturer's instructions. During the isolation, the T cells were kept in FACS buffer. The number of purified T cells was determined using a hemocytometer. Purity was checked by flow cytometry.

Unstimulated human T cells were cultured in T-cell media with 10 IU IL-2 (equivalent to 10ng/ml) at a density of $5x10^6$ cells per ml overnight at 37°C before nucleofection. For stimulation, plates are coated with 2.5 µg/ml human anti-CD3 in PBS for 2 h at 37°C. Plates were washed three times with PBS and cells were cultured in T-cell media containing 10 IU IL-2 and 1 µg/ml human anti-CD28 at a density of $1x10^6$ cells per ml. Cells were stimulated for 3 d before nucleofection.

8.2.2.6 RNP complex formation

Annealed gRNA (crRNA-tracrRNA), 3 µl (~150 pmol) of each was mixed with 2 µl (~60 pmol or 10 µg) of recombinant Cas9 in RNase-free tubes to obtain 5 µl of RNP at 3:1 gRNA:Cas9 ratio and incubated at RT for 10 mins to ensure RNP complex formation. For nucleofection in mouse or human T cells, 3 'gene-specific' RNPs (prepared using 3 different guides per gene) were mixed (3 µl each) and kept on ice until nucleofection. When only one gRNA was used to target a gene or for the NTC group, 5 µl of RNP was used for nucleofection. RNPs were always prepared fresh before nucleofection.

8.2.2.7 Nucleofection of human T cells

Human stimulated or unstimulated $CD3^+$ or $CD8^+$ T cells were counted and the required number of T cells was harvested in a 50 ml tube, washed with PBS at 1400 rpm at 4°C for 5 mins. P2 or P3 complete nucleofection solution was prepared according to manufacturer's instruction by combining 16.4 µl of Nucleofector solution with 3.6 µl Supplement. Cells

($2.5x10^6$) were resuspended in 20 µl P2 or P3 nucleofection solution and immediately added to the RNP mix kept in an RNase-free tube. The mixture was incubated at RT for 2 mins and followed by transferring into nucleofection cuvettes. Cuvettes were transferred into the Nucleofector 4D and nucleofection programs EH-100 (for P2) or EO-115 (for P3) were applied. Pre-warmed 100 µl of T-cell media (with 10 ng/ml IL-2) was added to the cells immediately after nucleofection and cells were rested at 37°C for 10 mins before transferring into 96-well culture plates. To each well, an additional 100 µl T-cell media supplemented with IL-2 was added.

8.2.2.8 CAR T-cell generation with CRISPR/Cas9 knockout of NFAT

$CD8^+$ T cells were isolated from PBMCs using a negative selection kit and stimulated with Dynabeads Human T-Activator CD3/CD28 at a 1:1 ratio for 48 h in CTL media with 50 IU/ml IL-2 following the manufacturer's instructions. Cells were harvested and washed with PBS at 1400 rpm for 5 mins. Cells were resuspended in a P3 nucleofection buffer at a density of $1x10^8$ per ml. Using the program FI-115, $2x10^6$ cells were nucleofected in the Nucleofector 4D with 0.5 µg SB100X minicircle (MC), 0.5 µg CD19-CAR MC along with RNPs. NTC RNP (5 µl) was prepared combining 3 µl NTC gRNA (˜150 pmol) and 2 µl (˜60 pmol or 10µg) Cas9. For targeting one gene, a total of 7.5 µl RNP was used prepared with 1.5 µl of each of 3 gRNAs and 3 µl Cas9. For targeting two genes simultaneously, a total of 9 µl RNP was used prepared with 0.9 µl of each of the total 6 gRNAs (3 per gene) and 3.6 µl Cas9. Pre-warmed CTL media (100 µl) was immediately added to the cells and those rested at 37°C for 10 mins. Cells were transferred into 48-well plates and 0.9 ml pre-warmed CTL media was added. Media (0.8 ml) was removed from the top after 4 h and 25 µl washed Dynabeads Human T-Activator CD3/CD28 were added with 0.8 ml fresh CTL + 50 IU/ml IL-2 to each well. Cells were incubated for 5 d and subcultured 3 d later. Beads were removed from cells 5 d later, cells were cultured in CTL+50 IU/ml IL-2 media for another 8 d and EGFRt expression, and knockout efficiency was analysed.

CAR T cells were expanded by coculturing with irradiated TM-LCL (80 Gy, 12.8 mins) cells at a T cell to TM-LCL ratio of 1:7. The next day, cultures were supplemented with 50 IU/ml of IL-2, and cells were fed with fresh CTL + 50 IU/ml IL-2 every second day. The phenotype of the expanded CAR T cells was analysed on 7 d of expansion.

Before functional testing, EGFRt$^+$ T cells were enriched using biotin-conjugated anti-EGFR mAb and anti-biotin microbeads in LS columns following the manufacturer's instructions. The phenotype of the purified T cells was analysed the next day.

8.2.3 Allogeneic hematopoietic cell transplantation

BALB/c recipient mice (H-2^d CD90.2$^+$) were conditioned by myeloablative total body irradiation (TBI) at a dose of 8.0 Gy using a Faxitron CP-160 X-ray system. Two hours after irradiation, a retro-orbital injection was performed with sex- and age-matched 5×10^6 B6 BM cells from *Rag1*$^{-/-}$ mice (H-2^b CD90.2$^+$) with or without 2.5×10^6 stimulated or 0.6×10^6 naïve CRISPR/Cas9-edited T cells from B6.*Cas9*.*Cd4cre*.luc.CD90.1 (H-2^b CD90.1$^+$) mice into the irradiated BALB/c mice. Mice were given antibiotics (Baytril) for one week to avoid opportunistic infections. Transplanted mice were assessed daily for weight loss and clinical aGvHD score adapted from Cooke et al.[63, 67, 118]

Scoring criteria to determine aGvHD severity

To determine the GvHD severity in murine recipients, a clinical scoring system was used[118].

Table 2. **Assessment of Clinical GvHD in transplanted animals**

Criteria	**Grade 0**	**Grade 1**	**Grade 2**
Weight loss	<10%	>10% to <25%	>25% 2$^+$ point >30%
Posture	Normal	Hunching noted only at rest	Severe hunching impairs movement
Activity	Normal	Mild to moderately decreased	Stationary unless stimulated
Fur texture	Normal	Mild to moderate ruffling	Severe ruffling/poor grooming
Skin integrity	Normal	Scaling of paws/tail	Obvious areas of denuded skin
Eyes	Normal	Conjunctivitis one eye or slightly on both eyes	Severe conjunctivitis in both eyes
Licking/Scratching	Normal	<1x/min	>1x/min
Stool	Normal	Slight diarrhea	Severe diarrhea
Anemia	Normal	Reduced body temperature	Reduced body temperature, Pale skin on feet and tail
End point	**≥ 8 total score or 2$^+$ score for weight loss in 2 d consecutively**		

In vivo and *ex vivo* bioluminescence imaging

Mice were anesthetized by i.p. injection of 80 mg/kg body weight ketamine hydrochloride and 16 mg/kg xylazine. Together with anaesthesia, mice were injected with 150 mg/kg D-luciferin. After 10 min, BLI signals of the anesthetized mice were recorded using an IVIS Spectrum Imaging system. For *ex vivo* imaging of internal organs 6 d after allo-HCT, mice were injected with D-luciferin and sacrificed 10 min later. Internal organs were removed and subjected to BLI. All pictures were taken with a maximum of 5 min exposure time and analysed with the Living Image 4.0 software[63, 67].

8.2.4 Flow cytometry staining

Cells were washed once in FACS buffer and blocked with anti-FcgRII/FcgRIII. Cells were stained with Zombie Aqua™ Fixable Viability stain (0.1 µl per sample in 100 µl PBS) at RT for 15 mins. Cells were washed with 100 µl FACS buffer and surface staining was performed at RT for 15 mins. Intracellular staining of transcription factors were performed with respective fluorescent-conjugated antibodies and using the Foxp3-staining kit according to the manufacturer's instructions. Cytokine detection was performed after a 6 h *in vitro* restimulation with Phorbol myristate acetate (PMA; 30 nM) plus ionomycin (5 nM) in the presence of GolgiStop and GolgiPlug using the IC Fixation Buffer kit and respective fluorescent-conjugated antibodies. Data were acquired on a FACSCanto II flow cytometer and analysed with FlowJo software.

8.2.5 Metabolism study

Extracellular flux analysis was performed as previously described[119]. Briefly, 1 d prior to measurements, Seahorse XFe96 culture plates were coated with Corning™ Cell-Tak Cell and Tissue Adhesive with 0.1 M NaHCO3 according to the manufacturer's recommendations. A Seahorse XFe96 cartridge was loaded with XF Calibrant solution and incubated overnight at 37°C in a CO_2-free atmosphere. The next day, cells were harvested from the culture, washed in the assay-specific medium according to the manufacturer's recommendations, and viable cells were automatically counted on a Muse® Cell Analyzer. The cells were seeded at a density of $2.4x10^5$ T cells per well. The ports of the Seahorse cartridge were loaded with appropriate dilutions of the following compounds (final concentrations in brackets): glucose (10 mM), oligomycin (1 µM), and 2DG (100 mM) for the GST and oligomycin (1 µM), FCCP (1.5 µM), and antimycin A/rotenone (3 µM each) for the MST. After sensor calibration, assays were run as

detailed in the manufacturer's manual by recording ECAR (extracellular acidification rate) and OCR (oxygen consumption rate). Metabolic parameters were obtained from the XF Wave software and calculated using Microsoft Excel.

8.2.6 Luciferase reporter assay

EL4 cells were transiently transfected with an *Irf4* promoter luciferase-reporter construct. An 836 bp *Irf4* fragment, generated by PCR with *Irf4*-Pr_s 5' TTT GCT AGC CAT GAT TGA AAC TTT GGG G 3' and *Irf4*-Ex1-Nco_a 5' TTT CCA TGG TCC CAA GTT CAA GTG GTG 3', was cloned into pGL3 via NheI/NcoI restriction sites, thereby matching the translational start site of IRF4 with that of luciferase. Plasmids expressing constitutive active HA-NFATc2[113] or Flag-IRF4 were co-transfected by standard DEAE Dextran. 36 h post-transfection, luciferase activity was measured from the cells that were left untreated or treated with TPA (10 ng/ml), ionomycin (5 nM) overnight, and relative light units were corrected for the transfection efficacy based on total protein concentrations. Normalized mean values of at least 3 independent experiments are depicted in relative light units as fold activation over empty vector control.

8.2.7 Immunoblot

T cells of spleen and LNs were harvested from *Nfatc1*caaA mice[116] crossed to dLckcre[117] and activated by 2.5 µg/ml ConA. Whole-cell extracts were resolved by 10% SDS-PAGE followed by immunoblotting[120]. The primary antibodies used were rabbit anti-NFATc1/αA, goat anti-IRF4, and mouse anti-β-actin. Human T cells were harvested from culture, cytoplasmic and nuclear proteins were extracted by NE-PER™ Nuclear and Cytoplasmic Extraction Reagents according to the manufacturer's instruction. Extracts were resolved in 10% SDS-PAGE followed by immunoblotting with anti-NFATc1 7A6, anti-NFATc2, anti-human-β-Actin, anti-human-HDAC antibodies.

8.2.8 Cytotoxic assay of human T cells

T cells (Effector, E) and tumor cells (MV4-11, MOLM-13, and RPMI 8226) (Target, T) were harvested and washed with PBS at 1400 rpm, 4℃, 5 mins. Cells were seeded in a 96-well U-bottom plate in different E:T ratios. A total of 10,000 tumor cells were added per well (100 µl). Depending on the intended E:T ratio, different numbers of T cells were added to the tumor cells in 100 µl T-cell media. After 24 h, luciferase assay was performed using PJK luciferase assay kit according to manufacturer's instructions. Cells were washed with PBS, lysed and 50 µl of the lysate was taken in a white flat bottom plate and mixed with 50 µl of luciferin. Each

plate was incubated at RT for 5 mins and measured in a plate reader. The cytotoxic killing was measured according to the following formula.

$$Percentage\ Killing = \frac{100 \text{ x } (Luminescence\ of\ target\ alone - Luminescence\ of\ test)}{Luminescence\ of\ target\ alone}$$

8.2.9 Cytotoxic assay of CAR T cells

Purified CAR T cells (E) (in 100 µl CTL media) were seeded in a white flat bottom plate with 10^4 luc^+ tumor cells (T) (in 100 µl CTL media with 10 µl luciferin) in different E:T ratios. Luminescence was measured at different time points and the percentage of killing was measured using the following formula.

$$Percentage\ Killing = \frac{100 \text{ x } (Luminescence\ of\ target\ alone - Luminescence\ of\ test)}{Luminescence\ of\ target\ alone}$$

8.2.10 Statistical Analysis

Figures were prepared using GraphPad Prism 5 and Corel Draw software. Different groups were compared by Unpaired Student's t-test, Mann Whitney test, or ANOVA using GraphPad Prism 5 software. Differences with p values of less than 0.05 were considered significant: *p <0.05; **p<0.01, and ***p<0.001. Replicates, as indicated, are individual mice, donors, or experiments.

9 Results

9.1 Rapid and efficient NFAT ablation by CRISPR/Cas9 in primary mouse T cells to ameliorate aGvHD

The first objective of this study was to evaluate the proof of concept that, ablating NFAT by CRISPR/Cas9 in mouse T cells can ameliorate aGvHD similarly when transplanting NFAT-deficient T cells from *Cd4cre.Nfatc1*$^{fl/fl}$ or *Nfatc2*$^{-/-}$ mice, as demonstrated by our group earlier[63, 67]. To fulfill this aim, we intended to optimize a highly efficient CRISPR/Cas9-mediated gene editing strategy to knockout genes in primary mouse T cells. This method should be highly efficient and must result in gene-edited T cells suitable for transplantation in a major mismatch aGvHD mouse model. Using our optimized method, we examined aGvHD regression upon NFATc1 or/and NFATc2 depletion.

9.1.1 Lentiviral delivery of gRNA is inefficient in primary mouse T cells

To determine the ideal method of CRISPR/Cas9 gene editing in primary murine CD3$^+$ T cells, first, we wanted to transfer gRNA using lentiviral transduction in mouse T cells. We have used the lentiviral vector system (FgH1tUTG) consisting of a doxycycline (dox)-inducible gRNA-cassette and constitutively expressed tetracycline repressor (TetR) linked via the T2A peptide to GFP[112]. The GFP in this plasmid was replaced with either BFP or CFP to track the transfection of two 'gRNA-containing' plasmids simultaneously. Lentivirus was generated by transfecting HEK 293T cells with FgH1tUTG-BFP along with packaging mix resulting in transfection efficiency consistently above 90% when analysed by flow cytometry 3 d after transfection (Fig. 7A). Lentivirus transduction efficiency was compared between two mouse cell lines, i.e. mouse B-cell lymphoma WEHI-231 and mouse T-cell lymphoma EL4, as well as pre-stimulated primary mouse CD3$^+$ T cells. We could achieve 34.8% and 70.9% (Fig. 7B, C) transduction efficiency in EL4 cells and WEHI-231 cells, respectively. Primary mouse CD3$^+$ T cells were pre-stimulated with anti-CD3, anti-CD28, and IL-2 for 3 d before transduction with the FgH1t-BFP plasmid. However, we gained only 12.5% BFP$^+$ population in pre-stimulated murine CD3$^+$ T cells. (Fig. 7D). DEAE-Dextran addition did not improve the transduction efficiency compared to polybrene (data not shown), although some studies show DEAE-Dextran improves the transduction efficiency in murine and human lymphocytes[121, 122].

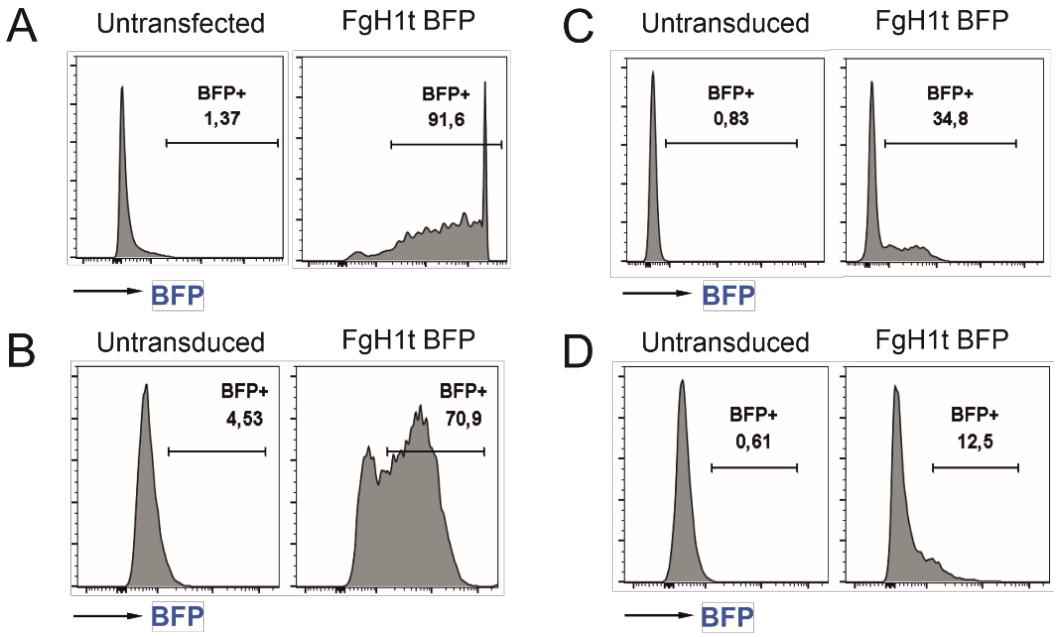

Figure 7. **Lentiviral transduction is inefficient in murine CD3⁺ T cells.**

BFP expression was measured by flow cytometry 3 d after **A.** transfection in HEK 293T cells with FgH1t-BFP plasmid and lentiviral packaging mix. **B.** FgH1t-BFP lentivirus transduction in EL4 cells. **C.** FgH1t-BFP lentivirus transduction in WEHI-231 cells. **D.** FgH1t-BFP lentivirus transduction in pre-stimulated (with 5 µg/ml plate-bound anti-CD3, 1 µg/ml soluble anti-CD28 +10 ng/ml IL-2 for 3 d) primary murine CD3⁺ T cells.

Next, 'gene-specific' gRNAs were designed by the CrispRGold tool and cloned into the FgH1t-BFP plasmid. EL4 cells were co-transduced with the lentivirus constitutively expressing FUCas9mcherry[112] as a source of Cas9 and gRNA-FgH1t-BFP plasmids. Cas9⁺mcherry and gRNA-FgH1t-BFP double-positive EL4 cells were purified by flow cytometry cell sorting with an efficiency of >90% (Fig. 8A). In Cas9⁺*Cd90* gRNA⁺ EL4 cells, 44% CD90-negative cells were detected upon dox treatment for 72 h (Fig. 8B). When *Cd40lg* or *Nfatc1* was targeted with specific gRNAs, there was a reduction in CD40L expression upon dox treatment as compared to Cas9-alone transduced cells (Fig. 8C, D). This suggested *Nfatc1* knockout-mediated downregulation in the expression of the NFAT target gene *Cd40lg* (Fig. 8D) since NFAT with its binding partner AP1 induces CD40L in T cells[123]. However, in Cas9⁺*Cd90* gRNA⁺ EL4 cells, 17% CD90-negative cells were detected before the treatment with dox, indicating leaky expression of *Cd90* gRNA probably due to less controlled tetR (Fig. 8B). Similar leaky expression of gRNA was also confirmed in Cas9⁺*Cd40lg* gRNA⁺ (Fig. 8C) and Cas9⁺*Nfatc1* gRNA⁺ EL4 cells (Fig. 8D). These experiments revealed that the use of a single gRNA per gene is moderately efficient, and the dox-inducible system is not tightly controlled in mouse cell lines. More importantly, lentiviral gene transfer is inefficient in primary mouse T cells.

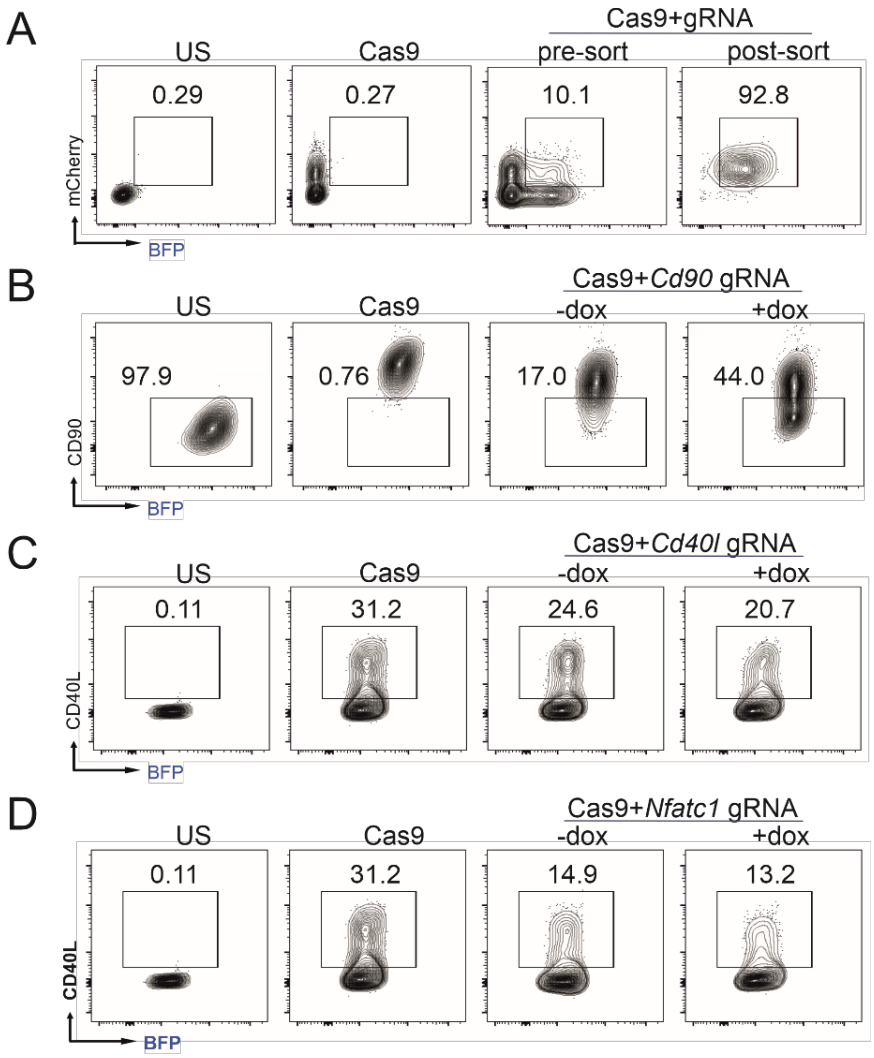

Figure 8. **Lentivirus mediated CRISPR/Cas9 knockout in EL4 cells.**

EL4 cells were transduced simultaneously with gRNA-FgH1tUTG-BFP and FuCas9mcherry lentivirus. **A.** Percentage of gRNA$^+$Cas9$^+$ double-positive cells, 72 h after transduction, pre-and post-flow cytometry cell sorting **B.** Sorted Cas9$^+$*Cd90* gRNA$^+$ double-positive EL4 cells were checked for CD90 knockout by flow cytometry after 72 h without and with 1 µg/ml dox treatment. **C.** Cas9$^+$*Cd40lg* gRNA$^+$ EL4 cells and **D.** Cas9$^+$*Nfatc1* gRNA$^+$ EL4 cells were treated with or without 1 µg/ml dox. CD40L expression was checked by flow cytometry after stimulating with 10 ng/ml TPA + 1 µg/ml ionomycin for 16 h.

9.1.2 Generation of *Cd4cre.*Cas9$^+$ transgenic mice for non-viral genome editing in mouse primary CD3$^+$ T cells

According to various studies and in our experience, viral genome editing methods require lengthy cloning processes of gRNA into plasmids, while viral transduction is inefficient in primary mouse T cells, requiring selection of transduced cells by antibiotic or flow cytometry cells sorting, and has the risk of immunogenicity as well as toxicity[124]. Additionally, one gRNA per gene is inefficient to completely lose gene expression, necessitating the administration of more than one gRNAs to achieve maximum knockout efficiency. To improve gene editing in 'hard-to-transfect' primary mouse CD3$^+$ T cells, we wanted to test non-viral genome editing methods. It has been previously shown that Cas9-expressing cells can be targeted by transduction using gRNA cloned in lentiviral or adeno-associated viral plasmids to ablate a gene of interest in mouse dendritic cells[125]. In pre-stimulated primary T cells, retroviral delivery of gRNA and Cas9 is only possible with suboptimal knockout efficiency[126]. A non-viral approach was recently demonstrated, where recombinant Cas9 protein-synthetic gRNA complexes (RNPs) were nucleofected into mouse primary T cells to achieve high knockout efficiency[91, 127]. However, it was not explored whether synthetic gRNAs can be directly nucleofected into Cas9$^+$ cells (gRNA-only nucleofection) which requires Cas9-gRNA complex formation inside the cell. To eliminate the need of using recombinant Cas9 protein, we utilized Cre-dependent Rosa26-floxed STOP-*Cas9* transgene knock-in mouse[114]. The transgene consists of *Streptococcus pyogenes* Cas9, linked to enhanced green fluorescent protein (EGFP) via P2A self-cleaving peptide to enable visualization of Cas9-expressing cells. We bred Rosa26-floxed STOP-*Cas9* to *Cd4cre*-expressing mice[115], which led to a deletion of the STOP cassette in CD4$^+$ and CD8$^+$ T cells (Fig. 9A). This mouse constitutively expresses Cas9 protein along with EGFP in all T cells which could be detected by flow cytometry in purified CD3$^+$ T cells (Fig. 9B). We also confirmed Cas9 protein expression in pre-stimulated CD3$^+$ T cells in western blot, using an antibody against 3xFLAG-tag, resulting in a ˜165KDa (Cas9 162KDa + 3x FLAG-tag 3kDa) band (Fig. 9C). This band could not be detected in CD19$^+$ B cells isolated from splenocytes of the same mice proving the specificity of CD4cre. For subsequent transfer studies, these mice were crossed to L2G85.*Cd90.1* transgenic mice, which express firefly luciferase and the CD90.1 congenic marker[63, 66, 67]. Thus, we generated B6.*Cas9.Cd4cre.luc.CD90.1* (Cas9$^+$) mice for non-viral genome editing in mouse CD3$^+$ T cells[68].

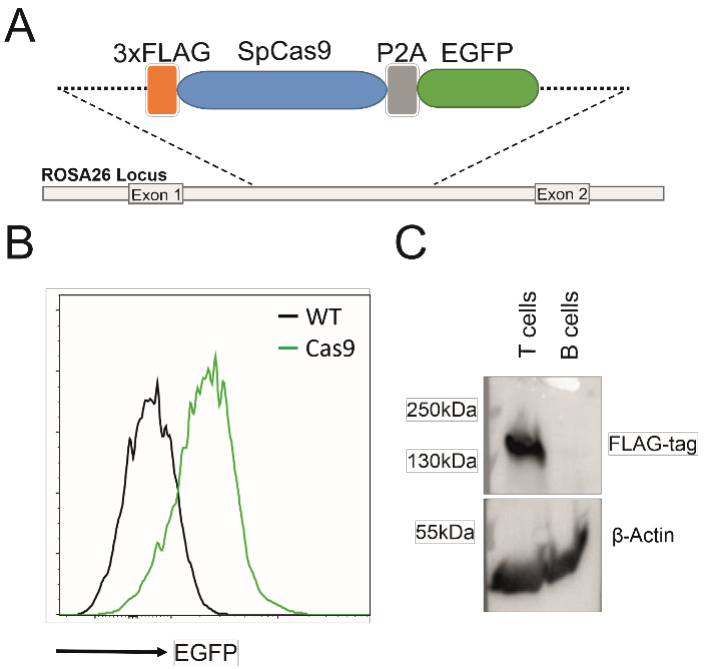

Figure 9. **Cas9 is expressed specifically in T cells from *Cd4cre*.Cas9⁺ mice.**

A. Schematic representation of the Cre-dependent Cas9 Rosa26-targeting vector. **B.** EGFP expression by flow cytometry in unstimulated CD3⁺ T cells from a *Cd4cre*.Cas9⁺ mouse, representing Cas9 expression in T cells. **C.** T cells and B cells were stimulated with TPA/ionomycin overnight before protein extraction. 3xFLAG-tag and β-Actin were detected in stimulated CD3⁺ T cells and CD19⁺ B cells by western blot.

9.1.3 Nucleofection of gRNAs into Cas9⁺ T cells is as effective as that of RNPs in WT T cells

We first wanted to compare the previously demonstrated RNP nucleofection method in wild type (WT) T cells[127] with gRNA-only nucleofection in T cells from the newly generated Cas9⁺ mice. CD3⁺ T cells were isolated from spleen and LNs of Cas9⁺ or WT mice, stimulated with anti-CD3, anti-CD28, IL-2 for 3 d or left unstimulated in IL-7 overnight before nucleofection[127] (Fig. 10A). To achieve high efficiency, first, we determined the optimum concentration of gRNA. We prepared gRNA by combining equimolar concentrations of chemically modified tracrRNA and crRNA[127, 128]. IL-7 pretreated, unstimulated Cas9⁺ T cells were nucleofected with 50 and 150 pmol *Cd90* gRNA_1 (Table 1). WT T cells were nucleofected with RNP, generated by combining 50 or 150 pmol gRNA with 10 µg recombinant Cas9. Nucleofection was performed in a Lonza Nucleofector IIb using the pre-set program X-001. Seven days after nucleofection, flow cytometry analysis was performed to determine surface protein loss and viability. A comparable knockout efficiency was observed between gRNA-only and RNP nucleofected IL-7-pretreated, but unstimulated mouse T cells, however, 150 pmol gRNA showed only a slight increase in knockout efficiency compared to 50 pmol (Fig. 10B). We

observed an overall increase in knockout efficiency when cells were cultured in RPMI (T-cell media), 60% versus Media A (recommended by nucleofection kit manufacturer, Amaxa/Lonza) 45% irrespective of the nucleofection method used (Fig. 10B). Viability was also enhanced for cells cultured in RPMI (25%) as compared to Media A (7%), irrespective of the nucleofection method used (Fig. 10C). Thus, we fixed our protocol for 150 pmol gRNA and RPMI as culture media but verified this in an extended approach comparing RNP and gRNA-only nucleofection of unstimulated (IL-7 pre-treated) and anti-CD3, anti-CD28 and IL-2 pre-stimulated $CD3^+$ T cells from WT and $Cas9^+$ mice. Viability was significantly enhanced in activated T cells (60%; Fig. 10D) as compared to unstimulated T cells (below 30%; Fig. 10C). Nevertheless, again no significant difference in knockout efficiency occurred between gRNA-only and RNP electroporation in neither unstimulated nor pre-stimulated T cells (Fig. 10E). Collectively, we identified optimized conditions and demonstrated that gRNA delivery in $Cas9^+$ unstimulated/naïve and pre-stimulated $CD3^+$ T cells is as efficient as RNP nucleofection in WT $CD3^+$ T cells.

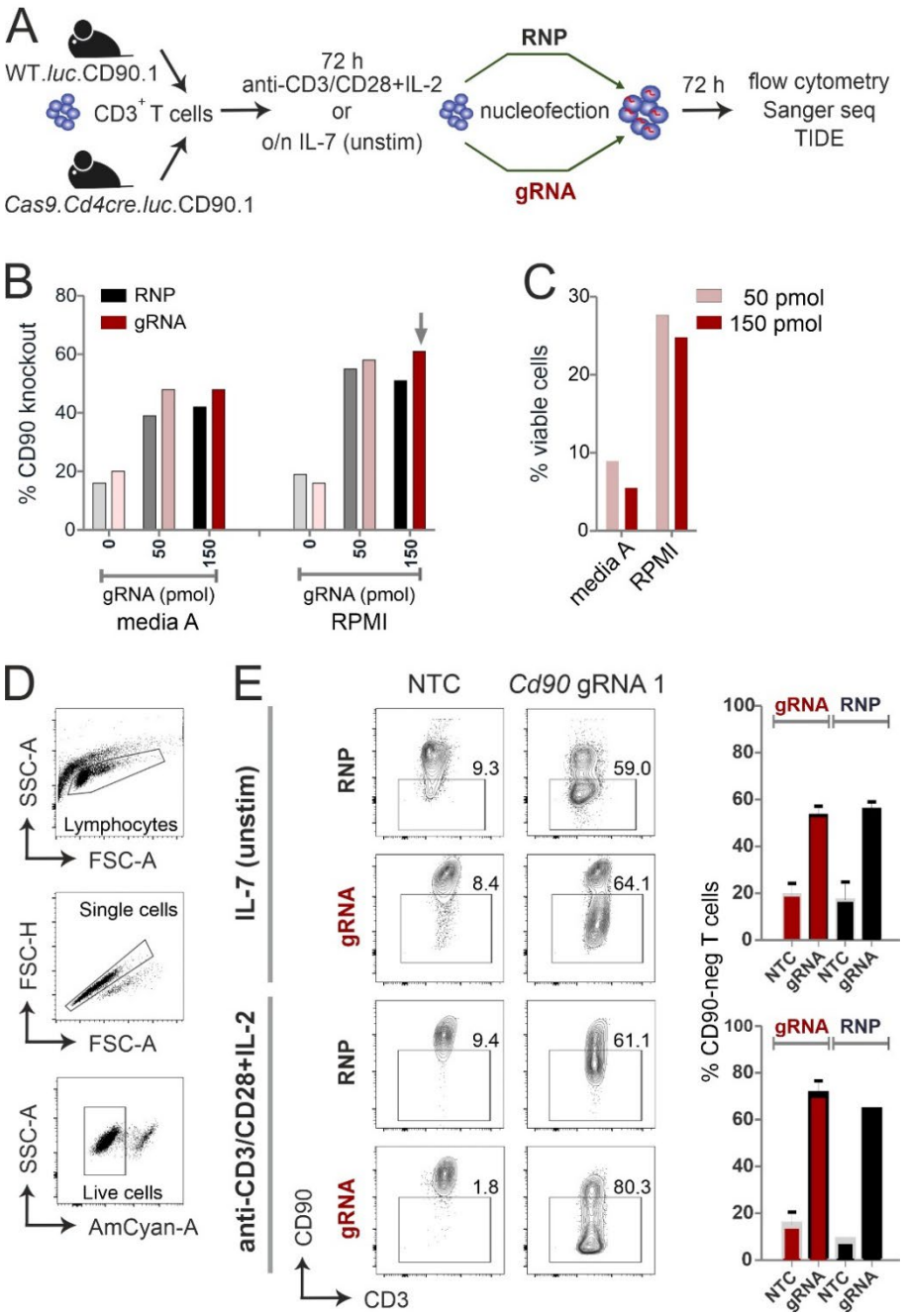

Figure 10. **CRISPR/Cas9-mediated knockout is equally efficient with RNP nucleofection in WT or gRNA-only nucleofection in Cas9$^+$CD3$^+$ primary mouse T cells.**

A. Flow chart of the CRISPR/Cas9 methods. **B-E.** All analyses were performed by surface antibody staining and flow cytometry. **B.** gRNA concentration optimization, comparison between Amaxa and RPMI media in resting CD3$^+$ T cells. **C.** Viability of resting CD3$^+$ T cells using gRNA-only nucleofection and different media. **D.** Gating strategy and viability of pre-stimulated CD3$^+$ T cells using gRNA-only nucleofection and RPMI. **E.** Comparison of CD90 KO efficiency between RNP nucleofection in WT T cells and gRNA-only nucleofection in Cas9$^+$ T cells, either resting (IL-7) or pre-stimulated CD3$^+$ T cells, 7 d or 3 d respectively after nucleofection using IIb/X-001 condition. Data are presented as mean ± SEM and representative of three independent experiments. NTC: Non-targeting control.

9.1.4 Two genes can be knocked out simultaneously in stimulated primary mouse Cas9$^+$CD3$^+$ T cells

We extended targeting to other genes encoding surface molecules by the gRNA-only nucleofection method in Cas9$^+$ T cells. We targeted *Cd4* in isolated CD3$^+$CD4$^+$ T cells and *Cd8* in isolated CD3$^+$CD8$^+$ T cells (Fig. 11A). Since efficacy and viability had been better with pre-stimulated T cells, we electroporated a combination of three gRNAs per gene this time using the Nucleofector 4D, CM-137 program. After 72 h, CD90 and both co-receptors were lost with a consistent efficiency of above 90%, all at once demonstrating that both T-cell subsets can be targeted equally well. Furthermore, different genes could be aimed at by a combination of three gRNAs per gene (Table 1) in the same cell, as proven by the concurrent loss of CD90 and CD8 in CD3$^+$CD8$^+$ T cells (Fig. 11B). Overall, in both CD4$^+$ and CD8$^+$ T cells, only a slight decrease of the mean knockout efficiency per gene was observed when one additional gene was targeted simultaneously (Fig. 11C).

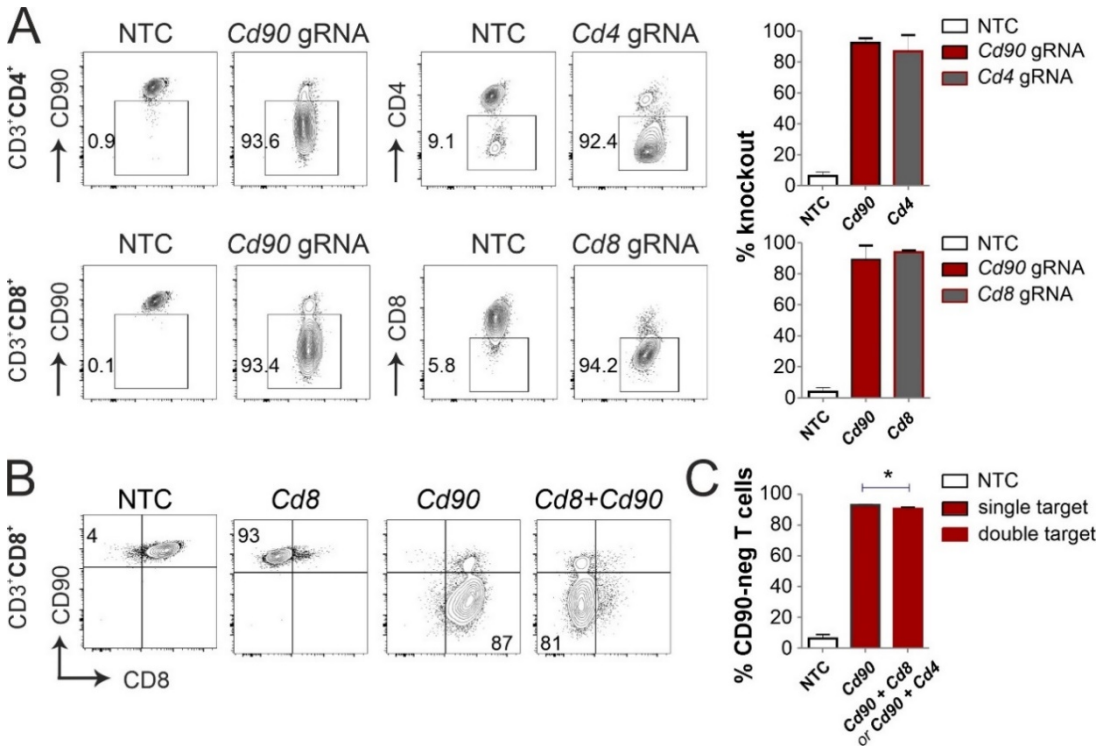

Figure 11. **gRNA-only nucleofection enables the simultaneous knockout of more than one gene in stimulated primary mouse Cas9$^+$CD3$^+$ T cells.**

A. Analyses by surface staining and flow cytometry of CD90 and CD4 or CD90 and CD8 knockout in stimulated CD3$^+$CD4$^+$ and CD3$^+$CD8$^+$ T cells 72 h post nucleofection, respectively (mean + SD), from two independent experiments. **B.** A flow cytometric example of simultaneous targeting of *Cd90* and *Cd8a* in CD3$^+$CD8$^+$ T cells; mean + SD, from two independent experiments; n=3, Student's unpaired t test (*p<0.05). **C.** Cumulative evaluation of concurrent knockout of CD90 and CD4 in CD3$^+$CD4$^+$ T cells or CD90 and CD8 in CD3$^+$CD8$^+$ T cells by flow cytometry, from two independent experiments. **A-C.** A combination of three gRNAs was used per targeted gene (Table 1).

9.1.5 The expression of transcription factors *Nfatc1* and *Nfatc2* is lost upon gRNA-only nucleofection in stimulated murine Cas9$^+$CD3$^+$ T cells

All NFAT proteins share a conserved core region composed of a DNA-binding RSD and a less conserved N-terminal regulatory domain, NHR (Fig. 4, Fig. 12A). We had shown that co-transplantation of NFAT-deficient T cells, as opposed to WT T cells, ameliorates GvHD after HCT in a major mismatch model[67]. At that time CD3$^+$ T cells were obtained from *Nfatc1$^{fl/fl}$.Cd4cre* or *Nfatc2$^{-/-}$* mice. For translational application, CRISPR/Cas9-mediated gene editing seemed feasible but needed to be examined. We designed several gRNAs for *Nfatc1* by the online tool DESKGEN (Table 1; Fig. 12B). Comparing the efficiency of all individual gRNAs by single nucleofection determined *Nfatc1* gRNA_4, which binds to exon 4, as superior to all others (Fig. 12C). The combination with exon 3-targeting gRNA_9 could enhance the degree of protein loss. Direct evaluation of the mutational burden on DNA level achieved by either cloning and sequencing or TIDE, revealed a similarly high degree after gRNA_4 nucleofection (Fig. 12D, E). In around 80% of the cells, a single G nucleotide was deleted, expected to cause a frameshift (Fig. 12D; above panel). About 7% of cells showed a deletion of six nucleotides as revealed by cloning PCR products of the target region in a TA vector and Sanger sequencing. Although we could not detect any insertions using Sanger sequencing, TIDE data showed insertion of 2 to 10 nucleotides in very low frequencies of cells (Fig. 12D; lower panel). Of note, although during NHEJ most of the indels are in the length of a few nucleotides, it is still possible to have longer ones, not detectable by either Sanger sequencing or TIDE. Interestingly, a reduction could be seen on mRNA level for both exon 1 and exon 2-containing isoforms even when the primers were chosen to bind 5' of the seeding sequence of the employed gRNAs (Fig. 12E). Loss of mRNA expression improved upon the combination of two or three gRNAs and did not alter when *Nfatc2* was additionally targeted (Fig. 12F).

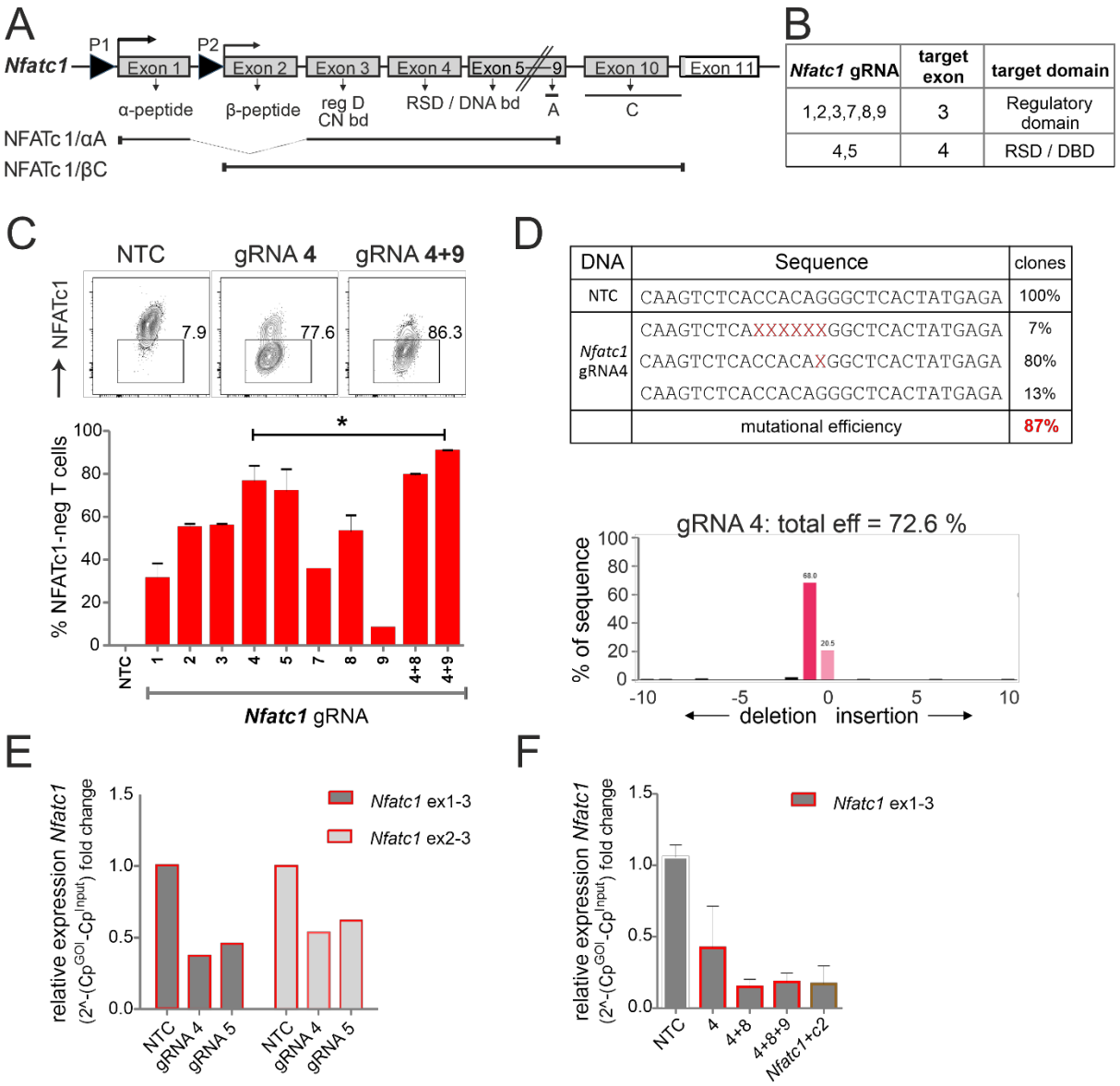

Figure 12. **The combination of exon 3 and exon 4-targeting gRNAs efficiently ablates *Nfatc1* in stimulated murine Cas9^{+}CD3^{+} T cells.**

A. Genomic structure of *Nfatc1* encoding six different isoforms due to two different promoters, of which P1 is inducible and P2 is constitutive, different splicing events and two non-depicted polyA sites. The most prominent isoforms NFATc1/αA and NFATc1/βC are indicated. The first common exon 3 encodes the regulatory domain, which includes calcineurin interaction and phosphorylation sites. Exon 4 is necessary for the expression of the RSD, which enforces DNA binding. **B.** Table with *Nfatc1* gRNAs and their target exons. **C.** Variation in knockout efficiency between gRNAs specific for *Nfatc1* measured by intracellular flow cytometry for NFATc1. The efficiency increases by the use of two gRNAs per gene mean + SEM, of three independent experiments, Student's unpaired t-test *, $P < 0.05$. **D.** Upper panel; Detection of indels in sequences of clones established after *Nfatc1* gRNA_4 nucleofection detected by Sanger sequencing, data are from one experiment. Lower panel; Recognition of indels using TIDE. **E.** mRNA isolated from cells collected 72 h post nucleofection. qRT-PCR with primers binding to exon 1 plus 3 or exon 2 plus 3 in *Nfatc1* RNA, i.e. 5' of the gRNA_4 binding site. **F.** qRT-PCR with primers binding to exon 1 plus 3 in Nfatc1 cDNA after nucleofection of one, two, or three *Nfatc1*-specific gRNAs, additionally with three *Nfatc1*-specific (4+8+9) and three *Nfatc2*-specific (1+2+3) gRNAs, mean + SEM, from two independent experiments.

NFATc2, like NFATc1, has several isoforms, in which at least exon 5, 6, 7 are expressed in all (Fig. 4, Fig. 13A). Resembling the strategy for *Nfatc1*, we had designed several *Nfatc2*-specific gRNAs, of which three gave the best results, i.e. two binding in exon 3 encoding most of the regulatory domain and one in exon 6 encoding part of the RSD (Table 1, Fig. 13B). We wanted to first detect NFATc2 knockout by flow cytometry with a fluorochrome-conjugated antibody (against NFATC2 amino acids 29-181). To check the specificity of the antibody, we used transgenic mouse-derived *Nfatc2*$^{-/-}$ T cells as a positive control. However, we could not detect any difference in expression of NFATc2 protein level in *Nfatc2*$^{-/-}$ T cells compared to WT T cells (Fig. 13C). In *Nfatc2*$^{-/-}$ mice, amino acids 398-444 in the RSD are replaced by the *neo cassette.* This results in a shorter polypeptide of NFATc2 which could be detected by the NFATc2 N-terminal-specific antibody (4G6-G5 specific for amino acids 145–189) in western blot analysis[129]. Similar to transgenic mouse-derived *Nfatc2*$^{-/-}$ T cells, in our CRISPR/Cas9-mediated *Nfatc2* knockout T cells, no difference in NFATc2 was observed by flow cytometry (Fig 13D). This could be either due to CRISPR/Cas9-mediated *Nfatc2* knockout giving rise to similar shorter polypeptide like in transgenic mouse-derived *Nfatc2*$^{-/-}$ T cells, or this fluorochrome-conjugated antibody is not specific to NFATc2. A specific antibody against targeted exons (3 and 6) is not commercially available to detect NFATc2 by flow cytometry. This necessitated the use of mRNA or DNA-based knockout detection methods. Here again, the knockout effect got stronger by combining *Nfatc2*-specific gRNAs specific for different exons (Fig. 13E). Mutations caused by one gRNA were less effective than in *Nfatc1*, but more complex (Fig. 13F, G). Additionally, we again observed very high knockout efficiency in mRNA levels when *Nfatc1* and *Nfatc2* were targeted at the same time (Fig. 12F, Fig. 13B). Taken together, we achieved above 85% knockout efficiency of the transcription factor NFAT by applying gRNA-only nucleofection, which we confirmed on DNA, RNA, and protein level.

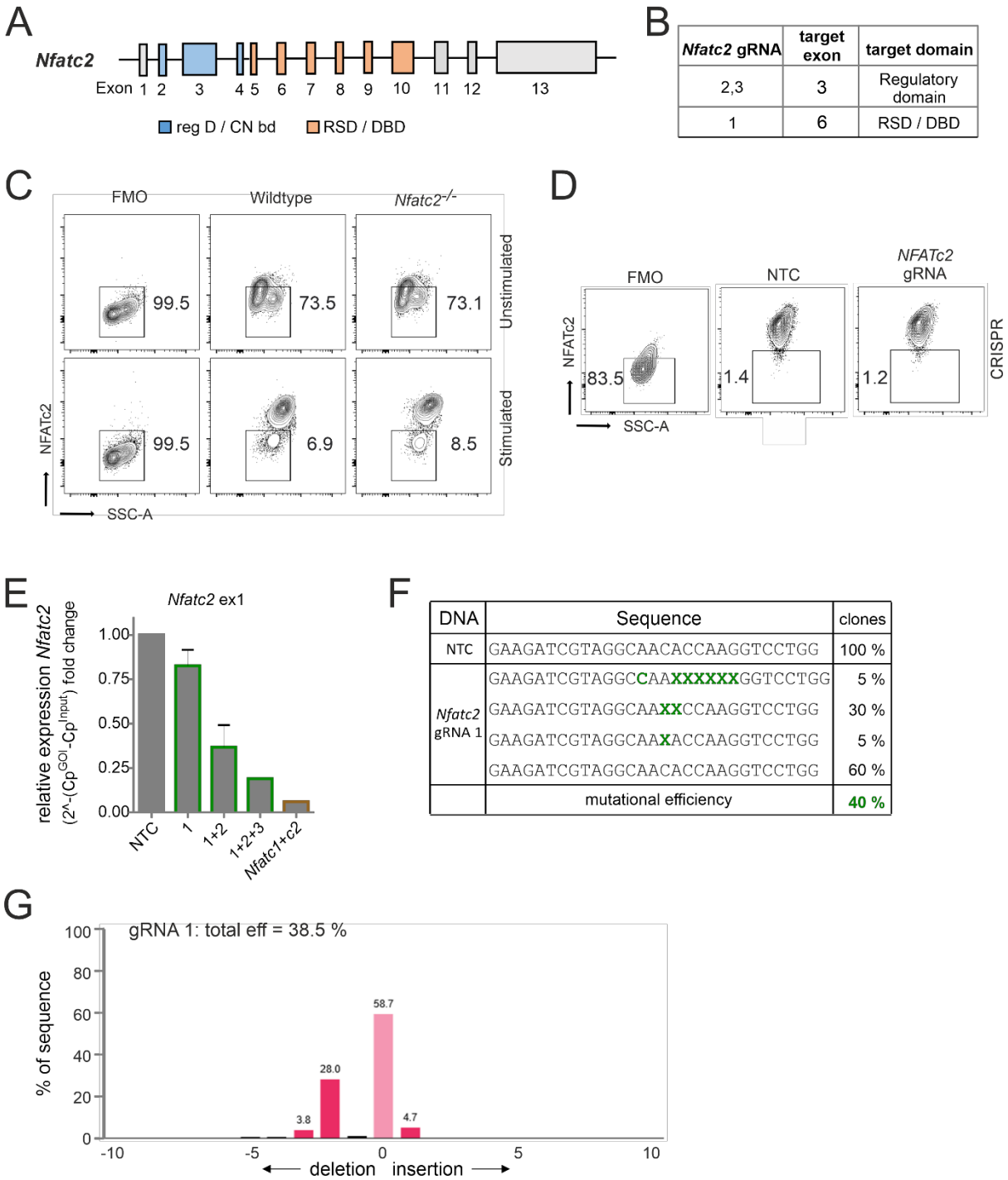

Figure 13. ***Nfatc2*-specific gRNAs lead to *Nfatc2* mutation and high efficiency when combined.**

A. Genomic structure of *Nfatc2* consists of 13 exons resulting in several isoforms known due to alternate splicing events. Exon 2-4 encode the regulatory domain, which includes calcineurin interaction sites. Exon 5-10 encode the RSD, which enforces DNA binding. **B.** Table with *Nfatc2* gRNAs and their target exons. **C**. T cells were isolated from WT or *Nfatc2*$^{-/-}$ mice and either directly used (unstimulated) or stimulated with anti-CD3+anti-CD28+IL-2 for 72 h. Cells were fixed and permeabilized for intracellular staining using FITC-conjugated NFATc2 antibody. **D**. CRISPR/Cas9 knockout of NFATc2 in mouse pre-stimulated Cas9^{+} T cells by nucleofection with gRNA 1+2. Three days after nucleofection cells were fixed and permeabilized for intracellular staining using FITC-conjugated NFATc2 antibody. Similar staining patterns were observed in all (total 7) gRNAs tested and also in combination of gRNAs. **E.** mRNA isolated from cells collected 72 h post nucleofection. qRT-PCR with primers binding to exon 1 in *Nfatc2* RNA after nucleofection of one, two, or three *Nfatc2*-specific gRNAs, additionally with three *Nfatc1*-specific (1+4+8) and three *Nfatc2*-specific gRNAs (1+2+3); mean ± SEM. Data are from three independent experiments. **F.** Detection of indels in sequences of clones; established 72 h after *Nfatc2* gRNA_1 nucleofection detected by Sanger sequencing using *Nfatc2* indel detection primers (Section 5.1.9). **G.** Recognition of indels using TIDE.

9.1.6 Effect of NFAT knockout on target gene expression

To evaluate the effect on NFAT-transactivated genes, we checked the expression of the cytokines IFN-γ, IL-2, and TNF-α as well as the surface molecule CD40L by flow cytometry. Although T cells had been stimulated for three days beforehand, which instigates instant NFAT activation, ablating either NFATc1 or NFATc2 could still reduce target gene expression (Fig. 14). The combination of three *Nfatc1*-specific gRNAs with three *Nfatc2*-specific gRNAs elicited an augmented effect on NFAT target genes as compared to ablating NFATc1 or NFATc2 alone (Fig. 14). A stronger effect was observed on the loss of target gene expression when NFATc2 was targeted compared to NFATc1.

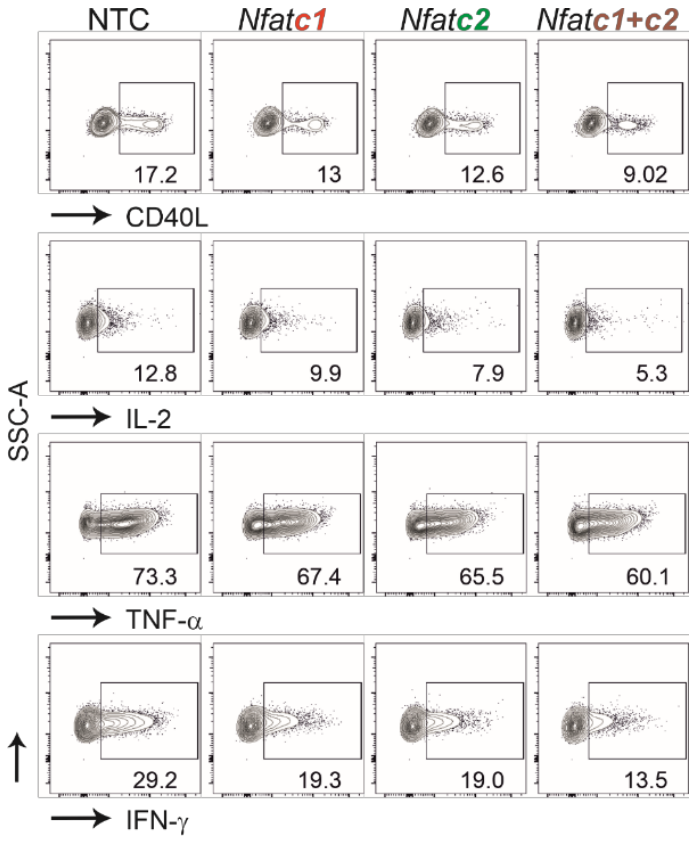

Figure 14: **Effect on target genes upon *Nfatc1* and/or *Nfatc2* knockout.**

NFAT knockout T cells were restimulated with PMA/ionomycin along with golgiplug and golgistop (Added 1 h after PMA/ionomycin addition) for a total of 6 h. Flow cytometry analysis of intracellular cytokines IL-2, TNF-α, and IFN-γ as well as surface protein CD40L. Data represent at least three independent experiments.

9.1.7 NFAT single-deficient pre-stimulated murine Cas9$^+$CD3$^+$ T cells expanded poorly during HCT

To explore whether NFAT ablation by CRISPR/Cas9 reduces the allo-reactivity like previously shown with T cells derived from transgenic mice[63], Cas9$^+$CD3$^+$luc$^+$CD90.1$^+$.H-2^b T cells were nucleofected by three gRNAs targeting either *Nfatc1* or *Nfatc2* (Fig. 15A). To achieve an enhanced degree of knockout (Fig. 10E), we pre-stimulated the T cells before nucleofection. Subsequently, they were co-transferred with CD90.2$^+$.H-2^b bone marrow (BM) from *Rag1*$^{-/-}$ mice into lethally irradiated CD90.2$^+$.H-2^d BALB/c mice. All mice, which received T cells, lost weight continuously over six days, but less with a prior NFATc1 knockout and significantly less upon NFATc2 knockout (Fig. 15B). Bioluminescence imaging (BLI) of the living mice over time revealed less proliferation and expansion of T cells, which had been NFAT-ablated vs transfected with NTC (Fig. 15C). This could be further corroborated *ex vivo* by BLI of all organs on 6 dpi (Fig. 15D). Detailed comparison of lymphoid and non-lymphoid organs of mice with NTC vs *Nfatc1*-specific gRNA-nucleofected T cells documented a significant decrease in the expansion of NFATc1 knockouts (Fig. 15E). This included the gut, one of the prime target organs during GvHD. Accordingly, the gut homing receptor α4β7 integrin was less expressed on NFATc1-ablated CD4$^+$ and CD8$^+$ T cells (Fig. 15F). Additionally, those T cells produced fewer IFN-γ, the dominant cytokine during aGvHD (Fig. 15G), while NFATc1 knockout Treg had an advantage over NTC-transfected ones (Fig. 15H).

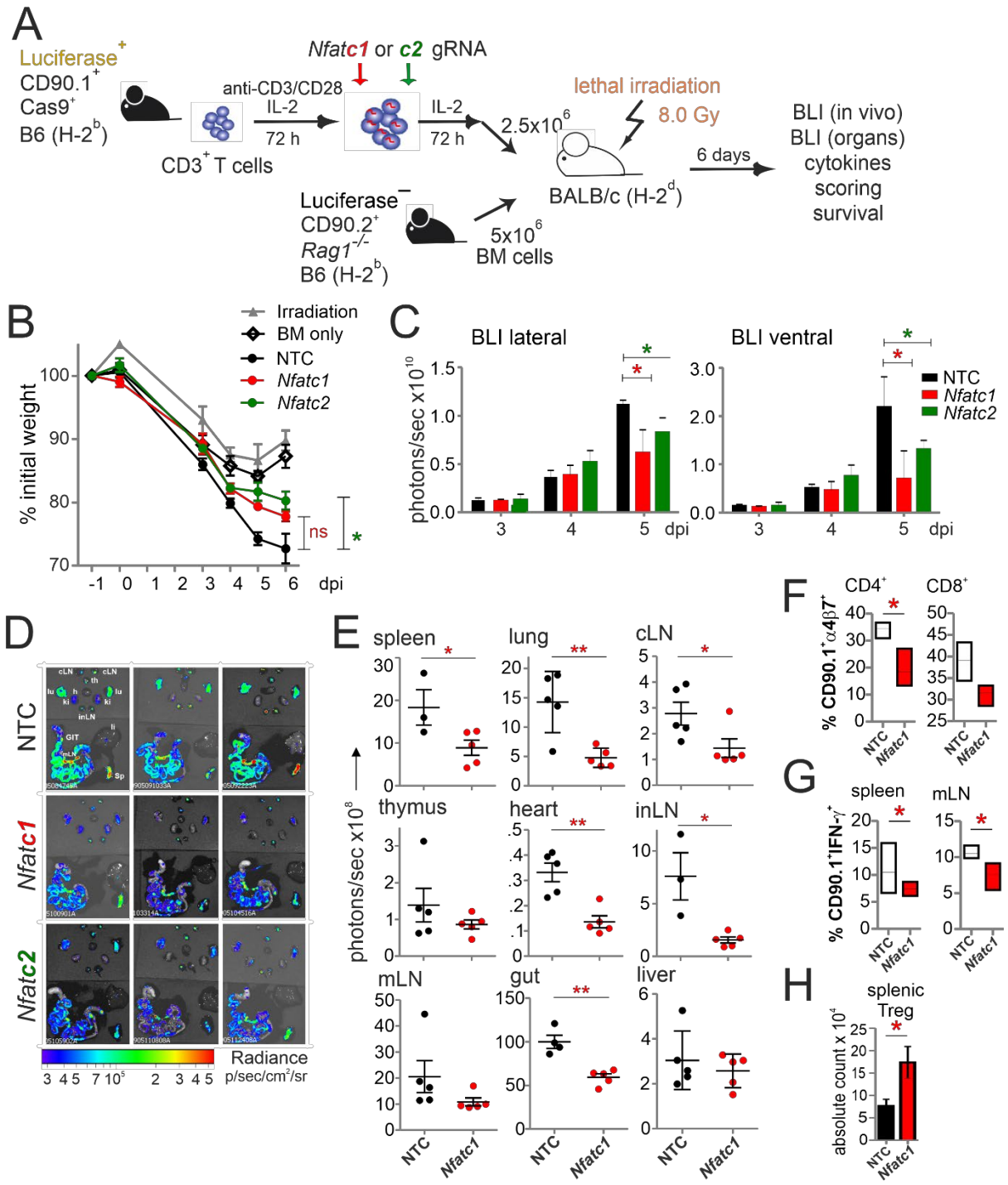

Figure 15. **Knockout of NFATc1 or NFATc2 in pre-stimulated murine Cas9⁺CD3⁺ T cells limit signs of GvHD after co-transfer in a major mismatch model**.

A. Experimental set up of NFAT-specific gRNA-only nucleofection and GvHD induction due to an H-2^b →H-2^d transfer with pre-stimulated Cas9⁺CD3⁺ T cells. **B-H.** gRNAs used: *Nfatc1* gRNA 4+8+9, *Nfatc2* gRNA 1+2+3. **B.** Weight changes of mice with NTC or NFAT-specific gRNA-nucleofected and co-transplanted Cas9⁺CD3⁺ T cells. Mice were evaluated every day weight loss were calculated considering -1 dpi weight as 100%. **C.** Lateral and ventral *in vivo* by BLI on 3, 4, and 5 dpi with NTC, NFATc1, or NFATc2-ablated pre-stimulated Cas9⁺CD3⁺ T cells. Plotted are photons per second; mean + SD. **D.** *Ex vivo* BLI images of lymphoid and non-lymphoid organs of the mice under C. at 6 dpi; mean ± SD. **E-H.** Analyses six days after GvHD induction with NTC and *Nfatc1* gRNA-nucleofected, pre-stimulated Cas9⁺CD3⁺ T cells; mean ± SD, Student's unpaired t-test (*p<0.05, **p<0.01), representative of two independent experiments. **E.** Quantitation of *ex vivo* BLI analyses of lymphoid and non-lymphoid organs. **F.** Staining of integrin α4β7 together with CD90.1, CD4 and CD8 followed by flow cytometry. **G.** Intracellular staining of IFN-γ after surface staining for CD90.1, CD4, and CD8 followed by flow cytometry. **H.** Intracellular staining of Foxp3 after surface staining for CD90.1, CD4, and CD25 followed by flow cytometry; dpi: days post irradiation.

Moreover, NFATc2 knockout T cells behaved similar to NFATc1 knockout T cells, showing reduced proliferation (Fig. 16A), increased Treg numbers (Fig. 16B), reduced α4β7 integrin expression (Fig. 16C), IFN-γ expression (Fig. 16D), and $CD8^+$ to $CD4^+$ T cell ratio (Fig. 16E). This supports our former data that Treg are less dependent on NFAT proteins and that they function well when one or two NFAT family members are missing[10, 63]. In sum, concerning allo-reactivity, ablating NFAT by gRNA-only in pre-stimulated $Cas9^+CD3^+$ T cells seemed to be equivalent to the loss achieved using T cells from knockout mice, as seen in our earlier work[63].

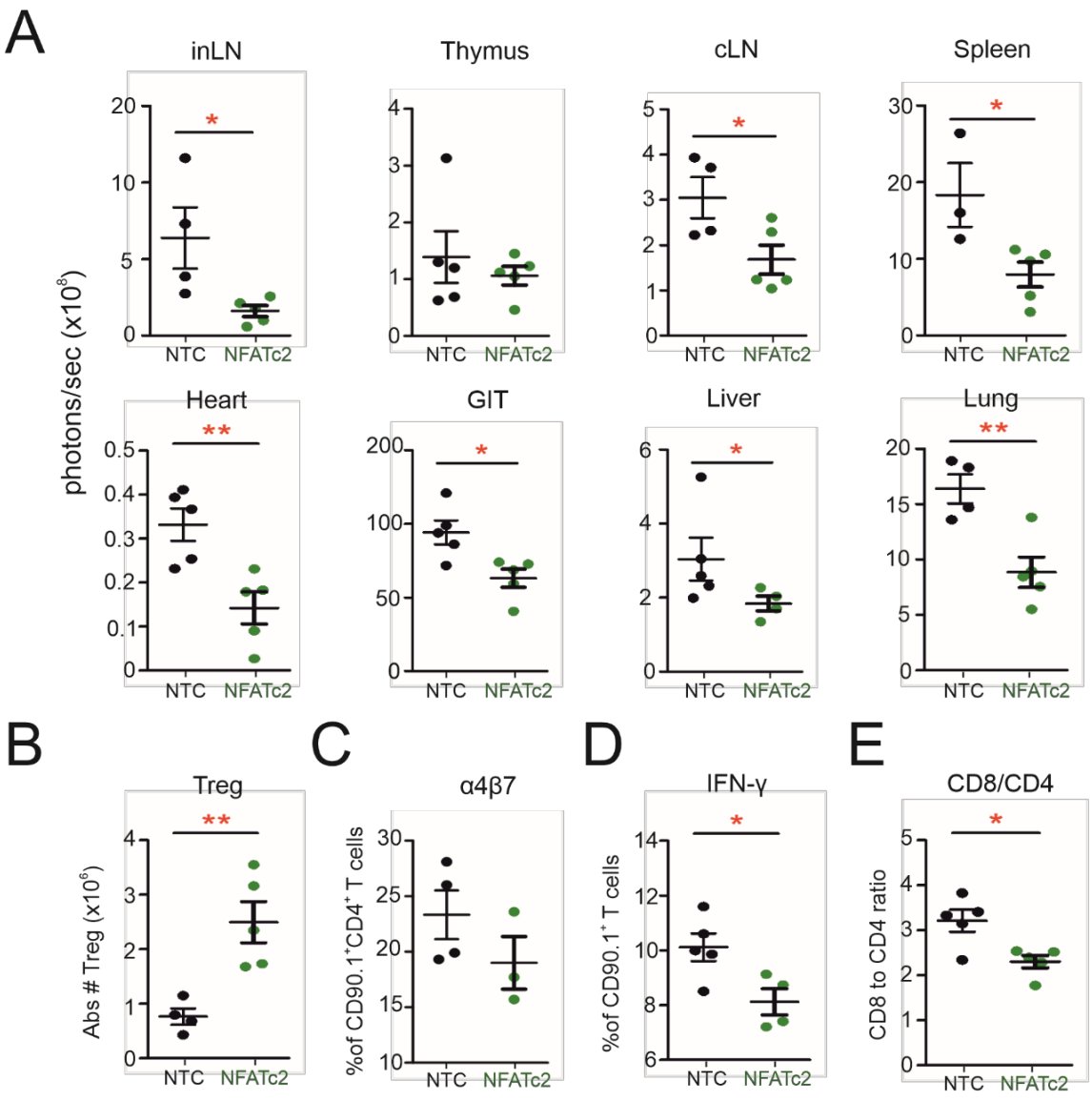

Figure 16: **CRISPR/Cas9 knockout of NFATc2 in pre-stimulated T cells reduces aGvHD at early time-point.**

A-E. Pre-stimulated NFATc2-ablated T cells were transplanted in recipient mice according to Fig. 15A. *Nfatc2*-specific gRNAs used are 1+2+3. At 6 dpi mice were used for *ex vivo* BLI analyses and sacrificed for flow cytometry analyses of spleen and LN cells. Data represent n=5, Student's unpaired t test (*p<0.05, **p<0.01). **A.** *Ex vivo* BLI of mice organ at 6 dpi. **B-E.** Gated on $CD90.1^+$ donor T cells. **B.** Absolute count of $CD90.1^+CD4^+CD25^+FoxP3^+$ Treg in splenocytes *ex vivo* at 6 dpi. Intracellular FoxP3 staining was performed using FoxP3 staining kit. **C.** α4β7 surface staining in $CD90.1^+CD4^+$ donor T cells *ex vivo* at 6 dpi. **D.** Intracellular IFN-γ staining in lymphocytes isolated from mLN *ex vivo* on 6 dpi, restimulated with PMA/ionomycin and brefeldin/monensin for 6 h. **E.** CD8 to CD4 T cell ratio in splenocytes *ex vivo* at 6 dpi.

9.1.8 Pre-stimulation of T cells alters their behaviour *in vivo*

We repeated the experiment according to Fig. 15A, but this time examined the recipient mice up to 35 dpi, to see if ablating single NFAT members in pre-stimulated donor T cells by gRNA-only nucleofection enhances long-term survival of recipient mice. We performed *ex vivo* BLI and flow cytometry analysis this time at 35 dpi. Unexpectedly, mice, which received NFATc1 or NFATc2-ablated T cells, were not protected over time and showed stronger clinical GvHD scores than the mice which received NTC-T cells. To envisage the cause, we investigated if the few T cells that could not be targeted by gRNA-only nucleofection outgrow at later time points. *Ex vivo* analyses at 35 dpi of spleen and LN cells revealed that NFATc1 deficiency was mostly conserved in the donor T cells of the NFATc1 KO group (Fig. 17A). This ensured that gRNA-only mediated NFATc1 loss was sustained at a later time point and outgrowth of the non-targeted cells was not the reason for less protection from GvHD in NFATc1 knockout T-cell recipient mice. Nevertheless, mice that received NFATc1 single KO T cells, exhibited increased weight loss (Fig. 17B) from 21 dpi, as well as enhanced clinical score starting at 17 dpi (Fig. 17C) compared to the NTC group. Due to the disease severity, all *Nfatc1*$^{-/-}$ T-cell recipient mice died within 33 dpi (Fig. 17D). Remarkably, the BLI signals, i.e. expansion of T cells, at 35 dpi did not correlate with the disease severity of the NFATc1 KO group (Fig. 17E). When analysing NFATc2-single knockout T cells, we found that they, although causing a similar weight loss as NTC T cells (Fig. 17B), especially triggered stronger skin GvHD, hence increased clinical scores (Fig. 17C). In contrast to 6 dpi (Fig. 16A), target organ homing (GIT, liver) of NFATc2-deficient T cells was no longer reduced compared to NTC-nucleofected T cells at 35 dpi. Especially, more NFATc2 KO donor T cells accumulated in thymus, kidney, and lung than NTC T cells, examined during *ex vivo* BLI analyses at 35 dpi (Fig. 17E). NFATc1c2 DKO group indicated less weight loss (Fig. 17B), less severe clinical score (Fig. 17C), weaker *ex vivo* BLI signals compared to the NTC group (Fig. 17E), and no mice in the DKO group died up to 35 dpi (Fig. 17D). In summary, this experiment revealed despite controlled aGvHD in the early weeks (1-2) post allo-HCT, single NFAT ablation in donor T cells by gRNA-only nucleofection worsened aGvHD progression from a later time point post-transplantation.

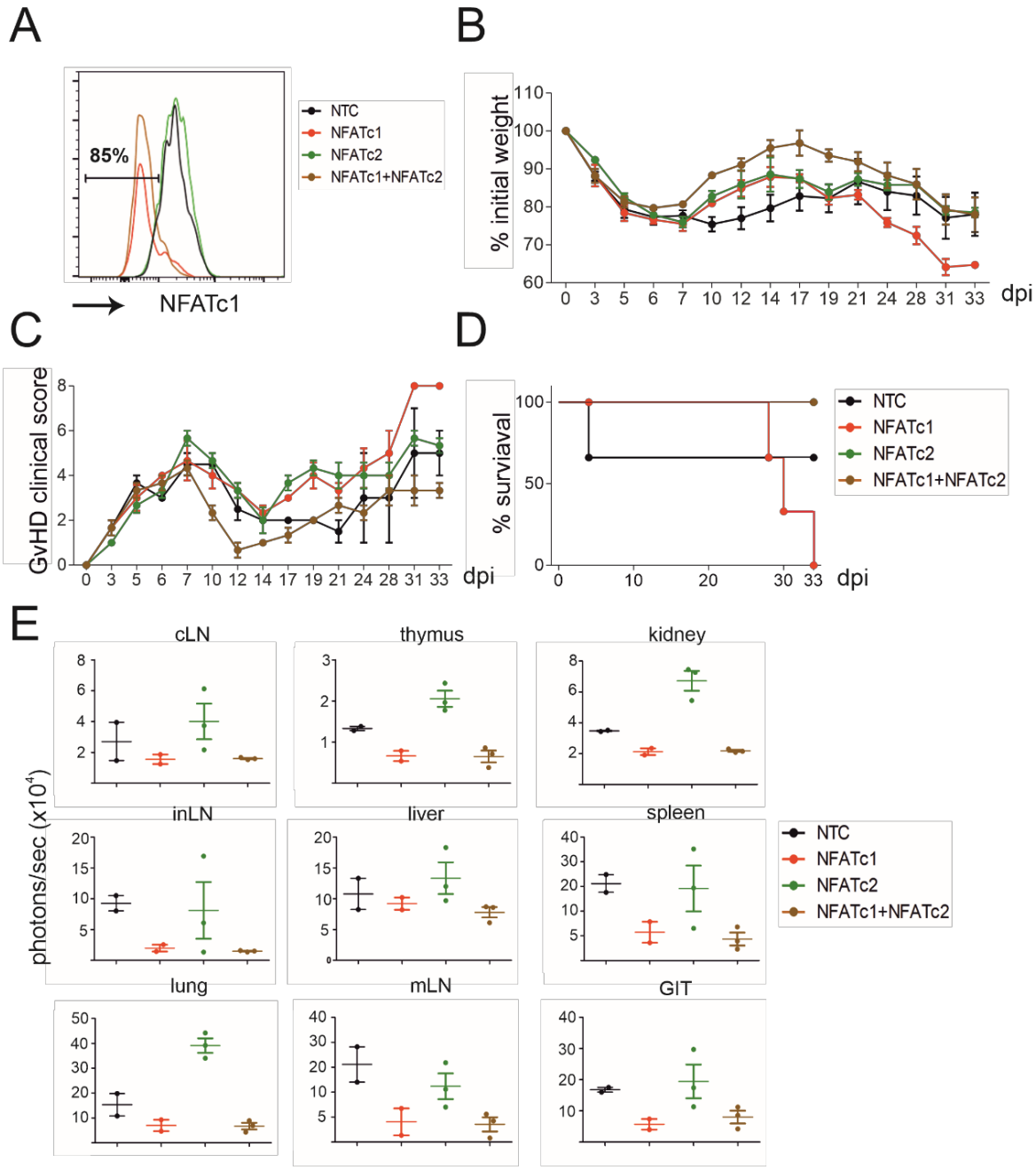

Figure 17: **Single NFAT knockout by CRISPR/Cas9 in pre-stimulated T cells aggravates aGvHD over time.**

A-E. GvHD induction due to an H-2^{b} -> H-2^{d} transfer with pre-stimulated Cas9^{+}CD3^{+} T cells (according to Fig. 15A). gRNAs used: NTC, *Nfatc1* gRNA 4+8+9, *Nfatc2* gRNA 1+2+3. Data represent n=3, mean ± SE; from one experiment. **A.** NFATc1 staining in NTC or *Nfatc1* knockout donor T cells from LNs 35 dpi. **B.** Percentage weight changes and **C**. GvHD clinical scores were measured every day post-transplantation up to 33 dpi. Percentage weight change was measured considering weight on 0 dpi as 100%. **D.** Survival of mice was measured up to 35 dpi. **E**. *Ex vivo* BLI analyses of organs were performed at 35 dpi.

9.1.9 NFAT single-deficient pre-stimulated T cells do not aggravate GvHD due to outgrowth of WT T cells or knocking out NFAT after pre-stimulation

One possibility of more severe GvHD in mice transplanted with NFAT single-deficient T cells could be the pre-stimulation of the T cells. Among other events, this results in TCR signaling-mediated expression of NFAT, which leads to transcriptional modifications of the cells before nucleofection. Therefore, we performed an experiment with NFATc1 and NFATc2-deficient T cells obtained from *Nfatc1*$^{fl/fl}$*.Cd4cre* and *Nfatc2*$^{-/-}$ mice, respectively[63]. Here, NFAT was already missing in T cells before *in vitro* pre-stimulation. This would have also proven another possible reason for more severe GvHD in single-deficient mice, which is that the few cells without knockout outcompeted the NFAT-deficient ones at later time points. We observed NFATc1-deficiency to be conserved in the *Nfatc1*-'CRISPR'-ed T-cell population (Fig. 17A) up to 35 dpi, ruling out this being true at least for the NFATc1-deficient group. Using T cells from *Nfatc1*$^{fl/fl}$*.Cd4cre* and *Nfatc2*$^{-/-}$ mice would revalidate this finding. We treated T cells from *Nfatc1*$^{fl/fl}$*.Cd4cre* and *Nfatc2*$^{-/-}$ mice according to our model (Fig. 15A) and compared them to NTC and gRNA-nucleofected for NFATc1 plus NFATc2. Very different from our results using these same NFAT-deficient T cells without stimulation, pre-activated CD3$^+$ T cells from either *Nfatc1*$^{fl/fl}$*.Cd4cre* or *Nfatc2*$^{-/-}$ caused long-term weight loss and enhanced clinical scores from the second week after transplantation in the major mismatch model of HCT (Fig. 18A). The NFAT single-deficient T cells were responsible for premature death in comparison to NTC-nucleofected or NFATc1c2 double-deficient ones, created by gRNA-only nucleofection of Cas9$^+$CD3$^+$ T cells. With this, the loss of a single NFAT member, both before (Fig. 18A) or after (Fig. 17B, C) *in vitro* stimulation prior to transplantation, caused more severe aGvHD. Moreover, this also verifies that non-manipulated Cas9$^+$CD3$^+$ T cells overgrowing the factually nucleofected ones were unlikely to be the cause of loss of protection over time. There are subtle differences between experiments (Fig. 17B-D, Fig. 18A) with pre-stimulated T cells may be due to varying knockout efficiency but in this context, not the topic, since first, we wanted to find a condition for translation into the clinic. One remaining possibility was that the 3 d pre-stimulation period changed the (allo-) reactivity of T cells. To understand, to what extent *in vitro* pre-stimulation changed CD4$^+$, CD8$^+$ Tcon, and Treg frequencies, we analysed the phenotype of the Cas9$^+$CD3$^+$ T cells before and after *in vitro* culture prior to transplantation (according to Fig. 15A). This revealed a stronger expansion of CD8$^+$ T cells (Fig. 18B), shifting the CD8 to CD4 ratio. However, Treg frequency was unchanged due to *in vitro* culture (Fig.

18C). To keep the CD8 to CD4 ratio more or less unchanged, we adapted our protocol to pre-stimulate $Cas9^+CD3^+$ T cells for only 24 h before gRNA nucleofection and transplanting them without a major rest. This kept the $CD8^+$ and $CD4^+$ T cells frequencies undisturbed (Fig. 18D). In parallel, we verified the knockout on the level of *Nfatc1* and *Nfatc2* mRNA (Fig. 18E). For additional safety measures, we chose to transfer just as many T cells ($1.2x10^6$) as we had done before with naive T cells from NFAT-deficient mice[63]. Now we observed a constant benefit upon NFAT ablation (Fig. 18F). Still, shortly pre-stimulated $Cas9^+$ T cells did not behave equally when knocked out for NFATc1 vs NFATc2 since NFATc1 deficiency was even more effective than the DKO regarding GvHD scores. This was in contrast to the former data with naive T cells from NFAT-deficient mice. Despite that, knocking out NFATc1, NFATc2, or both by gRNA-only in shorter pre-stimulated and directly co-transplanted $Cas9^+CD3^+$ T cells protected mice from aGvHD.

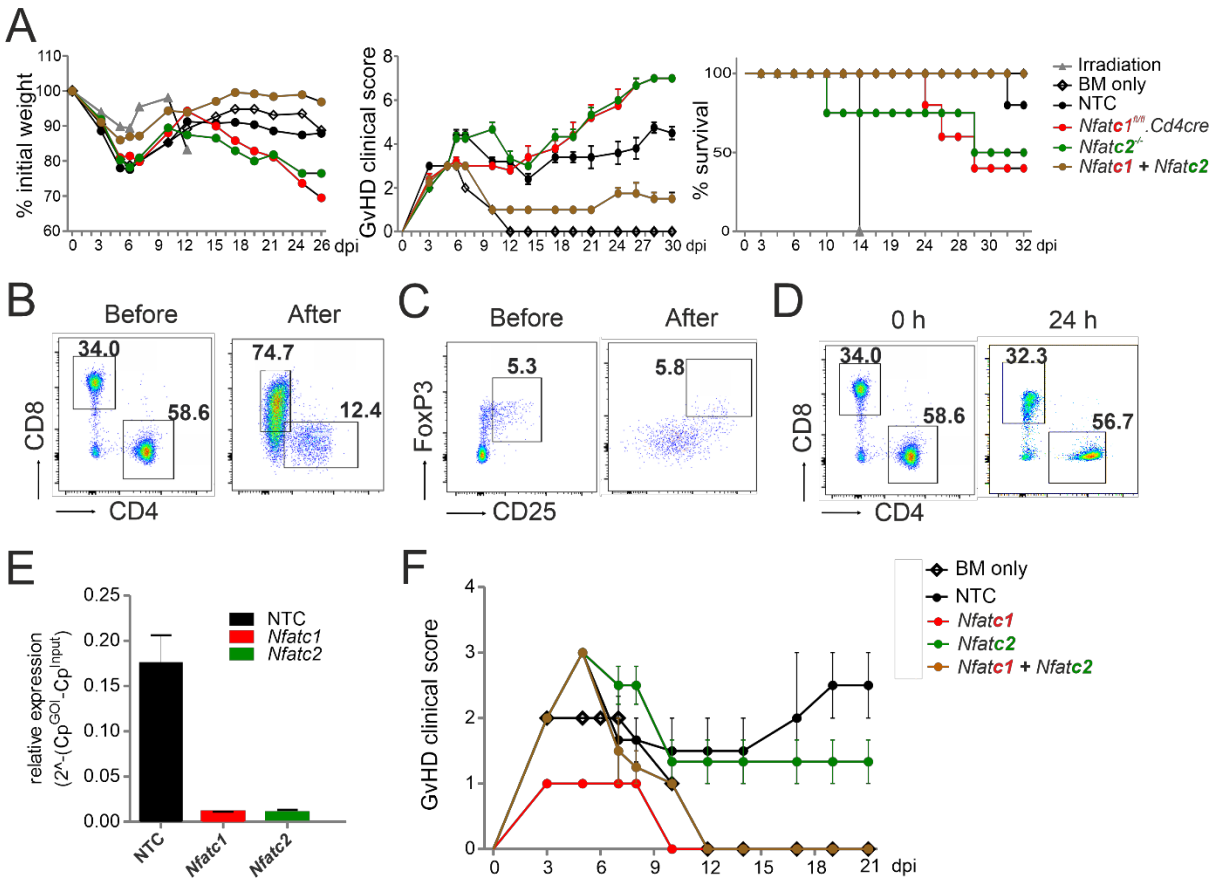

Figure 18. **Pre-stimulated *Nfatc1*$^{fl/fl}$*.Cd4cre* or *Nfatc2*$^{-/-}$ T cells aggravate aGVHD over time.**

A. GvHD induction due to an H-2^{b} -> H-2^{d} transfer with pre-stimulated Cas9^{+}CD3^{+} T cells. gRNA used: *Nfatc1* gRNA 4+8+9, *Nfatc2* gRNA 1+2+3. Weight changes, GvHD clinical score, and survival measured up to 32 dpi of mice transplanted with NTC or NFAT-specific gRNAs nucleofected in 3 d pre-stimulated Cas9^{+}CD3^{+} T cells for *Nfatc1+Nfatc2* group or similarly treated T cells isolated from *Nfatc1*$^{fl/fl}$*.Cd4cre* or *Nfatc2*$^{-/-}$ mice for the single knockout group; n≥4, mean ± SE; from one out of two independent experiments. **B-C.** T cells were isolated from Cas9^{+} mouse spleen and LNs, stimulated with anti-CD3+anti-CD28+IL-2 for 3 d, electroporated with NTC gRNA, and then cultured with IL-2 for 3 d. Cells were stained for surface markers CD4, CD8, CD25, and intracellular marker FoxP3 and analysed by flow cytometry. **B.** CD4^{+} and CD8^{+} percentage before and after *in vitro* culture. **C.** CD25^{+}FoxP3^{+} Treg population before and after *in vitro* culture. **D.** CD4^{+} and CD8^{+} percentage analysed by flow cytometry before and after 24 h *in vitro* stimulation of T cells isolated from Cas9^{+} mouse spleen, LNs with anti-CD3+anti-CD28+IL-2. Cells were electroporated with NTC gRNA before surface staining of CD4 and CD8. **E-F.** gRNA used: *Nfatc1* gRNA 4+8+9, *Nfatc2* gRNA 1+2+3. **E.** qRT-PCR with NFAT-specific primers from cells stimulated *in vitro* for 3 d post nucleofection in 24 h pre-stimulated Cas9^{+}CD3^{+} T cells; mean + SD; from one experiment. **F.** GvHD induction due to an H-2^{b} -> H-2^{d} transfer with pre-stimulated Cas9^{+}CD3^{+} T cells. GvHD clinical score measured up to 21 dpi of mice transplanted with 24 h pre-stimulated Cas9^{+}CD3^{+} T cells nucleofected with NFAT gRNAs; n=5; mean ± SE; from one experiment.

9.1.10 Pre-stimulated NFAT single-deficient T cells aggravate aGvHD over time due to the production of increased pro-inflammatory cytokines and perforin

Next, we attempted to detect possible causes of aggravated aGvHD in mice transplanted with NFAT single-deficient pre-stimulated T cells. We performed CRISPR/Cas9-mediated knockout of NFATc1 or NFATc2 in pre-stimulated T cells and transplanted T cells in recipient mice as described in Fig. 15A. Now on 35 dpi, *ex vivo* analyses of the spleen and LN lymphocytes were performed. *Nfatc1*$^{-/-}$ donor T cells showed a significant reduction in CD8 to CD4 ratio without any changes observed in *Nfatc2*$^{-/-}$ group (Fig. 19A). This was due to an increased frequency of CD4$^+$ T cells in the *Nfatc1*$^{-/-}$ group. Treg frequency was not significantly altered between WT and NFAT-depleted groups, suggesting that the worsening of the disease was not due to a lack of Treg (Fig. 19B). Two important markers for aGvHD progression are the gut homing receptors CCR9[130] and α4β7[131]. In NFAT single-deficient T cells, the reduction in α4β7 expression observed at the early time point 6 dpi (Fig. 15F, Fig. 16C) was not any more evident at 35 dpi (Fig. 19C). Additionally, NFATc2-depleted T cells had significantly increased CCR9 surface expression (Fig. 19D) accounting for the increased tendency of BLI signal in GIT at 35 dpi (Fig. 17E). We could not observe any considerable changes in the CD4$^+$ or CD8$^+$ T cell subpopulations (CD62L$^-$CD44$^+$ T_{EFF}/T_{EM}, CD62L$^+$CD44$^+$ T_{CM} and CD62L$^+$CD44$^-$ naive[132]) between the groups (Fig. 19E). When we restimulated the cells on 35 dpi *ex vivo* with PMA/ionomycin for 6 h, it revealed an increased amount of pro-inflammatory cytokine (IFN-γ, TNF-α) production by NFATc1 knockout donor T cells (Fig. 19F). Instead, NFATc2-ablated donor T cells even showed a reduced proinflammatory cytokine release (Fig. 19F). Furthermore, either NFATc1 or NFATc2-deficient CD8$^+$ T cells expressed significantly more perforin (Prf1), which could be the cause of CTL-mediated exacerbation of the disease. But, no changes in granzyme B (GzmB) and degranulation marker, CD107a expression were observed between groups.

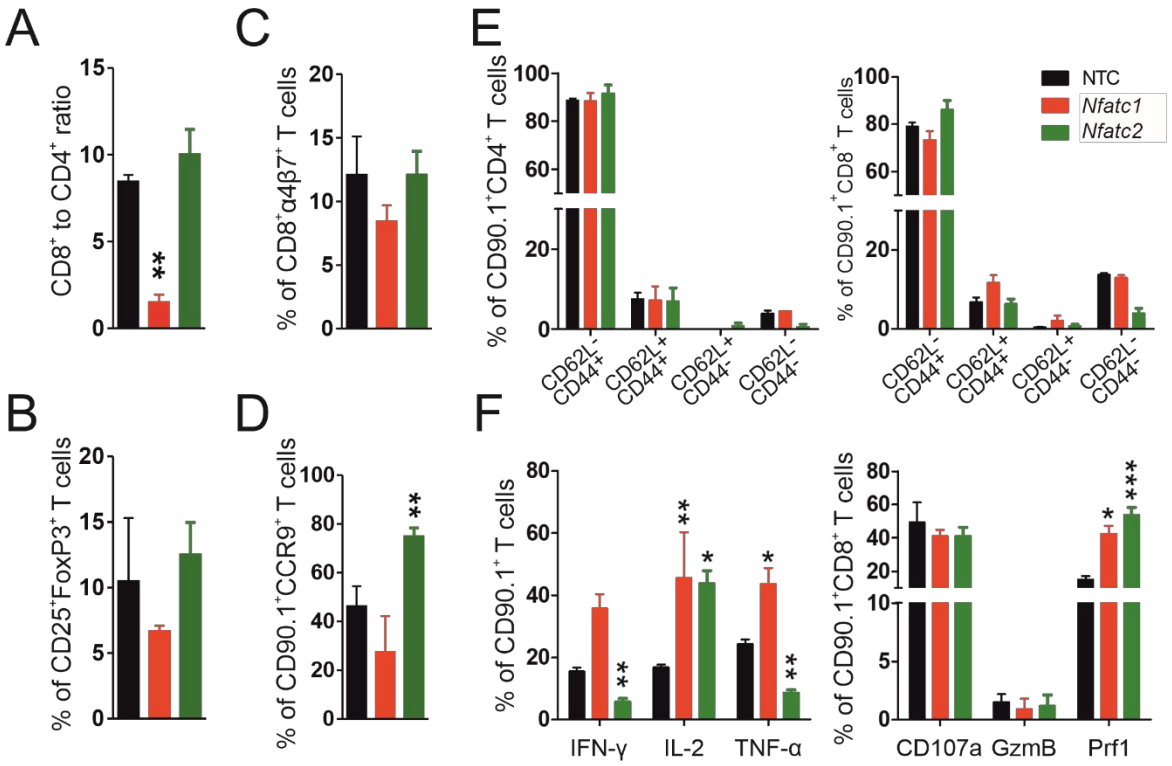

Figure 19: **Enhanced proinflammatory phenotype of NFAT single-depleted T cells in aGvHD over time.**

A-F. NFATc1 or NFATc2 is knocked out using a mix of three gRNAs (4+8+9 for *Nfatc1* or 1+2+3 for *Nfatc2*) in pre-stimulated T cells. Data represent n=3, Student's unpaired t test (*p<0.05, **p<0.01 ***p<0.001). Cells were cultured and transplanted in BALB/c recipients after irradiation according to Fig. 15A. On 35 dpi, mice were sacrificed, spleen and LNs were harvested and surface staining of **A.** CD90.1, CD4, CD8, **C.** α4β7 **D**. CCR9, **E.** CD62L, CD44 was performed. **A-F.** Flow cytometry analysis was performed to detect the phenotype of CD90.1$^+$ donor T cells. **A.** CD8 to CD4 ratio of donor T cells. **B.** Treg (CD90.1$^+$CD25$^+$FoxP3$^+$) frequency was quantified by surface CD25 and nuclear FoxP3 staining in LN cells using FoxP3 staining kit. **E**. Subpopulation frequencies of splenic T cells according to CD62L and CD44 surface expression. **F**. Splenocytes were stimulated with PMA/ionomycin along with brefeldin/monensin for 6 h. Intracellular staining of IFN-γ, IL-2, TNF-α, GzmB, Prf1 was performed. Anti-CD107a-PE antibody was added during culture to detect degranulation of CD8$^+$ T cells.

9.1.11 NFATc1 deficiency reduces the exhaustion of pre-stimulated donor T cells

Moreover, to elucidate an explanation for increased proinflammatory cytokine release by NFATc1-ablated donor T cells at 35 dpi (Fig. 19F), we experimented to compare between transplantation of naïve/unstimulated versus pre-stimulated T cells obtained from either WT or *Nfatc1$^{fl/fl}$.Cd4cre* mice. Again, pre-stimulated NFATc1-deficient T cell-recipient mice showed more severe GvHD from the third week post transplantation compared to WT T cell-recipient mice. In contrast, but similar to earlier study[63], mice which received unstimulated NFATc1-ablated T cells were protected from GvHD as compared to mice transplanted with WT unstimulated T cells. Previously, high co-expression of HMG-box transcription factor TOX, along with PD1 (TOX^{hi}PD1^{hi}) by CD8$^+$ T cells has been shown to be the attribute of T_{EX} cells[133] (Fig. 20A). In this experiment, we sacrificed the mice at 30 dpi. Surface expression of co-inhibitory molecules (PD1, Tim3) and intracellular TOX expression was performed to identify

T_{EX} cells by flow cytometry within splenocytes. We consistently observed reduced PD1 (NFAT target gene) expression, as well as a diminished TOX^{+} and $TOX^{hi}PD1^{hi}$ population within NFATc1-deficient donor T cells as compared to WT donor T cells (20B, C). This was consistent irrespective of whether pre-stimulated or unstimulated T cells were transplanted. However, Tim3 expression only decreased although not reaching significance in NFATc1-deficient donor T cells when pre-stimulated cells were transplanted and not when unstimulated T cells were used for transplantation (Fig. 20B, C). Overall, we observed an augmented amount of pre-stimulated WT $CD8^{+}$ T_{EX} population ($TOX^{hi}PD1^{hi}$) at 30 dpi (70%) compared to unstimulated WT T cells (40%) (Fig. 20B, C). Generally, T_{EX} cells also demonstrate impairment in effector cytokine production[134]. In our experiments, lessened exhaustion of pre-stimulated NFATc1-deficient T cells was supported by enhanced cytokine production observed at 35 dpi (Fig. 19F). In contrast, although we detected $TOX^{hi}PD1^{hi}$ donor T_{EX} cells when unstimulated T cells were transplanted, still NFATc1 deficiency reduced the level of cytokines, especially IFN-γ, at 30 dpi (Fig. 20D). Moreover, a higher percentage of NFATc1-deficient Treg was sustained even at 30 dpi (Fig. 20E) compared to WT, which was not the case with transplantation of pre-stimulated NFATc1-deficient T cells (Fig. 19B). In spite of those differences, CD8 to CD4 ratio changed in unstimulated NFATc1-deficient donor T cells (Fig. 20F) similar to pre-stimulated NFATc1-ablated donor T cells. (Fig. 19A).

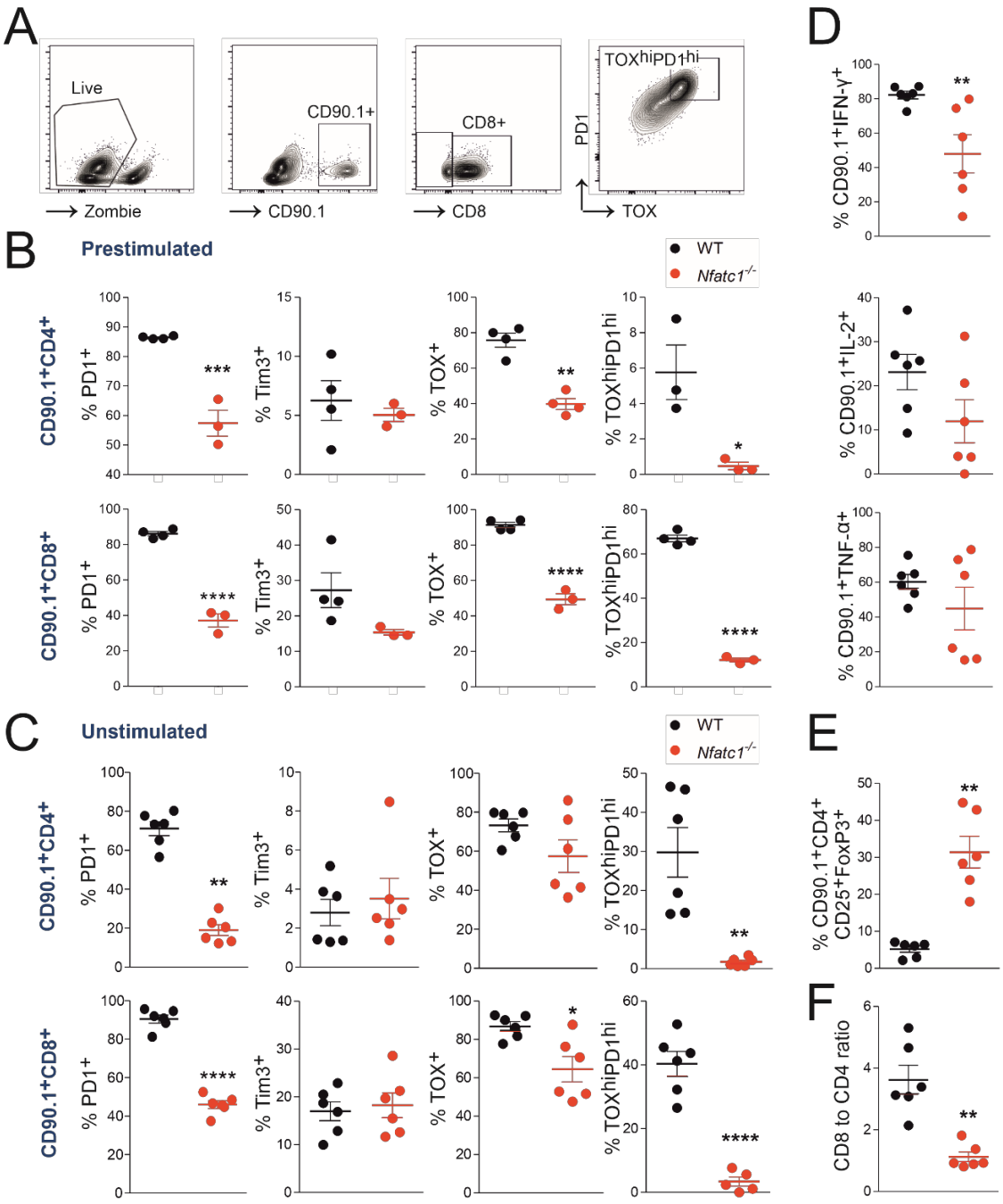

Figure 20. **NFATc1 is required for the exhaustion of donor T cells in the allo-HCT model.**

A. Gating strategy for identifying TOX^{hi}PD1^{hi} T_{EX} cells. **B-E.** Data represent n≥3, Student's unpaired t test (*p<0.05, **p<0.01 ***p<0.001, ****p<0.0001). **B.** CD3$^+$ T cells obtained from WT or *Nfatc1$^{fl/fl}$.Cd4cre* mice were pre-stimulated with anti-CD3+anti-CD28+IL-2 for 3 d and rested in IL-2 containing media for another 3 d before transplantion into irradiated BALB/c recipients according to Fig. 15A. On 30 dpi mice were sacrificed and splenocytes were stained for surface markers CD90.1, CD8, PD1, Tim3, and intracellular marker TOX and analysed by flow cytometry. CD8$^-$ T cells were considered as CD4$^+$ T cells. **C-F.** Unstimulated CD3$^+$ T cells (0.5x10^6) obtained from WT or *Nfatc1$^{fl/fl}$.Cd4cre* mice were directly transplanted in irradiated BALB/c recipients along with 5x10^6 BM cells obtained from *Rag1$^{-/-}$* mice. CD8$^-$ T cells were considered as CD4$^+$ T cells. **C.** Mice were sacrificed 30 dpi and splenocytes were stained for surface markers CD90.1, CD8, PD1, Tim3, and intracellular marker TOX and analysed by flow cytometry. **D.** At 30 dpi splenocytes were re-stimulated with PMA/ionomycin along with brefeldin/monensin for 6 h. Cells were stained for surface markers CD90.1 and CD8. Intracellular staining of IFN-γ, IL-2, and TNF-α was performed. **E.** Treg (CD90.1$^+$CD8$^-$CD25$^+$FoxP3$^+$) frequency was quantified by surface CD25 and nuclear FoxP3 staining in splenocytes at 30 dpi using FoxP3 staining kit. **F.** CD8 to CD4 ratio of donor T cells from splenocytes at 30 dpi.

9.1.12 In unstimulated T cells, CRISPR efficiency depends on the electroporator

Realizing that single NFAT ablation in pre-stimulated T cells can worsen aGvHD over time, we had to reconsider manipulating and transferring unstimulated/naive T cells, although the efficiency of gene ablation, as well as retained viability, had been so much superior with pre-stimulated T cells (Fig. 10). We simply tried to nucleofect by making use of a more recent version of the electroporator, 'Nucleofector 4D'. The technology and electrode material are different between these instruments (Aluminium for IIb and conductive polymer for 4D) and even the pre-set programs are not comparable between them. CD90, PD1, and NFATc1 expression were evaluated after two gRNAs per gene had been transfected into naive Cas9^{+}CD3^{+} T cells and all three proteins could now competently be reduced (Fig. 21A, B). Survival of naive T cells had been another issue (Fig. 10C). First, we re-evaluated the need for pre-culturing the naive Cas9^{+}CD3^{+} T cells in IL-7[91]. No influence on survival could be observed by the addition of IL-7 for overnight rest, but undoubtedly, an improved knockout efficiency in the absence of IL-7 before nucleofection for three genes tested (*Cd90* in Fig. 21C).

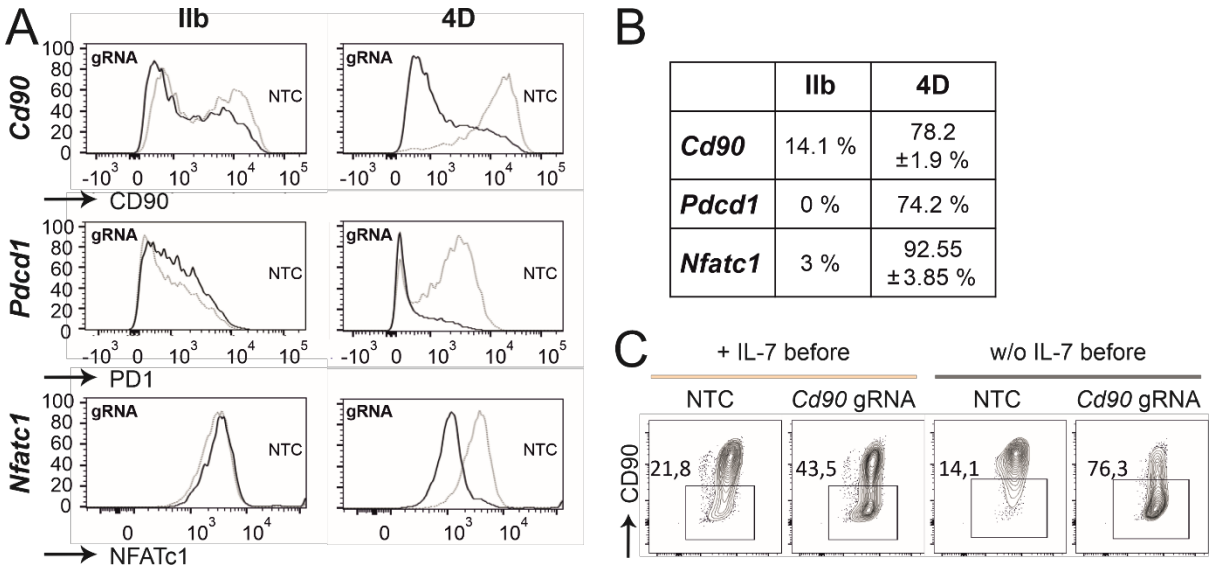

Figure 21. **Nucleofector 4D is superior to Nucleofector IIb for gene-ablation in naive Cas9^{+}CD3^{+} T cells.**

A. Comparison of two nucleofector versions for knocking out CD90 (gRNA 2+3), PD1 (gRNA 1+2), and NFATc1 (gRNA 4+8+9) by gRNA-only nucleofection in resting Cas9^{+}CD3^{+} T cells analysed by flow cytometry after 3 d rest with IL-7 and 3 d of stimulation. **B.** Table for unstimulated T cells comparing the knockout efficiencies with two versions of the electroporator; mean ± SD. **C.** CD90 KO (gRNA 2+3) with and without overnight IL-7 pre-incubation, followed by nucleofection, 3 d rest with IL-7, and 3 d of stimulation.

Next, we evaluated how nucleofected cells could be supported *in vitro* before stimulation. Different concentrations of IL-7 were given alone or in combination with IL-2 over three days after nucleofection. In the presence of IL-7, nucleofected naive $Cas9^{+}CD3^{+}$ T cells survived better (Fig. 22A). Here, any addition to 5 ng/ml IL-7 was not superior. $CD62L^{+}CD44^{-}$ naïve T cell frequency was kept up, while T_{CM} and T_{EM} occurrence was even counteracted by IL-7 in $CD4^{+}$ and $CD8^{+}$ T cells (Fig. 22B). Treg, which are highly sensitive *in vitro*, survived in sufficient frequencies, but surprisingly did not benefit from a further addition of IL-2. To test whether IL-2 was functional, we repeated the experiment including IL-2 alone (Fig. 22C-E). Compared to IL-7 or IL-7 plus IL-2, IL-2 alone negatively affected the overall survival of $CD3^{+}$ T cells, but could in a known feedback loop via STAT5 activation upregulate CD25 (Fig. 22C). The percentage of Treg was indeed supported by IL-2, although absolute Treg numbers did not differ between IL-2, IL-7, or double treatment (Fig. 22D). Since IL-2 enforces T_{CM} in $CD4^{+}$ and T_{EM} in $CD8^{+}$ T cells (Fig. 22E), such treatment is not advisable if one wants naive T cells for analyses or transfer.

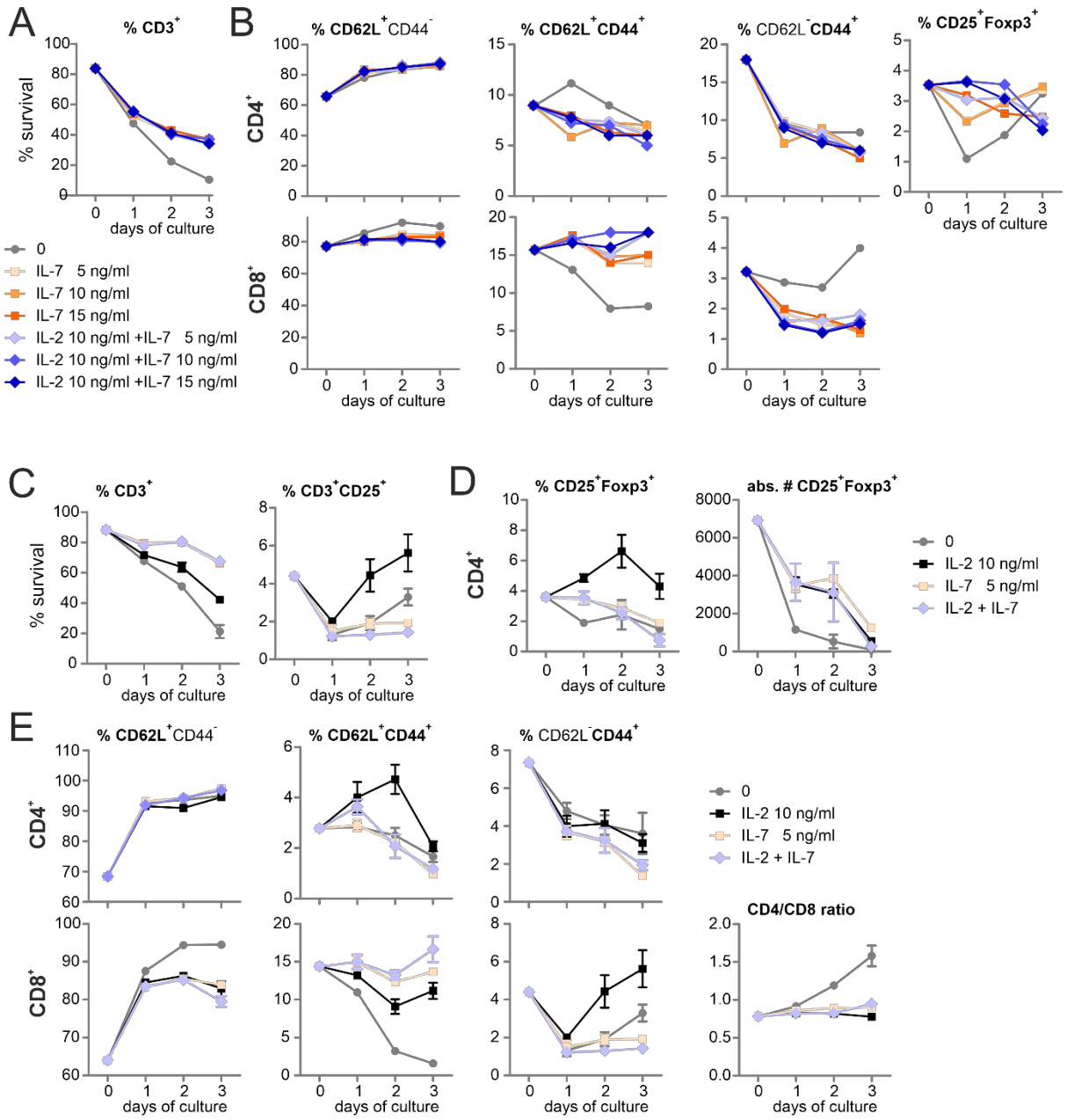

Figure 22. **Low dose IL-7 treatment after nucleofection preserves the naive status and survival the best during *in vitro*-cultures.**

A-B. Flow cytometry analyses over three days of resting Cas9$^+$CD3$^+$ T cells treated with 5, 10, and 15 ng/ml IL-7 in the absence or presence of 10 ng/ml IL-2 after NTC nucleofection. **A.** Percentage of living CD3$^+$ T cells analysed by Zombie live-dead staining, mean, n=3. **B.** Frequency of CD62L$^+$CD44$^-$ naive, CD62L$^+$CD44$^+$ T_{CM} and CD62L$^-$ CD44$^+$ T_{EM} CD4$^+$ and CD8$^+$ T cells as well as CD4$^+$CD25$^+$Foxp3$^+$ Treg determined by surface and intracellular staining followed by flow cytometry. **C-E.** Flow cytometry analyses of Cas9$^+$CD3$^+$ T cells nucleofected with NTC gRNA and cultured *in vitro* with/without 5ng/ml IL-7 and/or 10ng/ml IL-2 up to 3 d; mean ± SD, n=3. **C.** Viability measured by Zombie live-dead staining, staining of CD3 and CD25 to measure activated T cells. **D.** Treg percentage and absolute count by staining of CD4, CD25, and intracellular staining of Foxp3. **E.** Frequency of CD62L$^+$CD44$^-$ naive, CD62L$^+$CD44$^+$ T_{CM} and CD62L$^+$CD44$^+$ T_{EM} CD4$^+$ and CD8$^+$ T cells. CD4 to CD8 ratio was calculated from percentage.

For *in vivo* experiments, many cells might be needed, but doubling the number of naive Cas9$^+$CD3$^+$ T cells per cuvette during nucleofection decreased the knockout efficiency, which was noticeable for CD90 and NFATc1 (Fig. 23A). Lastly, we tested if gRNA-only nucleofected naive Cas9$^+$CD3$^+$ T cells need to be rested *in vitro* to achieve the loss of target gene expression during transfer mouse models. After three days of *in vitro* stimulation, the 2 d period of rest appeared to enhance the number of gene-ablated cells (Fig. 23B). On the other hand, cells, which were immediately transferred after nucleofection, exhibited the same high degree of 80% knockout, when regained after six days as when they had been rested in IL-7 post nucleofection for two days prior to transplantation (Fig. 23B). Since we nucleofected the mixture of resting CD3$^+$ T cells, it was necessary to document whether the minor, but important subtype of Treg got targeted together with Tcons. Indeed, the knockout efficiency was high in Treg as well, when measured *ex vivo*, six days after GvHD induction (Fig. 23C).

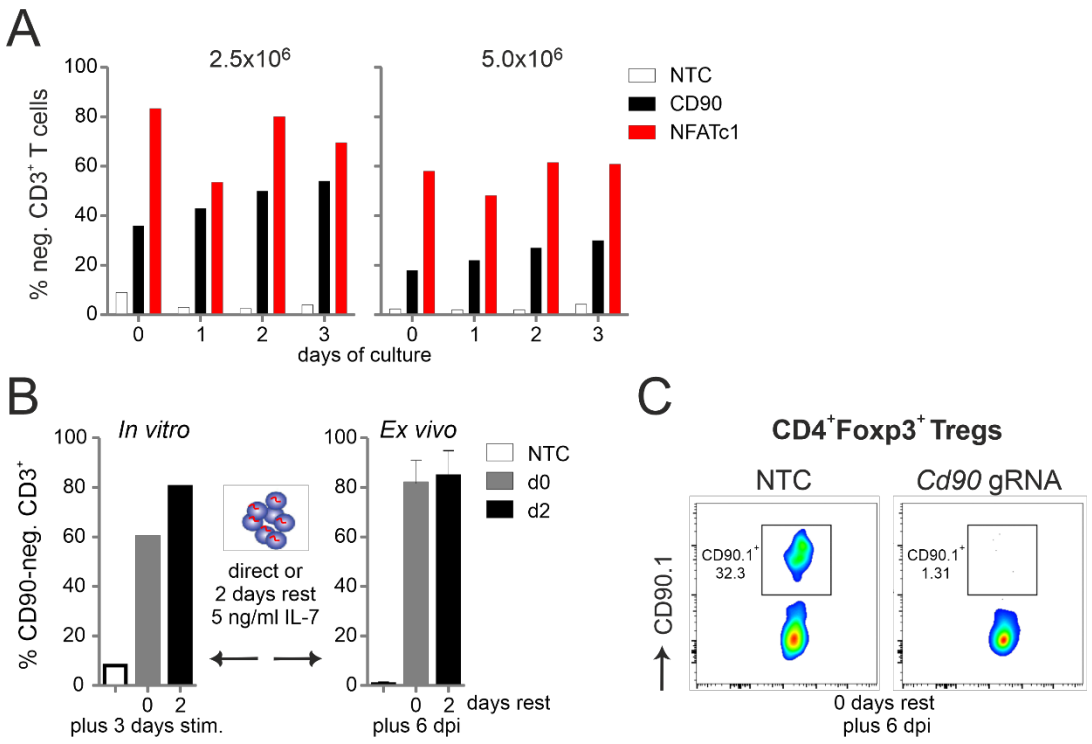

Figure 23. **Resting cells with low dose IL-7 is required for efficient gene editing in naive Cas9$^+$CD3$^+$ T cells *in vitro* but not *in vivo*.**

A. 2.5x10^6 or 5x10^6 Cas9$^+$CD3$^+$ T cells were nucleofected with *Cd90* gRNA_2 or *Nfatc1* gRNA_4, cultured with IL-7 for indicated times, and analyzed by flow cytometry after 3 d stimulation. **B.** CD90.1 staining and flow cytometry analysis of CD3$^+$ T cells not rested or rested for 2 d with IL-7 post gRNA nucleofection (*Cd90* gRNA 1+2+3) followed by 3 d *in vitro* stimulation, n = 1; For *ex vivo* analysis nucleofected T cells (0.6x10^6) were directly or after 2 d rest transplanted into irradiated BALB/c recipients along with BM cells (5x10^6) and analysed *ex vivo* 6 dpi; n=2, mean + SD. **C.** CD90.1 expression on CD4$^+$Foxp3$^+$ T cells *ex vivo* 6 dpi from LN cells.

We ensured that the degree of protein loss of NFATc1 achieved by our CRISPR/Cas9 method is comparable with the T cells isolated from *Cd4cre.Nfatc1*$^{fl/fl}$ mouse (Fig. 24). This proved NFATc1 knockout by our method to be highly efficient. Thus, all Cas9^{+}CD3^{+} T cells can be efficiently gene-targeted by gRNA-only without pre-stimulation if the right nucleofector is used, they are supported directly by the *in vivo*-situation or by low-dose IL-7 after nucleofection and before activation *in vitro*.

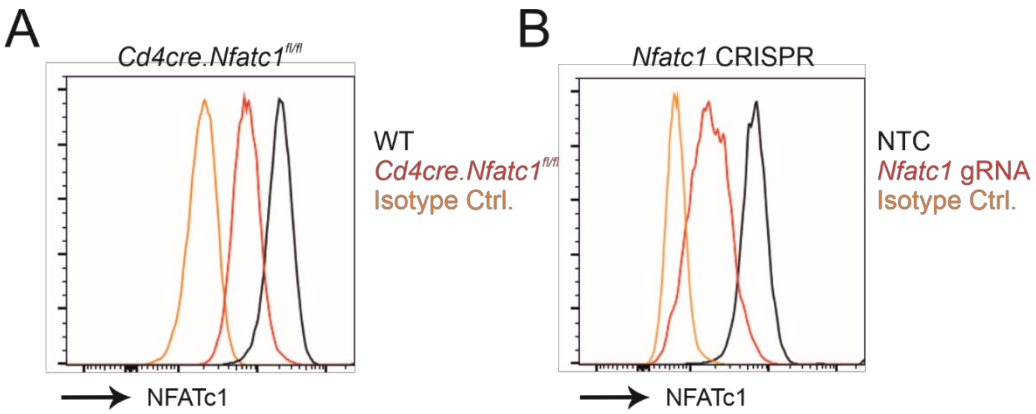

Figure 24. **CRISPR/Cas9 knockout of NFATc1 in Cas9^{+} T cells is comparable to *Cd4cre.Nfatc1*$^{fl/fl}$ mouse T cells.**

A. CD3^{+} T cells were isolated from *Cd4cre.Nfatc1*$^{fl/fl}$ or WT mice stimulated with anti-CD3+anti-CD28+IL-2 for 3 d followed by PMA/ionomycin restimulation for 5 h. **B.** CD3^{+} T cells were isolated from Cas9^{+} mice and immediately nucleofected with NTC or *Nfatc1* gRNA 4+8+9, rested for 2 d with IL7, and then stimulated with anti-CD3+anti-CD28+IL-2 for 3 d followed by PMA/ionomycin restimulation for 5 h. Cells were harvested after stimulation and nuclear staining of NFATc1 with 7A6 mAb or IgG isotype control (Ctrl.) was performed using FoxP3 staining kit.

9.1.13 The procedure of nucleofection only minimally affects the metabolism of Cas9^{+}CD3^{+} T cells

From their naïve to effector function, T cells undergo metabolic reprogramming and shift from oxidative phosphorylation (OXPHOS) towards aerobic glycolysis. The co-secretion of protons and lactate during aerobic glycolysis results in the acidification of the media, which can be measured as the extracellular acidification rate (ECAR) in the Glycolysis Stress Test (GST). The Mitochondrial Stress Test (MST) is based on changes in the oxygen consumption rate (OCR) that is indicative of OXPHOS. To determine whether nucleofection of naive Cas9^{+}CD3^{+} T cells influences their metabolic plasticity during activation, we performed metabolic flux analyses in cells, which underwent nucleofection with or without NTC in comparison to stimulated cells. As anticipated, without stimulation, ECAR and OCR activity were hardly detectable (data not shown) in T cells, while overnight (15 h) stimulation revealed substantial glycolytic and OXPHOS activity. Nucleofection, irrespective of incorporated RNA, affected both glycolysis and OXPHOS. The strongest effects were observed for maximal glycolytic capacity and

glycolytic reserve, while the basal OCR/ECAR ratio was not skewed suggesting a balanced effect on the basal bioenergetic phenotype (Fig. 25A). Strikingly, continuously (for 72 h) stimulated T cells did not display any differences in terms of their metabolic profile (Fig. 25B). The latter observation indicates that nucleofection of naive $Cas9^{+}CD3^{+}$ T cells might stress them (metabolically) only transiently and that upon a short recovery period T cells preserve their full capacity to meet their basic bioenergetic demands, but also to adapt to increased demands through upregulation of aerobic glycolysis or OXPHOS.

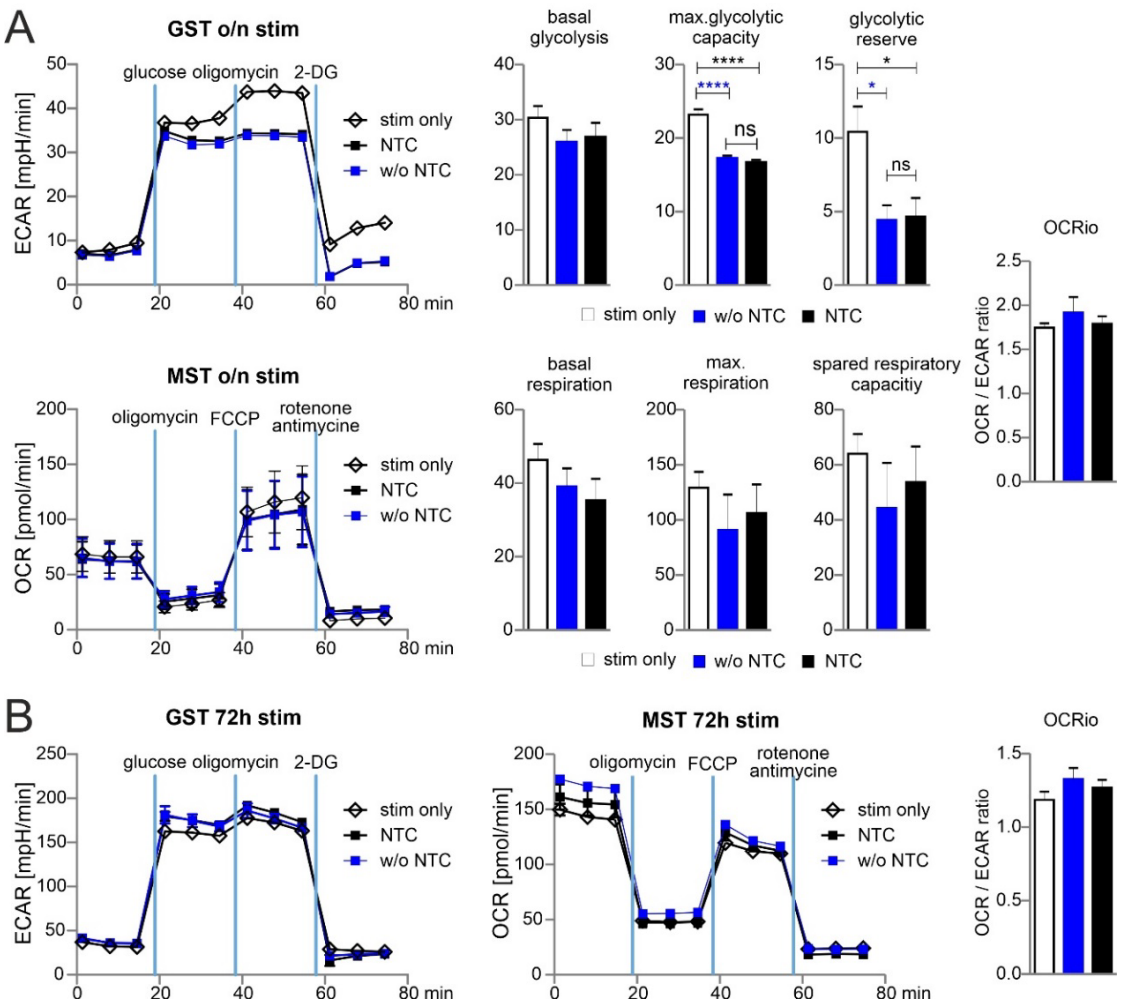

Figure 25. **The glycolytic reserve has been compromised upon electroporation of T cells.**

A. Mouse $Cas9^{+}CD3^{+}$ T cells were nucleofected followed by overnight stimulation with anti-CD3+anti-CD28+IL-2. Metabolic status was analysed by performing a GST and MST on the XFe96 Seahorse metabolic flux analyzer. ECAR was measured at baseline, in response to glucose to calculate basal glycolysis, after oligomycin injection for max. glycolytic capacity and reserve, and after 2-DG injection for non-glycolytic acidification. Basal glycolysis = glucose - baseline; glycolytic capacity = oligomycin - baseline; glycolytic reserve = capacity - glycolysis. Oxygen consumption rate (OCR) was measured under basal condition followed by sequential injection of oligomycin, FCCP, and rotenone together with antimycin A to shut down mitochondrial respiration (values represent non-mitochondrial respiration). Basal respiration = baseline - non-mitochondrial respiration; maximal respiration = FCCP - non-mitochondrial respiration; spare respiratory capacity = maximal respiration - basal respiration. Student's unpaired two-tailed t-test; n=3, mean ± SD of two independent experiments, (*$p<0.05$, ****$p<0.0001$). **B.** Naive mouse $Cas9^{+}CD3^{+}$ T cells were nucleofected followed by 72 h stimulation with anti-CD3+anti-CD28+IL-2. Metabolic status was determined as for A. n=3, mean + SD of two independent experiments.

9.1.14 Naive NFAT-targeted Cas9$^+$CD3$^+$ T cells do not cause severe GvHD

Pre-stimulated and nucleofected Cas9$^+$CD3$^+$ T cells were able to cause GvHD in a major mismatch model, during which NFAT deficiency reduced T-cell expansion and proliferation (Fig. 15, Fig. 16). However, the clinical score was untypically low with pre-stimulated T cells, while NFAT single-ablated T cells could not protect over time (Fig. 17, Fig. 18). Now we co-transplanted naive Cas9$^+$CD3$^+$ T cells with BM cells (Fig. 26A). The clinical scores doubled, demonstrating the undisturbed power of naive T cells (Fig. 26B). Knockout of NFATc1, NFATc2, or both reduced the clinical scores. Accordingly, NFAT-ablated cells measured by *in vivo* BLI, expanded significantly less (Fig. 26C, D). Next, we analysed whether it would be advisable to rest naive, NFAT-ablated Cas9$^+$CD3$^+$ T cells in IL-7 before transfer. We transferred the same number of BM cells, but a substantially downgraded number of T cells, still causing a clinical score above 6 (Fig. 26E). Two days of rest enabled the T cells to transmit the high GvHD score earlier, but their potential for induction of clinical scores and weight loss were alike irrespective of rest or immediate transfer after nucleofection. Knockout of NFATc1 by gRNA-only in naive Cas9$^+$CD3$^+$ T cells limited GvHD symptoms significantly in both settings (Fig. 26E). We conclude that gRNA-only nucleofection of unstimulated Cas9$^+$CD3$^+$ T cells not only leads to efficient gene editing but preserves their functional abilities upon allo-HCT.

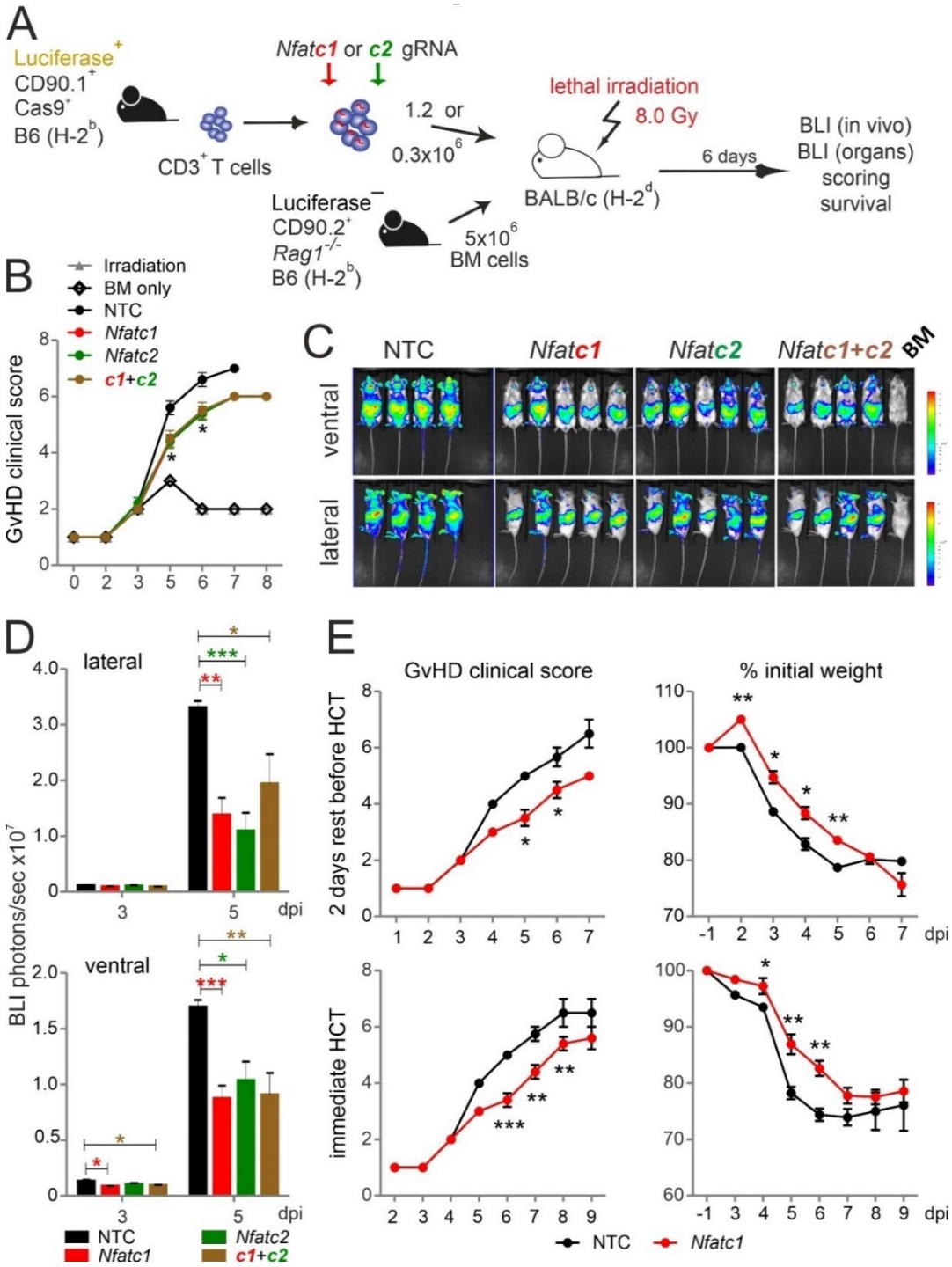

Figure 26. ***Nfatc1*$^{-/-}$ 'CRISPR'ed unstimulated murine Cas9^{+}CD3^{+} T cells ameliorate aGvHD**.

A. Experimental set up of sole NFAT-specific gRNA nucleofection and GvHD induction due to an H-2^{b} → H-2^{d} transfer with naive Cas9^{+}CD3^{+} T cells. **B-E.** gRNA used: Nfatc1 gRNA 4+8+9, Nfatc2 gRNA 1+2+3. **B-D.** Naive Cas9^{+}CD3^{+} T cells were nucleofected with NTC, *Nfatc1*, *Nfatc2*, and *Nfatc1* plus *Nfatc2* targeting gRNAs and 1.2x10^{6} cells transplanted immediately thereafter. **B.** Clinical scores of GvHD-induced mice determined daily for 8 days. **C.** Ventral and lateral *in vivo* BLI at 5 dpi. Data represent two independent experiments. **D.** Quantitation and statistical analyses of BLI of living mice in lateral and ventral view on 3 and 5 dpi. Plotted are photons per second. Student's two-tailed t-test (*p<0.05, **p<0.01, ***p<0.001); n=5, mean +SD. **E.** Naive Cas9^{+}CD3^{+} T cells were nucleofected by NTC or *Nfatc1* targeting gRNAs and 0.3x10^{6} cells transplanted after 2 days of rest in comparison to immediately. Clinical scores and weight loss were assessed daily over the indicated period. Student's two-tailed unpaired t-test (*p<0.05, **p<0.01, ***p<0.001); n=5, Mean ± SD.

9.1.15 Transfer of NFAT-ablated naive T cells protect mice from GvHD over time

To evaluate if the direct transfer of NFAT-deficient T cells created by gRNA-only nucleofection in naive $Cas9^+CD3^+$ T cells impinged long-term protection from severe GvHD, we once again knocked out NFATc1. NFATc1 ablation was verified in the total $CD3^+$ T cell population and individually in $CD4^+$ and $CD8^+$ Tcon as well as $CD4^+Foxp3^+$ Treg, each time in comparison to NTC nucleofection, by intracellular flow cytometry (Fig. 27A). When we rested some of those cells in IL-7 for two days, stimulated them with anti-CD3+anti-28+IL-2 and restimulated them with PMA/Ionomycin for 5 h *in vitro*, IL-2, and IFN-γ expression was compromised due to NFATc1 deficiency (Fig. 27B). *In vivo*, different from the transfer with pre-stimulated T cells, clinical scores, as well as weight loss, remained less severe over time in comparison to the transfer of naive WT $Cas9^+CD3^+$ T cells (Fig. 27C). Accordingly, all mice, which received NTC nucleofected $Cas9^+CD3^+$ T cells, had died by 35 dpi, while half of all mice getting NFATc1 knockout T cells were still alive after 90 dpi. Similarly, NFATc2 ablation in naive $Cas9^+CD3^+$ T cells and their subsequent transfer limited the degree of GvHD stably over time (Fig. 27D). With this, naive T cells behaved the same in our major mismatch model irrespective of whether they were gathered from NFAT-deficient mice[63] or whether they were knocked out *in vitro* by gRNA-only nucleofection of $Cas9^+CD3^+$ T cells.

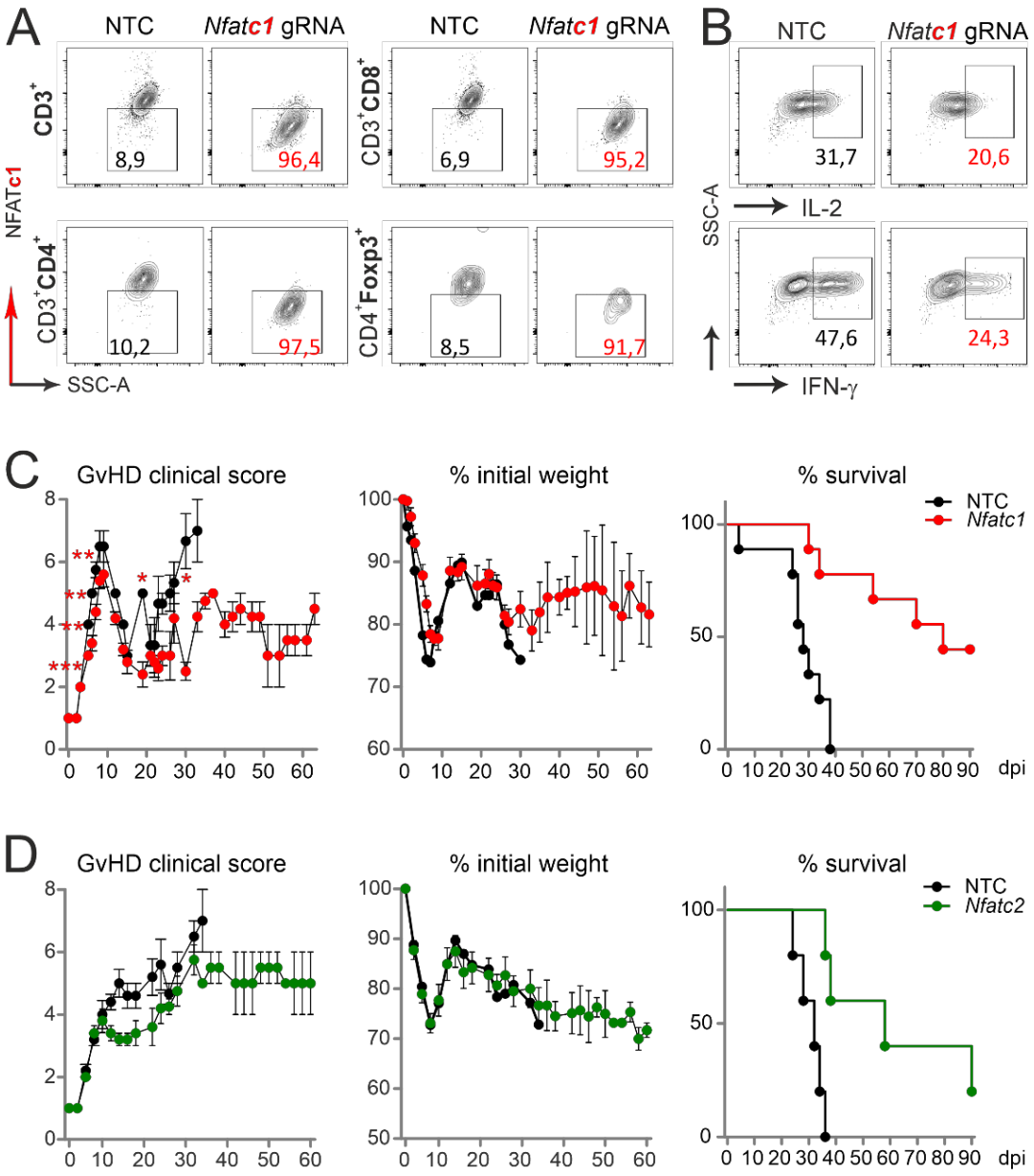

Figure 27. ***Nfatc1*$^{-/-}$ and *Nfatc2*$^{-/-}$ 'CRISPR'ed unstimulated murine Cas9^{+}CD3^{+} T cells protect over time and prolong survival.**

A-B. Naive Cas9^{+}CD3^{+} T cells were nucleofected by NTC or *Nfatc1*-targeting gRNAs and knockout efficiency was assessed by surface and intracellular flow cytometry after 2 days of IL-7 rest and 3 days of stimulation *in vitro*. **A.** Detection of NFATc1 in CD4^{+} and CD8^{+} as well as CD4^{+}Foxp3^{+} T cells. **B.** Intracellular IL-2 and IFN-ɣ staining in *Nfatc1* gRNA-nucleofected naïve Cas9^{+}CD3^{+} T cells. **C-D.** Naive Cas9^{+}CD3^{+} T cells were nucleofected by NTC or NFAT-specific gRNAs (*Nfatc1* gRNA 4+8+9, *Nfatc2* gRNA 1+2+3) and 0.3x10^{6} cells transplanted directly thereafter (H-2^{b} → H-2^{d} transfer). Clinical scores and weight loss were determined over 60 days, whereas survival over 90 days. Student's two-tailed t-test (*p<0.05, **p<0.01, ***p<0.001); mean ± SEM, n≥5. Data represent two independent experiments.

9.1.16 Ablation of the NFAT target gene *Irf4* in donor T cells ameliorates GvHD

Next, we wanted to demonstrate that our gRNA-only nucleofection method in Cas9$^+$ T cells can be utilized to investigate the role of any gene expressed in T cells during allo-HCT, without the need of availability of gene-knockout transgenic mice. Besides effector molecules like CD40L or cytokines, NFAT induces transcription factors, thereby extensively influencing gene expression. As we found NFAT to upregulate and cooperate with IRF4[135, 136], we determined whether IRF4 is a direct target gene. Both NFATc1 and NFATc2 are bound to the immediate upstream region of *Irf4* in ChIPseq experiments of CD8$^+$ T cells (Fig. 28A)[24, 90]. Accordingly, constitutive active NFATc2 transactivated the *Irf4* promoter in a reporter assay (Fig. 28B), while activation of T cells from *Nfatc1^{caaA}*.dLckcre mice, which express constitutive active NFATc1/αA in post-thymic T cells, had a strong positive impact on IRF4 protein levels (Fig. 28C). This prompted us to test our established method of CRISPR/Cas9 editing by gRNA-only nucleofection with this NFAT target gene for allo-HCT. gRNAs for exon 1 and exon 6 were tested in different combinations. The combination of three exon-1-specific gRNAs for nucleofection of naive Cas9$^+$CD3$^+$CD90.1$^+$ T cells achieved 80% IRF4-negative T cells after 2 days rest with IL-7 and 3 days of stimulation *in vitro* (Fig. 28D). Editing of *Irf4* and direct transfer in conjunction with allo-HCT did not prevent weight loss but reduced the clinical score significantly (Fig. 28E, F). Proliferation and expansion of transplanted T cells were extensively impaired (Fig. 28G). This could also be observed *ex vivo* in individual organs (Fig. 28H, I).

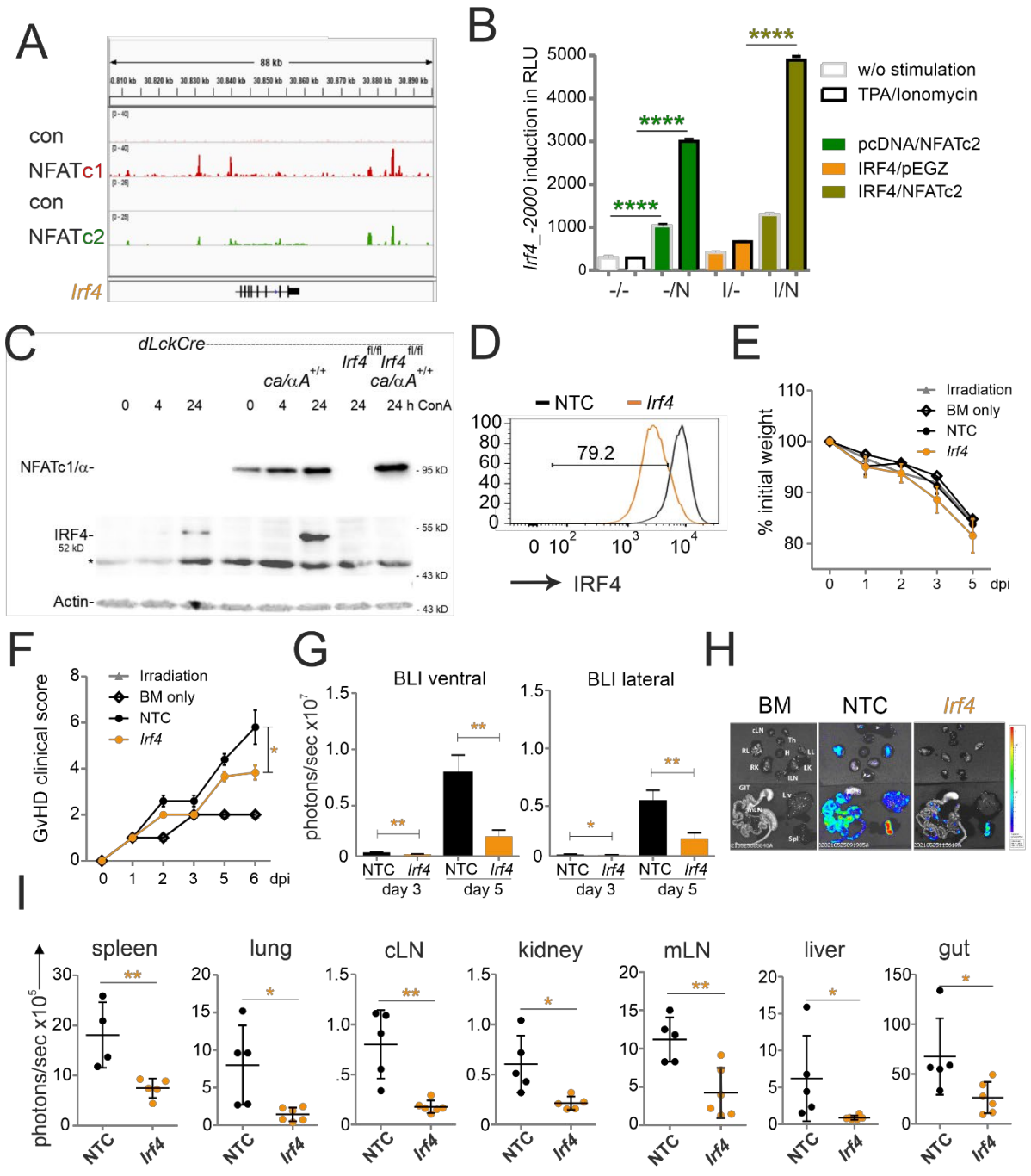

Figure 28. **NFAT target gene *Irf4* knockout in naïve T cells ameliorates aGvHD.**

A. Binding of NFATc1 and NFATc2 to the *Irf4* locus. Shown are own and publicly available ChIP-seq data for CD8⁺ T cells. **B.** Luciferase assays of *Irf4* proximal promoter (836 bp) in EL4 cells. Cells were co-transfected with the empty vectors pEGZ and/or pcDNA (-/-), as well as constructs encoding either constitutive active NFATc2 (-/N), IRF4 (-/I), or both (N/I). Cells were left unstimulated or activated with TPA/Ionomycin; n≥3. **C.** *In vitro* ConA-stimulated lymphocytes collected from spleen and LNs of *dLckCre* (WT), *Nfatc1caaA.dLckCre* (*ca/αA*$^{+/+}$), *Irf4*$^{fl/fl}$*.dLckCre* (*Irf4*$^{fl/fl}$), and double transgenic (*Irf4*$^{fl/fl}$*.ca/αA*$^{+/+}$) mice were analysed by whole-cell extracts and immunoblots with anti-NFATc1/α (specific for the α-peptide), anti-IRF4, and anti-β-Actin. **D-I.** Naive Cas9⁺CD3⁺ T cells were nucleofected with either NTC or a combination of three gRNAs targeting *Irf4*. **D.** IRF4 knockout efficiency was analysed in Cas9⁺CD3⁺ T cells by intracellular staining and flow cytometry post 2 d rest with IL-7 and 3 d of stimulation. **E-I.** GvHD induction due to an H-2^{b} →H-2^{d} transfer with naïve Cas9⁺CD3⁺ T cells. Data represent mean ± SD from one experiment with n≥5 mice per group; Mann Whitney test (*p<0.05, **p<0.01). **E.** Weight was measured post-transplantation up to 5 dpi and the percentage of weight loss was calculated considering d0-weight as 100%. **F.** Clinical score of GvHD-induced mice determined daily until 6 dpi. **G.** Quantitation of ventral and lateral *in vivo* BLI at 3 and 5 dpi. **H.** *Ex vivo* BLI images of lymphoid and non-lymphoid organs at 6 dpi. **I.** Quantitation of *ex vivo* BLI analyses of lymphoid and non-lymphoid organs at 6 dpi.

Accordingly, the absolute number of *Irf4*$^{-/-}$ CD90.1^{+} T cells, including that of tTreg was less compared to NTC-nucleofected T cells (Fig. 29A). However, the frequency of *Irf4*$^{-/-}$ Treg was preserved within the transplanted T-cell fraction (Fig. 29A). This might be due to relatively more IL-2 and TNF-α-expressing CD4^{+} and CD8^{+} splenic T cells (Fig. 29B, C), which support Treg via CD25, and TNFR2. On the other hand, we observed an enhanced Th1 phenotype, i.e. IFN-γ and again TNF-α production, caused by IRF4 ablation in CD4^{+} and CD8^{+} T cells (Fig. 29B, C). Nevertheless, the absolute numbers of cytokine expressing as well as GzmB and Prf1-positive CD4^{+} and CD8^{+} *Irf4*$^{-/-}$ T cells were contracted significantly in comparison to NTC-nucleofected T cells (Fig. 29D, E). In sum, despite the shift towards an unfavourable Th1 differentiation, deletion of the NFAT target gene IRF4 in co-transplanted naive T cells during allo-HCT protected from severe GvHD.

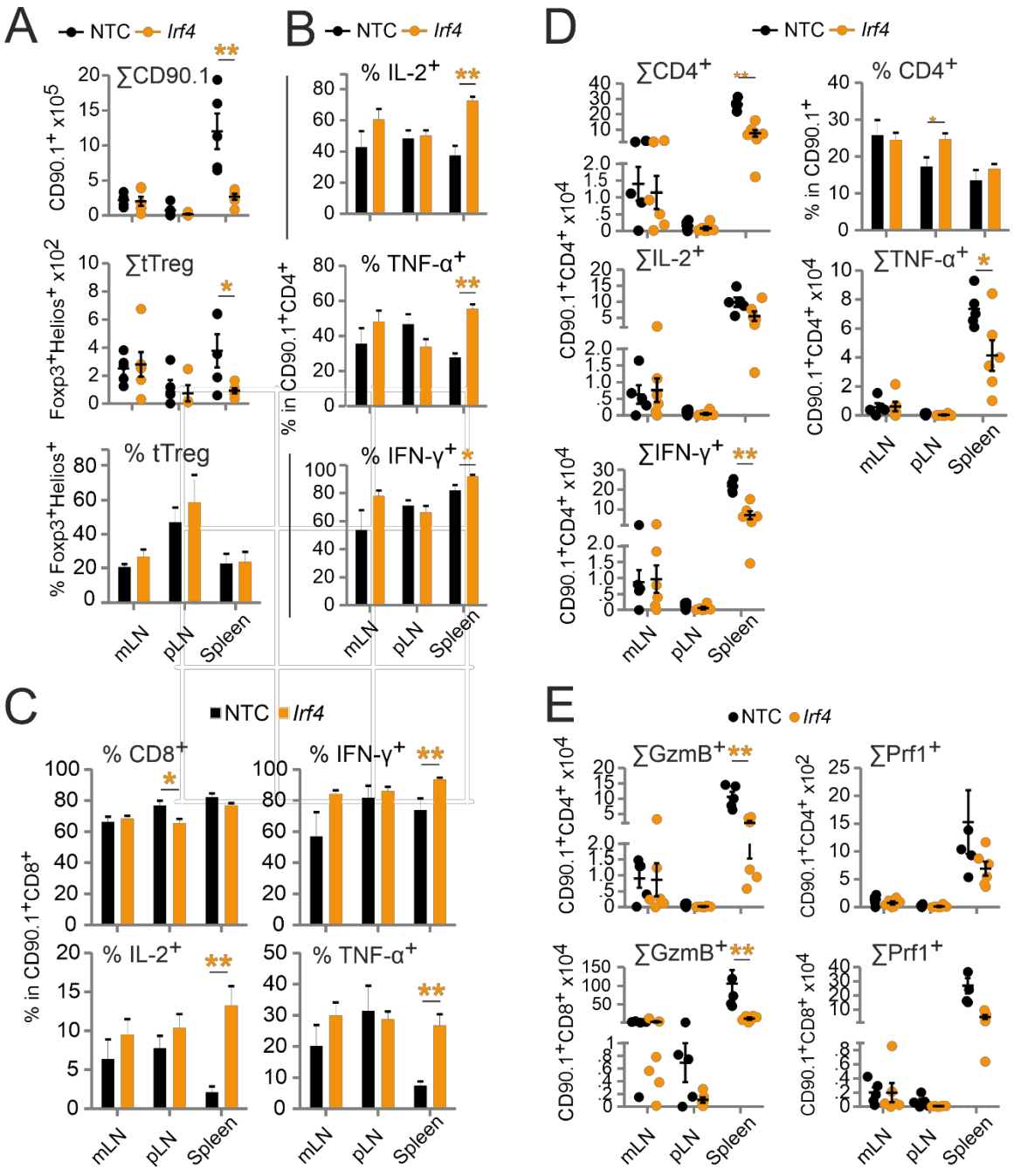

Figure 29. ***Irf4*$^{-/-}$ 'CRISPR'ed unstimulated murine Cas9$^+$CD3$^+$ T cells ameliorate GvHD despite enhanced Th1 differentiation.**

A-E. Naive Cas9$^+$CD3$^+$ T cells were nucleofected with either NTC or a combination of three gRNAs targeting *Irf4*. GvHD induction due to an H-2^b →H-2^d transfer with naïve Cas9$^+$CD3$^+$ T cells. Data represent mean ± SD from one experiment with n≥5 mice per group; Mann Whitney test (*p<0.05, **p<0.005). Mice were sacrificed and the organs analysed on 6 dpi. **A.** Absolute count of CD90.1$^+$ donor T cells and CD90.1$^+$CD4$^+$CD25$^+$Foxp3$^+$ donor T cells by flow cytometry. Percentage of Helios$^+$ tTreg within CD90.1$^+$CD4$^+$CD25$^+$Foxp3$^+$ donor T cells by intracellular flow cytometry. **B.** Frequency of IL-2$^+$, TNF-α$^+$, and IFN-γ$^+$ within CD90.1$^+$CD4$^+$ donor T cells determined by intracellular staining and flow cytometry **C.** Frequency of CD8$^+$ in CD90.1$^+$ and IL-2$^+$, TNF-α$^+$, and IFN-γ$^+$ within CD90.1$^+$CD8$^+$ donor T cells determined by intracellular staining and flow cytometry. **D.** Frequency and absolute count of CD90.1$^+$CD4$^+$ donor T cells. Absolute count of CD90.1$^+$CD4$^+$IL-2$^+$, CD90.1$^+$CD4$^+$TNF-α$^+$, and CD90.1$^+$CD4$^+$IFN-γ$^+$ donor T cells. **E.** Absolute numbers of GzmB and Prf1-positive CD90.1$^+$CD4$^+$ and CD90.1$^+$CD8$^+$ T cells determined by intracellular staining and flow cytometry.

9.2 Targeting NFAT in primary human T cells by CRISPR/Cas9 to reduce aGvHD and still confer GvL

The role of NFAT in mouse T cells has been widely studied using T cell-specific NFATc1 and total NFATc2 as well as NFATc3 knockout mice. In line, we have shown earlier that single NFAT ablation of NFATc1 or NFATc2 ameliorates GvHD and still confers GvL efficacy in mice[63, 68]. However, studies focusing on functional analysis of NFAT knockout in human T cells have been limited. Therefore, we asked whether single NFAT member ablation will also help in ameliorating aGvHD and still confer GvL in humans. In this study, we have set up a highly efficient CRISPR/Cas9 non-viral gene editing method to ablate NFAT in unstimulated and pre-stimulated human T cells. We evaluated the function of human NFAT-KO T cells *in vitro.* We have focused on GvHD-inducing proinflammatory cytokine secretion and tumor cell-killing ability of NFAT-ablated T cells. Additionally, we have also studied the function of $CD8^+$ CAR T cells upon NFAT deletion in this section.

9.2.1 Optimization of ribonucleoprotein-mediated CRISPR/Cas9 knockout in human T cells

Gene editing in human T cells is extremely useful and crucial for gene therapy as well as adoptive T cells therapy in clinics. Lentivirus and adenovirus-mediated Cas9 and gRNA delivery has been demonstrated to be barely efficient by several studies[137, 138]. Retrovirus-mediated gene knockout is more commonly used in the clinic, but still only results in moderate efficiency and yet requires flow cytometry sorting of knockout cells[139]. Moreover, retrovirus-mediated gene editing additionally requires pre-stimulation of the T cells which activates the TCR signaling pathway. Another important drawback is that viral genes can induce genotoxicity[140], humoral[141], and cellular immune responses[124] against vector backbones or virus-specific proteins that eventually interfere with effective gene transfer[142, 143, 144]. Recently, ribonucleoprotein (RNP)-mediated knockout of genes in human T cells has been demonstrated in a few studies and shown to be highly efficient when 3 gRNAs are simultaneously used per gene[91, 127]. Hence we wanted to use the RNP-mediated CRISPR/Cas9 knockout system, to target individual NFAT members in primary human $CD3^+$ T cells. Peripheral blood mononuclear cells (PBMCs) were isolated from peripheral blood and primary human $CD3^+$T cells were isolated from PBMCs. The workflows of our optimized RNP-mediated

gene knockout method in unstimulated and stimulated CD3⁺ T cells are described in Fig. 30A &B, respectively.

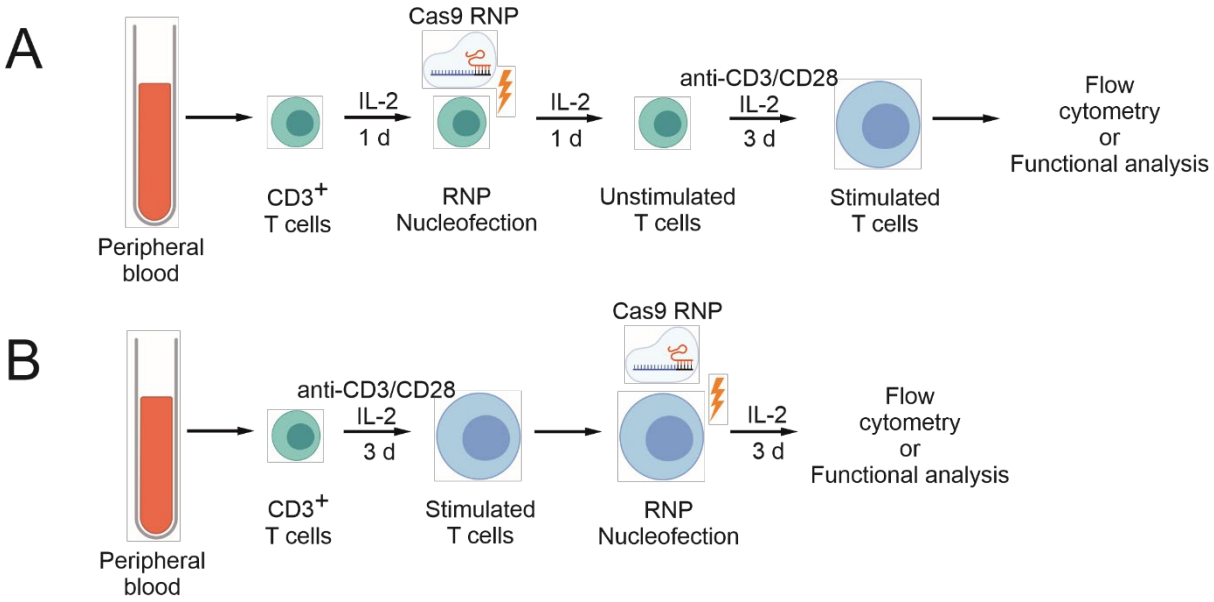

Figure 30. **Workflow of Cas9 RNP nucleofection-mediated CRISPR/Cas9 gene knockout in human T cells.**

A. Schematic of optimized CRISPR/Cas9 gene editing in unstimulated human T cells. **B.** Schematic of optimized CRISPR/Cas9 gene editing in stimulated human T cells.

To optimize a gene knockout in primary human T cells, we first targeted a cell surface chemokine receptor CXCR4 which is constitutively expressed on human CD3⁺ T cells using gRNAs tested by a previous study[91] (Table 1). First, we optimized the amount and ratio of Cas9 and gRNA. Also, the two manufacturer-recommended programs T-020 and T-023 were tested in Lonza Nucleofector IIb. For this, CD3⁺ T cells were stimulated with plate-bound 2.5 µg/ml anti-CD3, soluble 1 µg/ml anti-CD28 and 10 ng/ml IL-2 for 3 d before nucleofection (Fig. 30B). We prepared RNPs using *CXCR4* gRNA_1 and two different amounts, i.e. 10 µg or 5 µg of Cas9 protein to achieve 2:1 or 3:1 molar ratios of gRNA:Cas9. Three days after nucleofection, the loss of surface expression of CXCR4 was analysed by flow cytometry. A slight, but consistent increase in knockout efficiency and viability was observed when T cells were nucleofected using the T-023 program compared to the T-020 program (Fig. 31A, B). A clear improvement in loss of CXCR4 surface expression was detected with 10 µg compared to 5 µg of Cas9 when the T-023 nucleofection program was applied (Fig. 31A). Additionally, T-023 combined with a 3:1 ratio of gRNA:Cas9 resulted in a slightly superior knockout efficiency compared to the 2:1 ratio (Fig. 31A). We achieved a maximum loss in CXCR4 surface expression of 90.4% using T-

023, gRNA:Cas9 3:1, and 10 µg of Cas9 in pre-stimulated human CD3⁺ T cells with only one gRNA to target *CXCR4* (Fig. 31A, C). Hence, we chose T-023, gRNA:Cas9 3:1, and 10µg Cas9 as our optimized conditions. Similar to mouse experiments, non-targeting control (NTC) gRNA always served as the negative control. We further tested unstimulated CD3⁺ T cells. Purified human CD3⁺ T cells were cultured in 10 ng/ml IL-2 for 1 d before nucleofection with *CXCR4* gRNA_1-specific RNP using the T-023 program. One day after nucleofection, T cells were stimulated with anti-CD3, anti-CD28, and IL-2 for 3 d (Fig. 30A). After 3 d of stimulation, the loss in surface expression of CXCR4 was determined by flow cytometry. Similar to pre-stimulated T cells, we again achieved above 90% knockout efficiency when *CXCR4* was targeted in unstimulated human T cells using our optimized conditions (Fig. 31C).

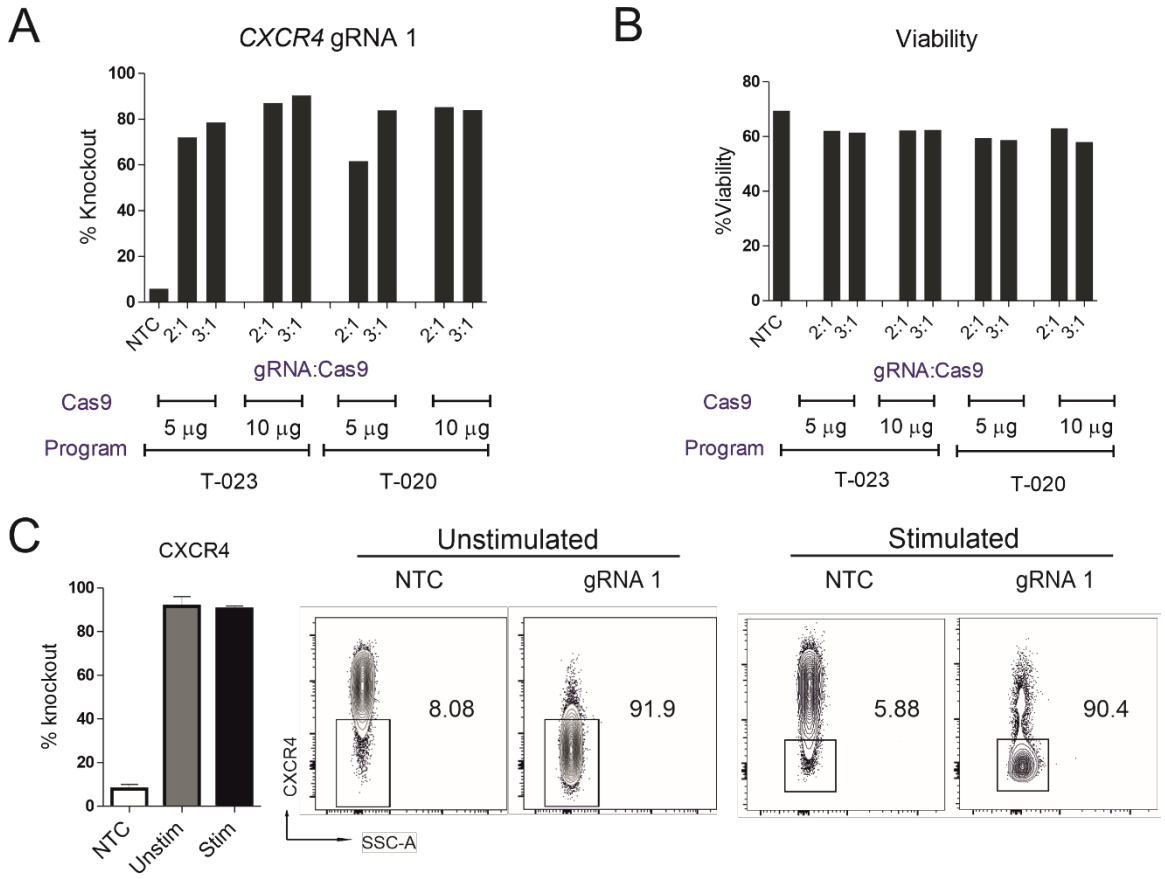

Figure 31. **Optimization of CRISPR/Cas9 gene editing in human T cells.**

A-B. Primary human CD3⁺ T cells were stimulated with anti-CD3, anti-CD28, and IL-2 for 3 d prior to nucleofection with RNP consisting of *CXCR4* gRNA_1 and recombinant Cas9 following the workflow described in Fig. 30B; n=1 from one experiment. **A.** Graphical representation of CXCR4 knockout efficiency by flow cytometry 3 d post nucleofection with 5 or 10 µg of Cas9, 2:1 or 3:1 gRNA:Cas9 ratios and preset programs T-023 or T-020. **B.** Viability of T cells determined by flow cytometry 3 d post nucleofection with 5 or 10 µg of Cas9, 2:1 or 3:1 gRNA:Cas9 ratios and preset programs T-023 or T-020. **C.** Bar diagram of mean + SD, n=3, and flow cytometry plots showing a comparison of CXCR4 knockout in unstimulated T cells and stimulated T cells 3 d post nucleofection using *CXCR4* gRNA_1, 10 µg Cas9, 3:1 gRNA:Cas9 ratio and the program T-023 following workflow in Fig. 30A & Fig. 30B, respectively. Knockout efficiency was measured by surface staining of CXCR4 followed by flow cytometry. Data represent three independent experiments.

9.2.2 RNP-mediated knockout of NFAT in primary human T cells

With our optimized protocol, we aimed to knockout NFAT members in human $CD3^+$ T cells. We decided to follow a similar strategy like those with mouse T cells. First, three gRNAs for both human *NFATC1* and *NFATC2* were designed by the online tool DESKGEN targeting exons 3 and 4 (Table 1), which are the first ones to be commonly expressed in all isoforms. We made sure to choose gRNAs specific for both RSD and NHR domains and used them in combination to achieve maximum knockout efficiency. Three gRNAs specific for two exons were combined to attain large deletions which ensures high knockout efficiency. We used the optimized gRNA and Cas9 concentrations, T-023 program in the Nucleofector IIb, but a combination of 3 gRNAs to target *NFATC1* in pre-stimulated T cells. However, suboptimal and variable knockout efficiency of NFATC1 (ranging within 33-78%) between donors was observed (Fig. 32A). In addition, similar to mouse T cells using the Nucleofector IIb, we could only achieve low efficiency (32%) when targeting *NFATC1* in unstimulated human T cells (Fig. 32B), although the same setup results in high efficacy for constitutively expressed surface protein CXCR4 (Fig. 31C).

To achieve reliable and consistent knockout of the two NFAT members, we next used Nucleofector 4D. Preset program P2 EH-100 for both pre-stimulated and unstimulated human $CD3^+$ T cells were chosen. These parameters proved to be efficient for several other genes in a previous study[91]. The gRNA, Cas9 concentrations, and ratios were kept the same as optimized for the Nucleofector IIb. In stimulated and also unstimulated T cells we now consistently detected >80% loss of *NFATC1* expression by intracellular NFATC1 staining 3 days after nucleofection (Fig. 32C, D). The knockout was equally efficient in both $CD4^+$ and $CD8^+$ subsets (Fig. 32C) and donor variability was negligible (Fig. 32D). Efficient NFATC1 knockout in unstimulated T cells was confirmed by western blot analysis, where we observed a complete loss of all isoforms (A, B, and C) of NFATC1 in nuclear extracts using the 7A6 antibody (Fig. 32E). This suggested that flow cytometry analysis of NFATC1 knockout efficiency was undervalued. Cytoplasmic NFATC1 could not be detected after restimulation with PMA/Ionomycin for 5 h (Fig. 32E). HDAC2 and β-Actin expression were checked in nuclear and cytoplasmic extracts, respectively, as subcellular loading controls. Another preset program P3 EO-115 which resulted in efficient gene knockout in pre-stimulated T cells in the previous studies[145, 146], proved to be equally efficient in both pre-stimulated and unstimulated $CD3^+$ T

cells in our setup (Fig. 32C). Moreover, similar to mouse T cells, we could not establish reliable NFATC2 staining for flow cytometry using an antibody specific for NFATC2. When three specific gRNAs were used to knockout NFATC2 in pre-stimulated human T cells, flow cytometry analysis could not detect any NFATC2 negative cells (Fig. 32F). Nevertheless, using three *NFATC2*-specific gRNAs simultaneously with the P2 EH100 program in the Nucleofector 4D, we detected a complete loss of NFATC2 protein by western blot analysis (Fig. 32G). In summary, using our optimized gRNA:Cas9 ratio (3:1), combined with the P2 EH100 program in the Nucleofector 4D we achieved a complete loss of *NFATC1* and *NFATC2* expression verified by western blot analysis.

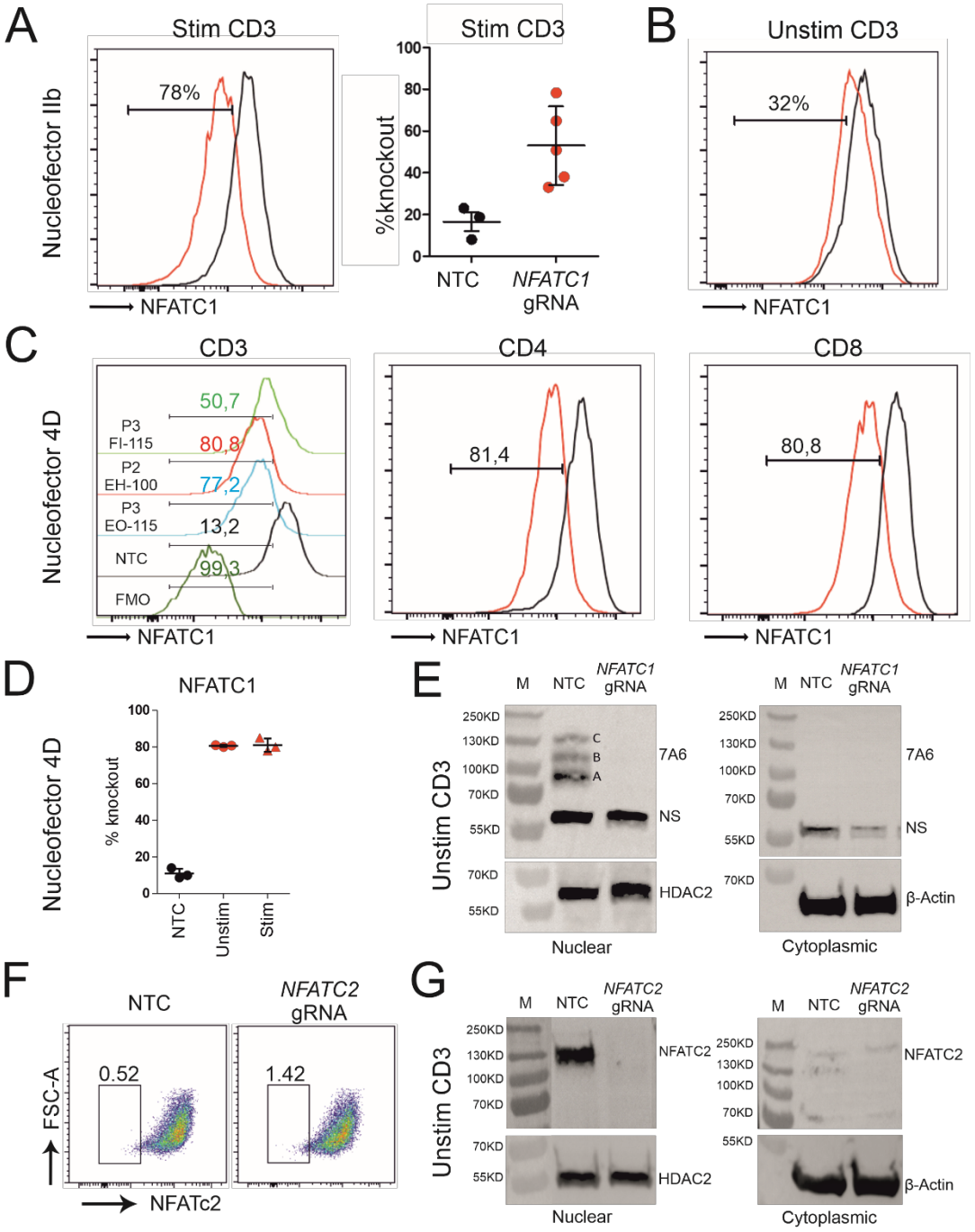

Figure 32. **NFAT knockout by CRISPR/Cas9 in human T cells.**

A-E. NFATC1-specific RNPs were prepared with three gRNAs in a gRNA:Cas9 ratio of 3:1. **A.** Nucleofection was performed using the T-023 program in the Nucleofector IIb to target *NFATC1* in stimulated CD3⁺ T cells (following the workflow in Fig. 30B). Histograms of flow cytometry and graphical representation of NFATC1 knockout (n=5). **B.** NFATC1 knockout analysis by flow cytometry in unstimulated CD3⁺ T cells using the Nucleofector IIb or **C-E.** using P2 EH-100 in the Nucleofector 4D following the workflow in Fig. 30A. **C.** Left panel: A comparison of the programs. Middle & right panel: CD4⁺ and CD8⁺ subset-specific knockout using P2 EH-100. **D.** Graphical representation of knockout efficiency in unstimulated and stimulated CD3⁺ T cells. **E.** Western blot analyses of NFATC1 knockout in unstimulated CD3⁺ T cells, detected by 7A6 mAb in nucleus and cytoplasm after 5 h of restimulation with PMA/ion. NS: nonspecific or uncharacterized band detected by 7A6 mAb. Different isoforms (A, B, C) of NFATC1 with anti-NFATC1 (7A6) mAb. **E,G.** Anti-HDAC2 and anti-β-Actin were used to detect loading controls in nuclear and cytoplasmic extracts, respectively. M: Molecular weight marker; **F-G.** Naïve CD3⁺ T cells were nucleofected with an RNP mixture of three *NFATC2*-specific gRNAs according to Fig. 30B. Cells were restimulated with PMA/ion for 5 h and **F.** intracellular staining of NFATC2 was performed with an NFATC2-specific antibody followed by flow cytometry. **G.** Western blot analyses of NFATC2 in the cytoplasmic and nuclear extract using anti-NFATC2 antibody.

9.2.3 Frequencies of Treg and other T cell subpopulations are mostly unaffected by NFAT ablation in human T cells

Of note, especially naïve T cells account for more severe aGvHD. Now, due to the fact that Treg are important for controlling other T-cell subpopulations and thereby aGvHD, it is important to determine whether *in vitro* culture condition and NFAT ablation changes the composition of human T-cell populations. We first checked the effect of *in vitro* stimulation on T-cell subtype frequencies. A rapid increase in the frequency of Treg ($CD4^+CD25^+FoxP3^+$) (Fig. 33A, B) was observed, but CD8 to CD4 ratio was unaltered (Fig. 33B) upon stimulation with antiCD3, anti-CD28, and IL-2 for 72 h. T_{EFF} ($CD45RO^-CCR7^-$), naive (CD45RO-$CCR7^+$), and T_{EM} ($CD45RO^+CCR7^-$) were reduced at the expense of a significant increase in T_{CM} ($CD45RO^+CCR7^+$) in both $CD4^+$ and $CD8^+$ T-cell compartment (Fig. 33B). Upon NFAT single or double-knockout in stimulated $CD3^+$ T cells following the scheme in Fig. 30B, 3 d after nucleofection, the CD8 to CD4 ratio was slightly but insignificantly reduced (Fig. 33C). Additionally, Treg frequency was not affected upon NFATC1 or/and NFATC2 knockout (Fig. 33C), which again ensures one or two NFAT members being missing does not affect Treg frequency. T_{CM}, T_{EM}, naïve, and T_{EFF} cell frequencies remained unchanged both in $CD8^+$ and $CD4^+$ subsets upon NFAT ablation (Fig. 33D). Next, we performed RNP nucleofection to target NFAT in unstimulated $CD3^+$ T cells following Fig. 30A. One day after nucleofection, T cells were stimulated for 72 h followed by surface staining of CD4, CD8, CCR7, CD45RA, and CD45RO. CD8 to CD4 ratio again remains unchanged in *NFATC1*$^{-/-}$, *NFATC2*$^{-/-}$ or DKO T cells compared to T cells nucleofected with NTC RNP. Moreover, naive, T_{CM}, $T_{EM,}$ and T_{EFF} subpopulation frequencies were more or less undisturbed (Fig. 33E). A slight rise in Treg population was observed in one donor upon NFATC1 (10.8%), NFATC2 (12.1%), and NFATC1+NFATC2 (10.5%) knockout compared to NTC control (9.89%), whereas in another donor T cell populations, Treg frequencies reduced a little upon NFAT ablation (NTC: 25.5%, NFATC1: 24.1%, NFATC2: 21%, NFATC1+NFATC2: 24.6%) (Fig. 33F). CD25 surface expression was somewhat diminished upon targeting *NFATC1* or *NFATC2* and further reduced in DKO T cells in two donors tested (Fig. 33F). In summary, T-cell subtype frequencies remained unchanged upon single or double NFAT ablation in unstimulated or pre-stimulated $CD3^+$ T cells by CRISPR/Cas9 *in vitro*.

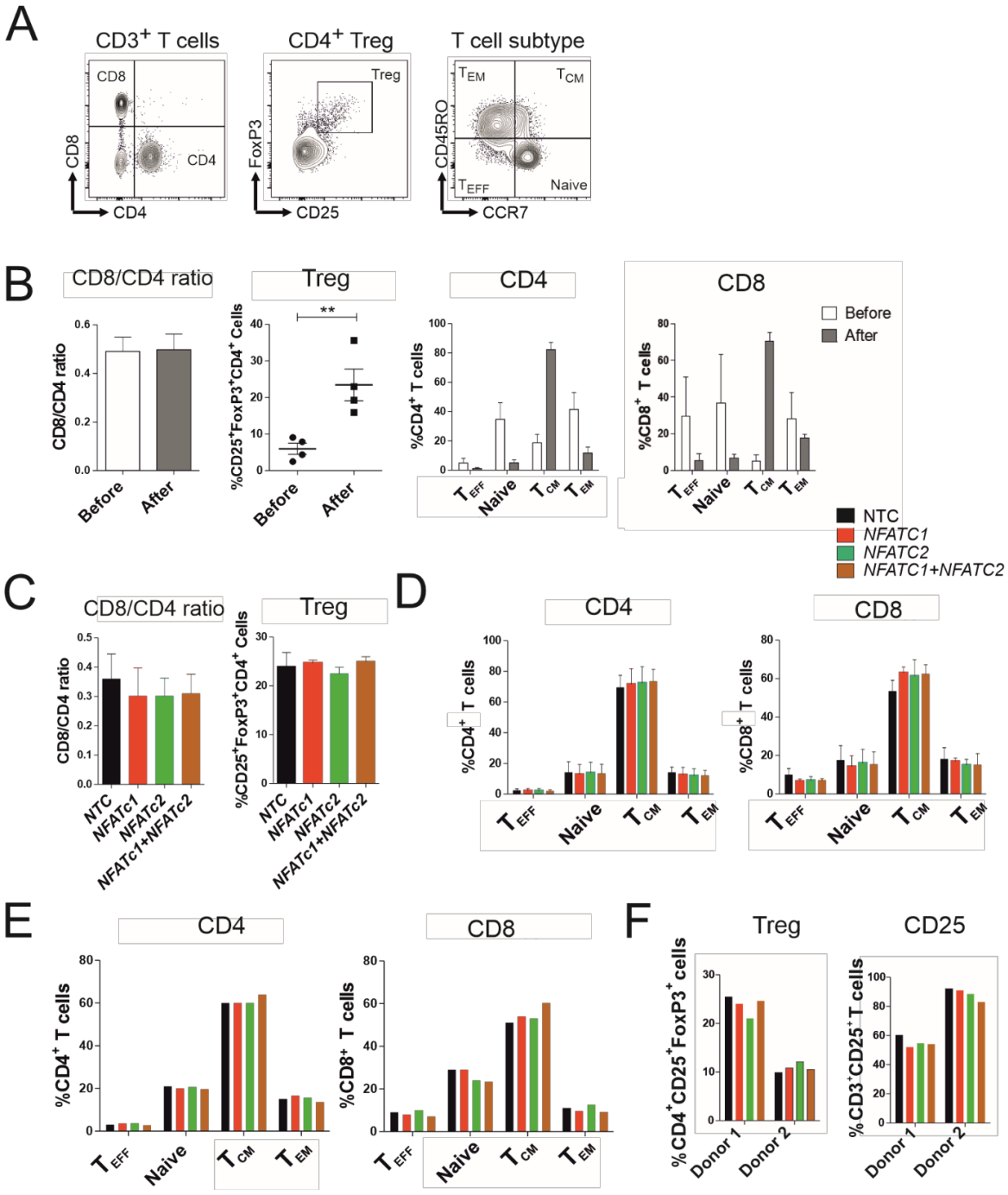

Figure 33. **NFAT knockout does not affect the subtype frequency of T cells.**

A. Flow cytometry representative plots of CD4, CD8, Treg, and different subpopulations of T cells distinguished by CCR7 and CD45RO expression. **B.** Changes in CD8/CD4 ratio, Treg, subpopulations of $CD4^+$ T cell and $CD8^+$ T cell frequency before and after anti-CD3, anti-CD28+IL-2 stimulation for 3 d. **C-F.** To prepare NFAT specific RNPs, three gRNAs (Table 1) per gene-specific for 2 different exons were used in a gRNA:Cas9 ratio of 3:1. **C-D.** NFAT knockout in stimulated $CD3^+$ T cells using P2 EH-100 in the Nucleofector 4D following Fig. 30B. Data represent 4 independent experiments using T cells from 4 different donors; mean + SE, Mann Whitney test (**p<0.01). **C.** CD8/CD4 ratio and Treg frequency; **D.** subpopulations of $CD4^+$ T cell and $CD8^+$ T cell frequency. **E-F**. NFAT knockout in unstimulated $CD3^+$ T cells using P2 EH-100 in the Nucleofector 4D following scheme in Fig. 30A. Data represent 2 independent experiments using T cells from 2 different donors. **E.** Naïve and memory $CD4^+$ and $CD8^+$ subpopulations in T cells. **F.** $CD4^+CD25^+FoxP3^+$ Treg frequency and overall $CD3^+CD25^+$ T cells.

9.2.4 Effect on target gene expression upon NFAT ablation in human T cells

Similar to mouse T cells, to examine whether NFAT knockout reduces proinflammatory cytokines in human T cells, we checked for NFAT target gene expression upon restimulation with PMA/ionomycin of the 'gene-edited' T cells. RNP nucleofection was performed following Fig. 30B in pre-stimulated human T cells. Consistent with our findings in mouse T cells, loss of IFN-γ, TNF-α, IL-2, and CD40L expression was observed when *NFATC2* was targeted in pre-stimulated human T cells. However, NFATC1 knockout only lessened IL-2 and CD40L expression significantly without changing the level of IFN-γ and TNF-α, analysed by flow cytometry (Fig. 34B). Significant loss of all target genes' expression was also observed when NFATC1 and NFATC2 were ablated simultaneously (Fig. 34B). We have also confirmed these findings by knocking out NFAT in unstimulated T cells according to Fig. 30A. We observed similar results like earlier in pre-stimulated T cells, that is NFATC1 knockout alone did not affect the expression of target genes (*IL2, TNF, IFNG, CD40LG*) massively (Fig. 34D). However, NFATC2 ablation alone or in combination with NFATC1 again immensely reduced effector gene expression in both $CD4^+$ and $CD8^+$ T cells (Fig. 34D). These findings indicate especially targeting *NFATC2* alone or in combination with *NFATC1* in human T cells may result in less severe aGvHD when transplanted during allo-HCT due to diminished expression of pro-inflammatory cytokines such as IFN-γ and TNF-α.

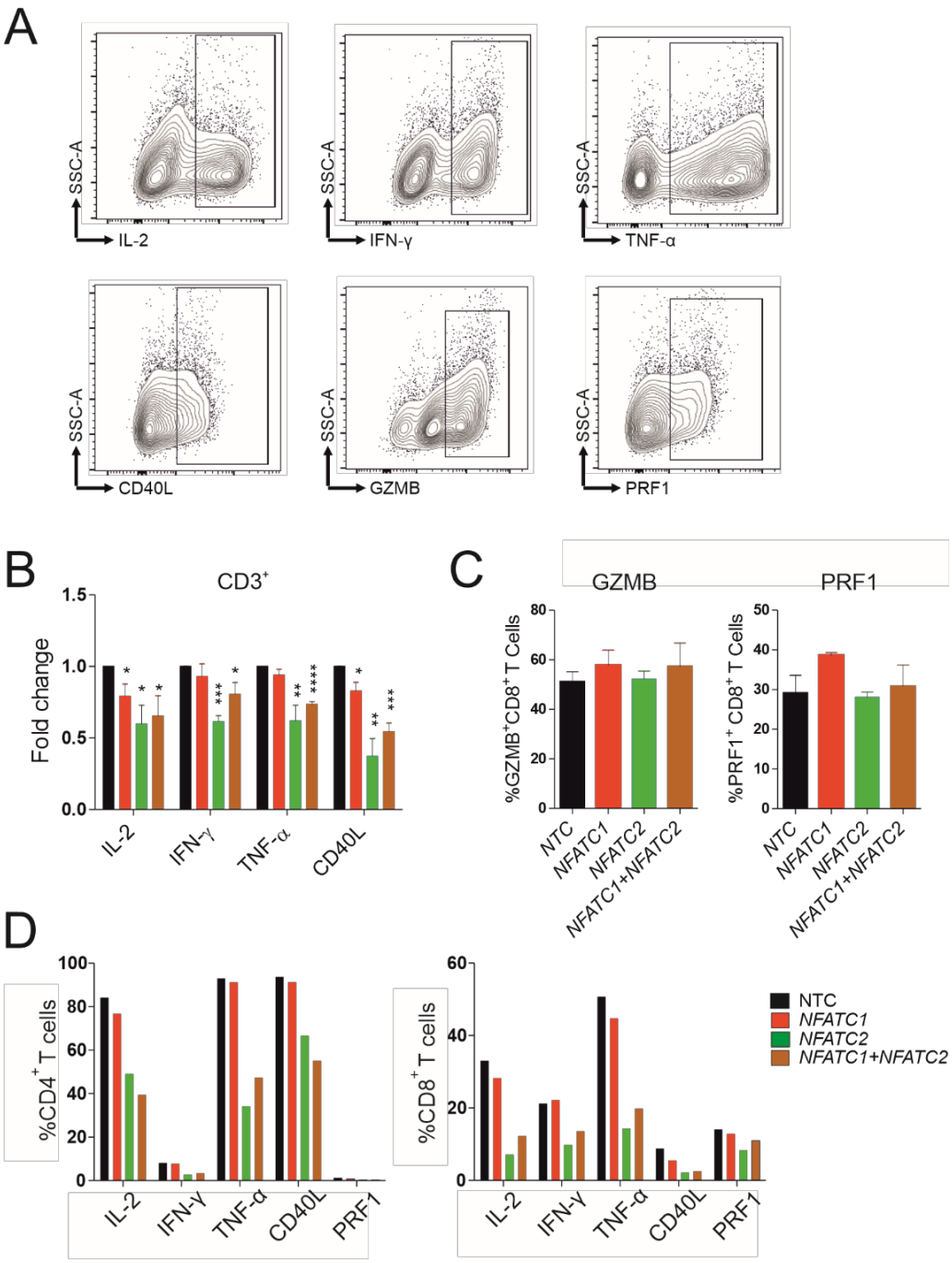

Figure 34. **Effect on NFAT target gene expression upon NFAT ablation in human T cells.**

A-C. Pre-stimulated CD3+ T cells were nucleofected with RNPs of 3 specific gRNAs per gene (Table 1) following the scheme in Fig. 30B using P2 EH100 in the Nucleofector 4D. **A-D.** Cells were restimulated with PMA/ionomycin in the presence of brefeldin and monensin for 5 h followed by surface staining of CD4, CD8, CD40L, and intracellular staining of IL-2, IFN-γ, TNF-α, granzyme B, perforin. **A.** Flow cytometry representative plots for expression of different NFAT target genes in T cells. **B.** Fold change in NFAT target gene expression (IL-2, IFN-γ, TNF-α, and CD40L) upon NFAT ablation. **C.** Granzyme B (GZMB) and perforin (PRF1) expression in CD8+ T cells. Data represent mean + SD from at least 3 independent experiments; Mann Whitney test (*p<0.05, **p<0.01, ***p<0.001). **D.** Unstimulated CD3+ T cells were NFAT ablated using RNPs of 3 specific gRNAs per gene (Table 1), following the scheme in Fig. 30A, using P2 EH100 in the Nucleofector 4D. One day after nucleofection, cells were stimulated with anti-CD3, anti-CD28, IL-2 for 3 d followed by restimulation with PMA/ionomycin to detect intracellular proteins. Data are from one experiment.

9.2.5 NFAT ablation does not hinder cytotoxicity-related gene expression in human CD8$^+$ T cells *in vitro*

Granzyme B, perforin, and CD107a are additional proteins important for the cytotoxicity of CD8$^+$ T cells against tumor cells. To investigate the role of NFATC1 and NFATC2 in the cytotoxicity of human CD8$^+$ T cells, we first analysed the intracellular expression of granzyme B (GZMB) and perforin (PRF1). We pre-stimulated CD3$^+$ T cells with anti-CD3, anti-CD28, and IL-2 for 3 d, ablated NFAT by RNP nucleofection, cultured with IL-2 for 3 d (Fig. 30B), and restimulated with PMA and ionomycin for 5 h to detect intracellular GZMB and PRF1 expression (representative gating in Fig. 34A) in CD8$^+$ T cells. We observed a slight increase in GZMB and PRF1 levels in *NFATC1*$^{-/-}$ CD8$^+$ T cells (Fig. 34C) compared to NTC-RNP-nucleofected T cells which are similar to the earlier findings in mouse T cells[90]. Targeting *NFATC2* alone or in combination with *NFATC1* did not affect the production of GZMB and PRF1 (Fig. 34C). RNP nucleofection in unstimulated CD3$^+$ T cells (Fig. 30A) did not affect the PRF1 level in *NFATC1*$^{-/-}$ CD8$^+$ T cells, but *NFATC2*$^{-/-}$ or DKO CD8$^+$ T cells showed a slight reduction in PRF1 level compared to the NTC control (Fig. 34D). Almost no expression of PRF1 in CD4$^+$ T cells (Fig. 34D) confirmed the fact that CD4$^+$ T cells typically do not possess granule-exocytosis-mediated cytotoxicity[147].

Next, we challenged the CD3$^+$ T cells with various tumor cells, i.e. MOLM-13 and MV4-11, both acute myeloid leukemia (AML) cell lines, and RPMI 8226, a multiple myeloma (MM) cell line. We again performed RNP nucleofection of pre-stimulated CD3$^+$ T cells following the method in Fig. 30B. Three days after nucleofection T cells were cocultured with tumor cells in a 1:1 ratio for 6 h (Fig. 35A). To minimize the donor-dependent gene expression variations, we calculated the fold change in GZMB and PRF1 levels in NFAT-deficient CD8$^+$ T cells compared to their respective NTC control. These variations are probably caused due to a varied level of MHC mismatches between donors and tumor cell lines owing to different levels of T-cell activation. Comparable to PMA and ionomycin restimulation, we observed an increase in GZMB expression in *NFATC1*$^{-/-}$ CD8$^+$ T cells when cocultured with MV4-11 or MOLM-13 tumor cells (Fig. 35B). In addition, *NFATC2*$^{-/-}$ CD8$^+$ T cells also responded with a slight but significant rise in GZMB level when cocultured with any of the 3 tumor cell lines (Fig. 35B). PRF1 was upregulated only in *NFATC1*$^{-/-}$ CD8$^+$ T cells when cocultured with MV4-11 cells (Fig. 35C). Consistent with PMA/ionomycin restimulation (Fig. 35C), NFATC1 along with

NFATC2 ablation did not affect the level of GZMB and PRF1. CsA is known to compromise the GvL efficacy of human T cells during allo-HCT. Hence, we wanted to investigate whether during our *in vitro* coculture of tumor cells and T cells, the addition of CsA influences the expression of cytotoxicity-related genes. The addition of CsA (10 ng/ml) during coculture reduced the fold change in $CD8^+PRF1^+$ T cells slightly without changing the $CD8^+GZMB^+$ T-cell subset (Fig. 35B, C). Furthermore, to test CD107a, a marker for $CD8^+$ T cell degranulation, RNP nucleofection was performed in unstimulated $CD3^+$ T cells (Fig. 30A). Cells were rested for 1 d in IL-2 and then stimulated for 3 d with anti-CD3+anti-CD28+IL-2 before coculturing with tumor cells for 6 h with PE-conjugated anti-human CD107a antibody to measure degranulation by flow cytometry. CD107a exhibited an augmented fold change in *NFATC1*$^{-/-}$, *NFATC2*$^{-/-}$ and DKO $CD8^+$ T cells (Fig. 35D). Addition of CsA (10 ng/ml) during the coculture left CD107a expression unaffected (Fig. 35D). To sum up, cytotoxicity-related genes expressed by $CD8^+$ T cells were not compromised by single or double NFAT depletion in human T cells irrespective of whether reactivated with PMA/ionomycin or challenged with AML or MM cell lines.

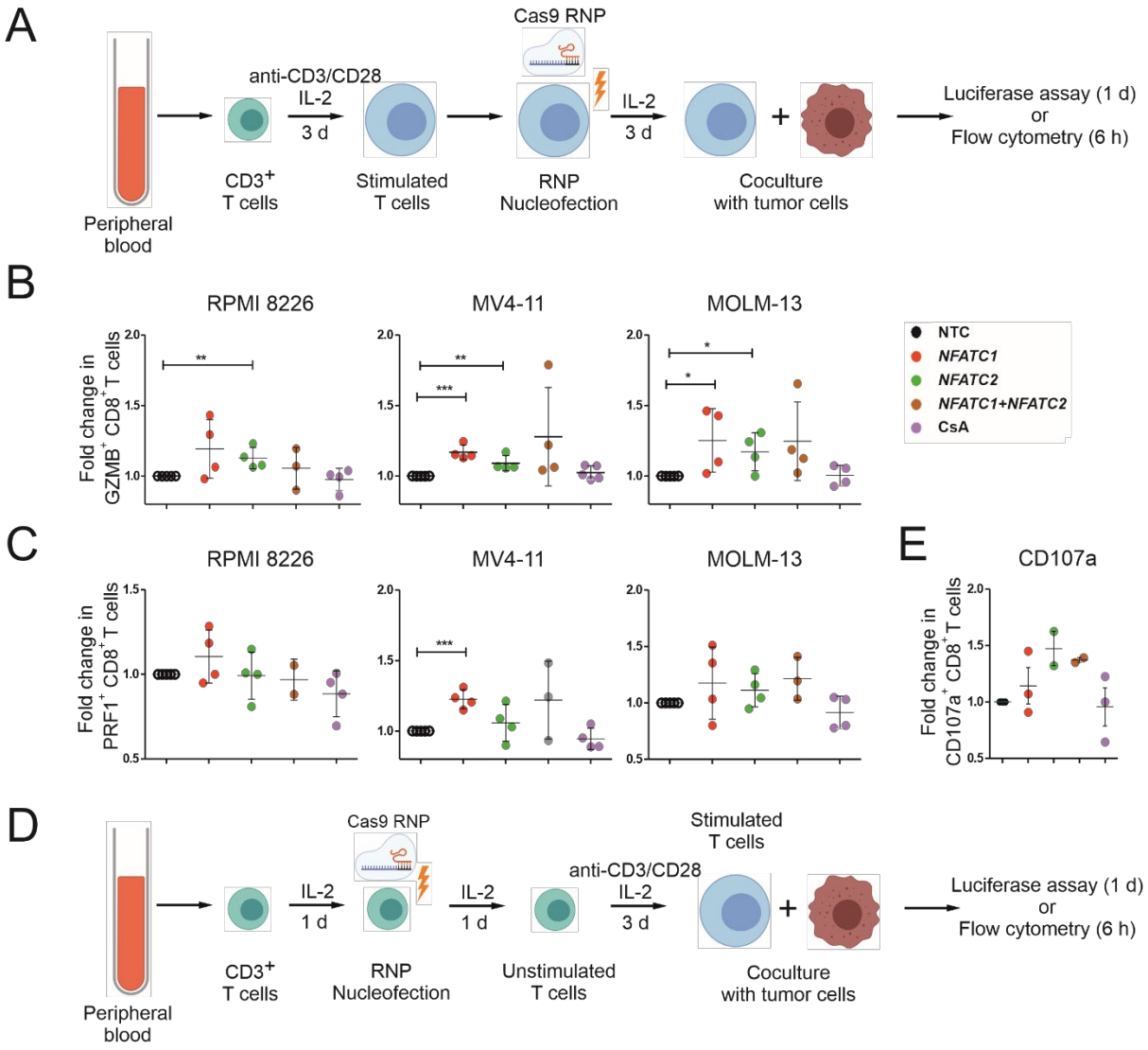

Figure 35. **Cytotoxicity-inducing genes are not reduced upon NFAT knockout in human CD8⁺ T cells.**

A-C. Pre-stimulated CD3⁺ T cells were nucleofected with RNPs of 3 specific gRNAs per gene (Table 1) following the scheme in Fig. 30B using P2 EH100 in the Nucleofector 4D. Cells were harvested 3 d after RNP nucleofection and cocultured with the tumor cells RPMI 8226, MV4-11, or MOLM-13 at a 1:1 ratio for 6 h followed by flow cytometry analysis after 6 h or by a luciferase assay after 1 d. After 6 h, intracellular staining of GZMB and PRF1 was performed. **A-E.** 10 ng/ml CsA was added at the beginning of coculturing T cells and tumor cells. **A.** Schematic of RNP nucleofection in pre-stimulated CD3⁺ human T cells and coculture with tumor cells. **B.** Flow cytometry analysis of GZMB expression gated on CD8⁺ T cells. Fold change was calculated compared to GZMB expression in NTC-treated CD8⁺ T cells. Mann Whitney test (*p<0.05, **p<0.01, ***p<0.001). **C.** Flow cytometry analysis of PRF1 expression gated on CD8⁺ T cells. Fold change was calculated compared to PRF1 expression in NTC-nucleofected CD8⁺ T cells. **D-E.** Unstimulated CD3⁺ T cells were NFAT-depleted by nucleofection with RNPs of 3 specific gRNAs per gene (Table 1) following the scheme in Fig. 30A using P2 EH100 in the Nucleofector 4D. After 1 d, T cells were stimulated with anti-CD3, anti-CD28, and IL-2 for 3 d and subsequently cocultured with tumor cells in a 1:1 ratio for 6 h for flow cytometry analysis or 1 d for luciferase assay. Degranulation of CD8⁺ T cells was measured by adding a PE-conjugated anti-human CD107a antibody during the 6 h-coculture with tumor cells. Flow cytometry analysis was performed and fold change was calculated compared to the CD107a⁺ frequency of NTC-nucleofected CD8⁺ T cells.

9.2.6 Human T cells retain *in vitro* cytotoxic activity upon NFAT ablation

We earlier showed that the absence of one NFAT member does not compromise the GvL efficacy of T cells in allo-HCT tumor-bearing mouse models[63]. Hence, we attempted to examine the consequence of single or double NFAT member deletion on the cytotoxicity of human T cells against AML and MM tumor cell lines. To establish an *in vitro* cytotoxicity assay, we used RPMI 8226 tumor cell line expressing luciferase. $CD3^+$ T cells (Effector, E) were activated with anti-CD3, anti-CD28, and IL-2 for 3 d, harvested and then cocultured with RPMI 8226-luc^+ cells (Target, T). To find out the optimal time and ratio required to observe a difference between cytotoxicity of NTC and NFAT-ablated $CD3^+$ T cells, cocultures were performed for 24 or 48 h in different E:T ratios, i.e. 1:1, 10:1, and 50:1. After 24 and 48 h cells were lysed and luciferin substrate was added to the cell extract to calculate the tumor-killing by T cells. Tumor cells cultured without T cells were considered as a control for no T cell-mediated killing. We observed >80% killing in 10:1 and 50:1 E:T ratio at 24 and 48 h (Fig. 36A). Since the 1:1 ratio at 24 h showed a moderate (around 30%) killing efficiency, we picked this time point and ratios around 1:1 to be able to see small differences in cytotoxicity, if any, between NTC RNP-nucleofected T cells and NFAT-ablated T cells. *NFATC1* or/and *NFATC2* was targeted in pre-stimulated T cells and 'gene-manipulated' T cells were cocultured with tumor cells for 24 h, 3 d after nucleofection (Fig. 35A). Apart from RPMI 8226-luc^+, we also used MV4-11-luc^+ and MOLM-13-luc^+ cell lines. NFATC1 or NFATC2 single-ablated $CD3^+$ T cells did not indicate any defect in tumor killing efficacy in cytotoxicity assays with three tumor cell lines (Fig. 36B, C, D). *NFATC1*$^{-/-}$*NFATC2*$^{-/-}$ DKO $CD3^+$ T cells showed a significant loss of killing efficacy only in the MOLM-13 cell line at an E:T 1:2 ratio (Fig. 36B, C, D). In contrast, the addition of 10 ng/ml CsA when coculturing $CD3^+$ T cells with any of the three tumor cells, significantly reduced killing efficacy by at least 50% (Fig. 36B, C, D).

Next, NFAT ablation was performed by RNP nucleofection in unstimulated human T cells followed by stimulation for 3 d with anti-CD3+anti-CD28+IL-2 before coculturing them with tumor cells following the workflow in Fig. 35D. Here again, we could not observe any reduction in killing efficiency of NFAT single or double-deficient T cells. Only CsA treatment reduced cytotoxicity drastically against all the three tumor cells (Fig. 36E). To summarize, single NFAT deletion does not affect the cytotoxicity of $CD3^+$ T cells *in vitro* against AML and MM cell lines and double-knockout minimally reduces cytotoxicity only when cocultured with

MOLM-13. In contrast, cytotoxicity of CD3$^+$ T cells was overall massively suppressed upon CsA treatment.

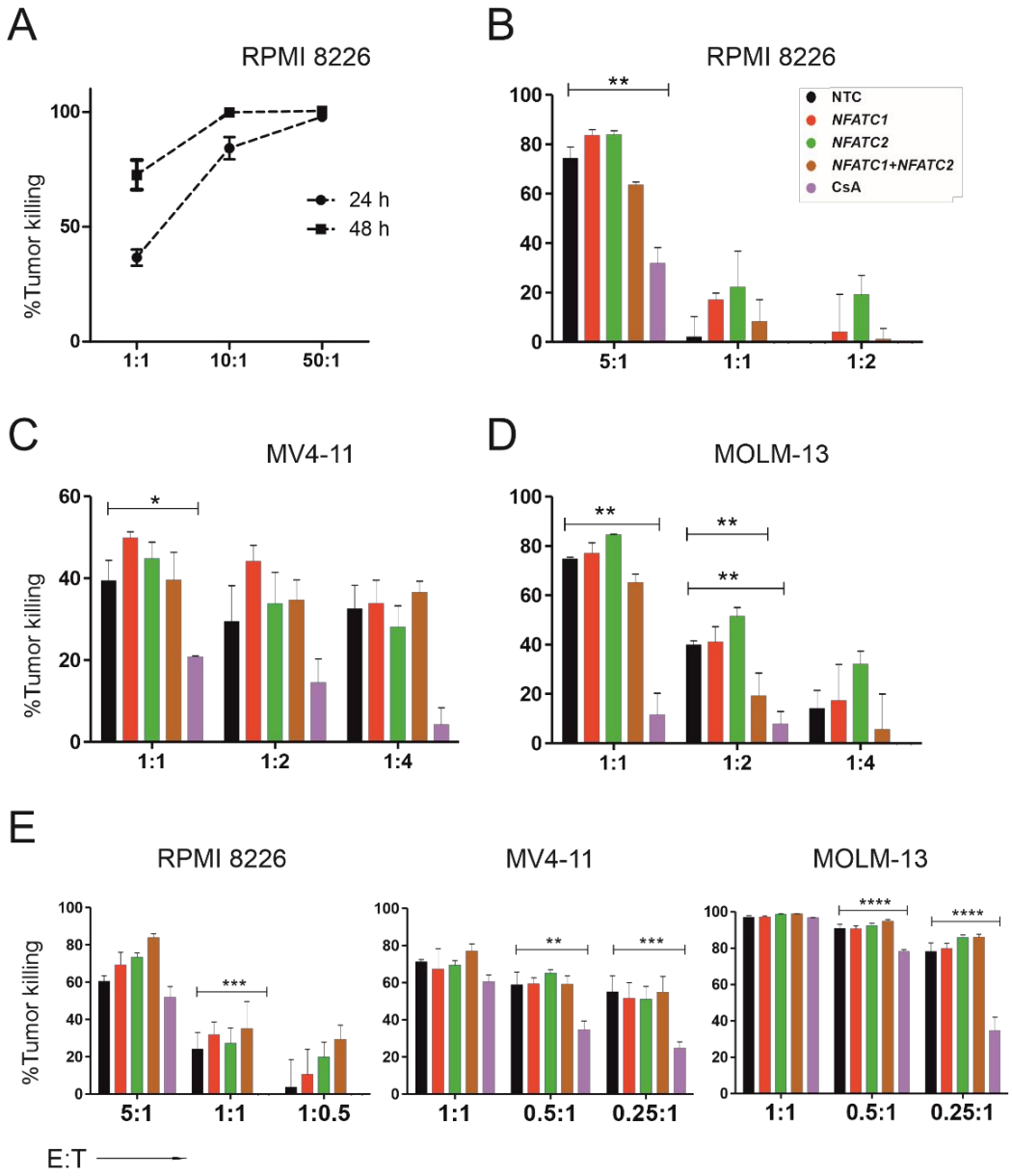

Figure 36. **Single NFAT-ablated T cells retain tumor-killing efficiency.**

A. CD3$^+$ T cells were stimulated with anti-CD3, anti-CD28, and IL-2 for 3 d prior to the coculture with RPMI 8226-luc$^+$ in different E:T ratios. The percentage of RPMI 8226-luc$^+$ tumor killing by CD3$^+$ T cells was measured by luciferase assay at 24 h or 48 h. **B-D.** CD3$^+$ T cells were nucleofected with NTC or 'gene-specific' RNPs and cocultured with tumor cells according to the scheme in Fig. 35A. Luciferase assay was performed 1 d after coculture Data represent mean + SD values of one out of 3 individual experiments with 3 different donors. **B-E.** Mann Whitney test (*p<0.05, **p<0.15, ***p<0.001, , ****p<0.0001). **B.** Killing of RPMI 8226-luc$^+$, **C.** MV4-11-luc$^+$ and **D.** MOLM-13-luc$^+$ tumor cells by NTC, NFATC1$^{-/-}$, NFATC2$^{-/-}$ and NFATC1$^{-/-}$ NFATC2$^{-/-}$ human CD3$^+$ T cells. In CsA treated group, NTC-T cells were used along with CsA (10 ng/ml) added at the beginning of the coculture with tumor cells. **E.** CRISPR/Cas9 editing was performed in unstimulated T cells, which were then stimulated with anti-CD3, anti-CD28, and IL-2 for 3 d according to Fig. 35D. Luciferase assay to estimate the percentage of tumor-killing was performed after 1 d of coculture with luc$^+$ tumor cells. In the CsA-treated group, NTC-T cells were used along with CsA (10 ng/ml) added at the beginning of coculture with luc$^+$ tumor cells.

9.3 Functional analysis of NFAT-depleted human CD19-CAR T cells

We observed variable killing efficiency against tumor cells of human CD3⁺ T cells from various donors. This could be due to variability in HLA types of the donors which can cause different levels of T-cell activation. To see more reliable antigen-specific responses, we created CD19-CAR T cells by the minicircle and sleeping beauty (SB) transposon system[102]. We incorporated our optimized RNP nucleofection-mediated NFAT depletion method in human T cells to generate *NFATC1*$^{-/-}$ or/and *NFATC2*$^{-/-}$ CAR T cells. The most commonly used CAR T cells in the clinic are generated by viral transduction which has safety issues. For specific 'gene-ablated' CAR T-cell generation using CRISPR/Cas9, researchers have used 'Cas9-mRNA' along with gRNA electroporation after viral transduction of a CAR construct[93]. To our knowledge, no study has yet shown the generation of endogenous gene-ablated CAR T cells in a single step of nucleofection. Here, we established a novel method of non-viral CAR T-cell generation in conjunction with RNP-mediated gene deletion all in a 'one-step nucleofection' (Fig. 37). This was performed in collaboration with Prof. Dr. Michael Hudecek's lab at the University of Würzburg.

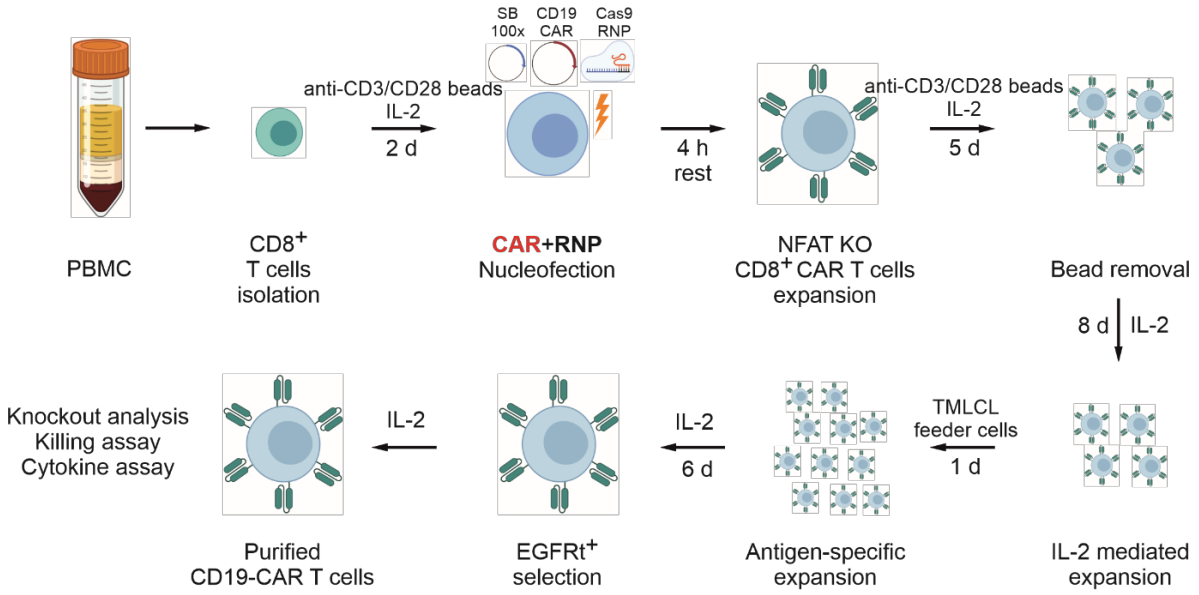

Figure 37. **Schematic of a simultaneous NFAT knockout and CAR T-cell generation.**

CD8⁺ T cells are isolated from PBMCs, stimulated with anti-CD3/CD28 beads+ IL-2, and nucleofected with anti-CD19-CAR minicircle (MC), sleeping beauty transposase MC (SB100x), and 'gene specific' RNPs using the Nucleofector 4D, P3 F-115 program. RNPs were prepared using a 3:1 gRNA:Cas9 molar ratio as optimized earlier in Fig. 31A. Three gRNAs were used per gene to achieve maximum KO efficiency. After 4 h, cells were restimulated with anti-CD3/CD28 beads+IL-2 for 5 d. The anti-CD3/CD28 beads were removed by magnetic separation and cells were cultured with IL-2 for a further 8 d. For rapid 10-20 fold antigen-specific expansion, CAR T cells were cocultured with irradiated CD19-expressing TMLCL feeder cells for in a total of 7 d. IL-2 was added after 1 d of starting the coculture. EGFRt⁺ CAR T cells were selected by magnetic separation and further used in functional analysis.

9.3.1 One-step generation of human CD19-CAR T cell with NFAT knockout by nucleofection

$CD8^+$ T cells were isolated from several donors' PBMCs and stimulated with anti-CD3/CD28 beads+IL-2 for 48 h. The cells were electroporated with anti-CD19-CAR minicircle (MC), sleeping beauty transposase MC (SB100x), and RNPs prepared with 'gene-specific' gRNAs. This 'one-step nucleofection' using the Nucleofector 4D, preset program P3 FI-115 facilitated the transfer of CD19 MC, SB100x, and RNPs at the same time in the cell (Fig. 37). We again used 3:1 of gRNA:Cas9 ratio and 3 gRNAs per gene like before. The cells which received the CAR-construct successfully, express EGFRt on the cell surface because the CAR transgene is fused to EGFRt by T2A sequence (Fig. 6). Accordingly, we first verified CD19-CAR transfer by EGFRt surface expression (Fig. 38A) and simultaneous RNP-mediated knockout using *CXCR4 gRNAs*. A combination of three *CXCR4* gRNA resulted in 84.7% knockout efficiency (Fig. 38B) gated on the total $CD8^+$ population. The CD19-CAR T cells were further expanded by coculturing them with CD19-expressing feeder cells (TMLCL), which rapidly expanded the $EGFRt^+$ CD19-CAR T-cell population (Fig. 38C). For our initial interest, similar to targeting *CXCR4*, we nucleofected anti-CD3/CD28 beads+IL-2-activated $CD8^+$ T cells with RNPs containing three *NFATC1* gRNAs (Table 1) mixed with CD19-CAR MC and SB100x. We observed suboptimal loss of intracellular NFATC1 in the total $CD8^+$ population (66.6%) (Fig. 38D left panel). However, when gated on $CD8^+EGFRt^+$ cells, i.e. CAR-expressing T cells, almost complete loss of NFATC1 protein expression (a flow cytometry underestimated 82.7%) was observed in this fraction (Fig. 38D right panel). This ensured *NFATC1* RNPs were received by all $CD8^+$ T cells which also successfully expressed the CAR construct. The $EGFRt^+$ CAR T cells were purified using an EGFRt-biotin-streptavidin magnetic isolation method, achieving consistently above 90% purity (Fig. 38E). Cells were kept in IL-2-containing media until functional assays were performed. We confirmed highly efficient NFATC1 knockout in purified $EGFRt^+$ CD19-CAR T cells by flow cytometry after PMA/ionomycin restimulation of 5 h and intracellular staining using PE-conjugated 7A6 mAb (Fig. 38F). Utilizing the same strategy, we also generated *NFATC2*$^{-/-}$ and *NFATC1*$^{-/-}$*NFATc2*$^{-/-}$ CAR T cells. In DKO $EGFRt^+$CAR T cells, 71.4% NFATC1-negative population was detected by flow cytometry (Fig. 38D, F). However, we had realized by western blot analysis of *NFATC1*$^{-/-}$ $CD3^+$ T cells that the true knockout efficiency would be more than estimated by flow cytometry (Fig. 32C, D, E). This is because, apart from NFATC1, 7A6 mAb also binds to another protein (~60KD) non-specifically which cannot be

distinguished by flow cytometry but can be clearly visualized in western blot (Fig. 32E). Additionally, we consistently observed an increase in *NFATC1* expression in *NFATC2*$^{-/-}$ CD8^{+}EGFRt^{+} CAR T cells (Fig. 38F).

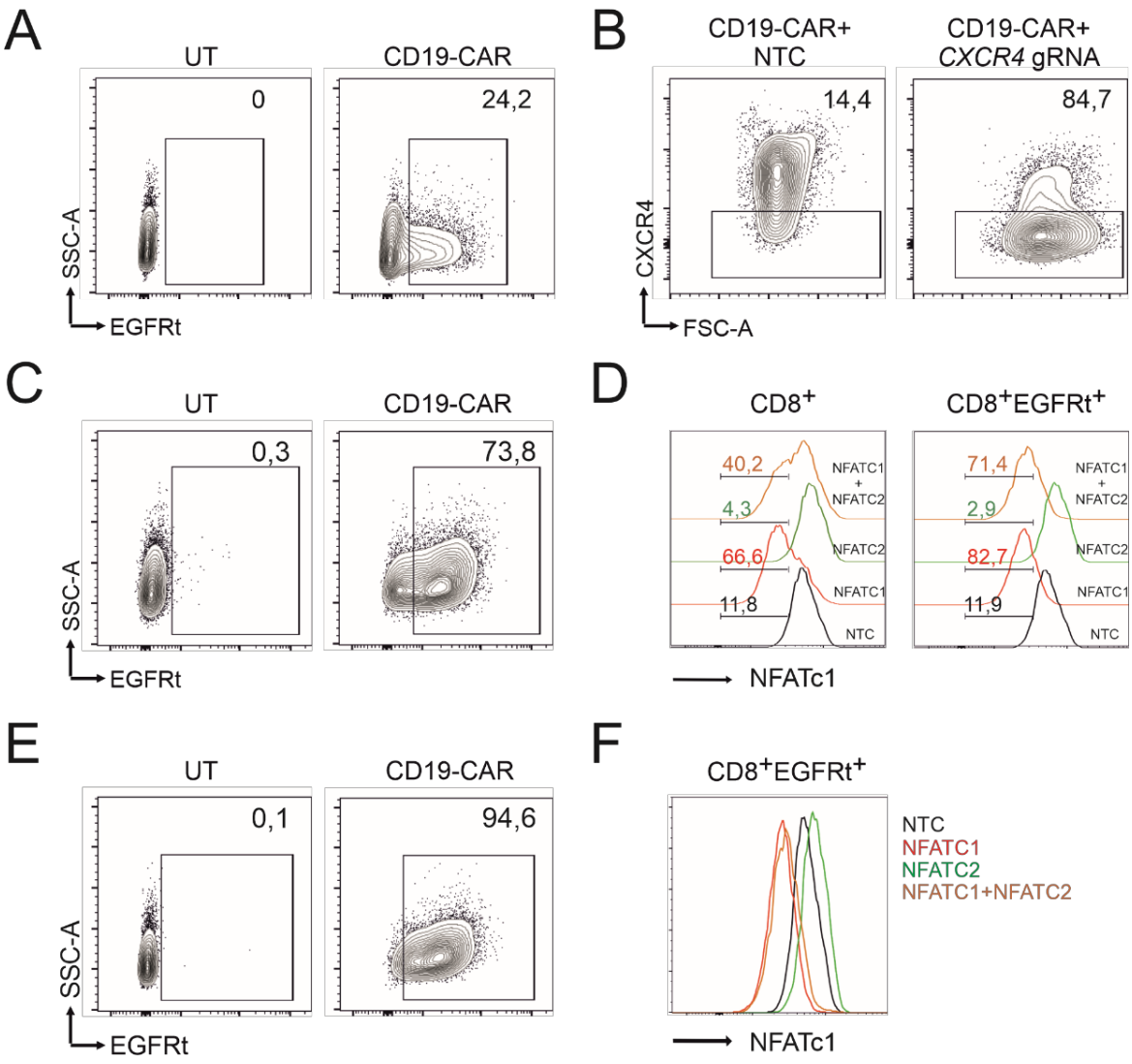

Figure 38. **Efficient gene knockout by CRISPR/Cas9 in CD8^{+} CAR T cell.**

A-F. CD8^{+} CD19-CAR T cells were generated following the workflow described in Fig. 37. **A.** EGFRt surface expression was analysed by flow cytometry in untransfected (UT) and CD19-CAR nucleofected CD8^{+} T cells 5 d after nucleofection. **B.** CXCR4 surface staining was performed in NTC or CXCR4 RNP nucleofected CD8^{+} CAR T cells 5 d after nucleofection. CXCR4 surface expression was determined by flow cytometry. **C.** EGFRt expression in TMLCL feeder cell-expanded CD19-CAR T cells 7d after coculture. **D.** *NFATC1*$^{-/-}$ CD19-CAR T cells were generated using 3 specific gRNAs (Table 1). Intracellular NFATC1 staining was performed in PMA/ionomycin-restimulated CAR T cells 5 d after nucleofection gated on total CD8^{+} or CD8^{+}EGFRt^{+} T cells. **E.** EGFRt^{+} CAR T cells were purified by the positive-selection method. EGFRt surface expression was analysed by flow cytometry in positive-selected CAR T cells. **F.** Following EGFRt^{+} positive-selection of NTC and NFAT-ablated CAR T cells, NFATC1 intracellular staining was performed in PMA/ionomycin-restimulated CD8^{+}EGFRt^{+} CAR T cells. Data represent one out of 4 independent experiments.

9.3.2 NFATC2 knockout affects gene expression in CD8$^+$ CD19-CAR T cells

To analyse whether targeting *NFAT* by RNP nucleofection has functional consequences on CD8$^+$ CD19-CAR T cells, again we examined NFAT target gene expression. CD8$^+$EGFRt$^+$ CD19-CAR T cells were restimulated with PMA/ionomycin after purification following scheme in Fig. 37 for 5 h. Similar to mouse and human CD3$^+$ T cells IL-2, IFN-γ, TNF-α, and CD40L level was examined. We observed a differential role of NFATC1 and NFATC2 in this context. NFATC1 ablation did not affect NFAT target gene expression, whereas *NFATC2*$^{-/-}$ CAR T cells rapidly reduced IL-2, IFN-γ, TNF-α, CD40L compared to NTC RNP-nucleofected CAR T cells (Fig. 39). In DKO CAR T cells, IL-2 expression declined like in *NFATC2*$^{-/-}$ T cells. Other target proteins, TNF-α, IFN-γ, and CD40L, were further reduced in DKO T cells compared to *NFATC2*$^{-/-}$ T cells. (Fig. 39). This is in line with our data from human CD3$^+$ T cells (Fig. 34B) that NFATC2 dominantly regulates the expression of human *IL2*, *IFNG*, *TNF,* and *CD40LG*. We further checked for the expression of the cytotoxicity-related genes *GZMB* and *PRF1* in CD8$^+$ CD19-CAR T cells. The effect of NFAT ablation on GZMB and PRF1 in CAR T cells was not found to be similar to human CD3$^+$ T cells. We observed no difference in GZMB$^+$ or PRF1$^+$ NTC and *NFATC1*$^{-/-}$ CAR T cells, while targeting *NFATC2* alone or in addition to *NFATC1* moderately reduced GZMB and PRF1 levels. Furthermore, no difference in CD107a expression was detected in CAR T cells upon NFAT ablation (data not shown).

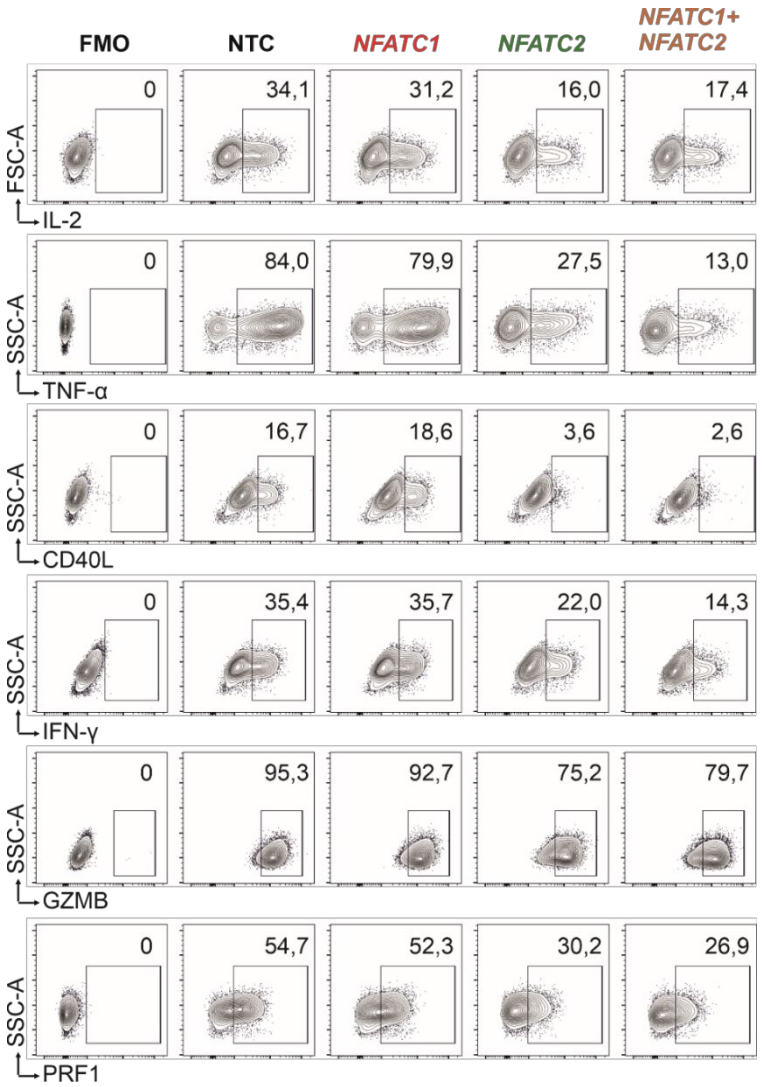

Figure 39. **NFAT target genes are repressed upon NFATC2 knockout by CRISPR/Cas9 in CD8⁺ CAR T cell.**

Intracellular IL-2, TNF-α, CD40L, IFN-γ, GZMB, and PRF1 expression in 5 h PMA/ionomycin-restimulated CD8⁺EGFRt⁺ CD19-CAR T cells with or without NFAT knockout (Fig. 37, Fig. 38). Data represent one out of 2 independent experiments.

9.3.3 Only NFAT double-knockout suppresses *in vitro* antigen-specific cytotoxicity of anti-CD19-CAR CD8⁺ T cells

Finally, we determined whether NFAT depletion affects the tumor-killing efficacy of CAR T cells *in vitro*. Luciferase assays were performed coculturing luciferase-expressing tumor cells (K562, K562-CD19, and Raji) with CAR CD8⁺ T cells in several E:T ratios. These CD8⁺EGFRt⁺ CD19-CAR T cells showed a very strong antigen-dependent killing efficacy, rapidly killing tumor cells specifically expressing CD19. No killing was observed of K562 tumor cells which do not express CD19. We tested several E:T ratios ranging from 5:1 to 1:5. NFAT single-knockout CAR T cells could kill the CD19⁺ K562-CD19 (at E:T 5:1) and Raji (at E:T 1:1 and 1:5) tumor cells with similar efficacy as NTC CAR T cells (Fig. 40A, B). However, NFAT single-deficient CAR T cells elicited

reduced K562-CD19 killing ability at E:T 1:5, although this did not reach significance (Fig. 40A, right panel). This depicts that NFATC1 or NFATC2 deficiency does not affect CAR T-cell cytotoxicity majorly. Remarkably, even *NFATC2*$^{-/-}$ CAR T cells are efficient in killing tumor cells in an *in vitro* situation despite reduced IFN-γ, TNF-α, GZMB, and PRF1, proteins important for cytotoxicity. DKO CAR T cells from two donors consistently exhibited significant compromise in tumor-killing ability. These CAR T cells killed fewer K562-CD19 cells and Raji cells at 1:5 of the E:T ratio. However, the killing ability of DKO CAR-T cells was still superior to CsA (100 ng/ml)-treated CAR T cells (Fig. 40A, B). A point to note is that CsA was added only during coculture of anti-CD19-CAR T cells with tumor cells, whereas in DKO CAR T cells NFATs were already ablated before coculture with tumor cells. To summarize, we again confirmed that human T cells, like mouse T cells, retain cytotoxicity upon single NFAT ablation. Double-knockout CAR T cells show slightly compromised cytotoxicity which was still superior to CsA treatment. This proved our findings of CD3^{+} T-cell cytotoxicity assay and importantly of our *in vivo* mouse leukemia model from the previous study of our group[63].

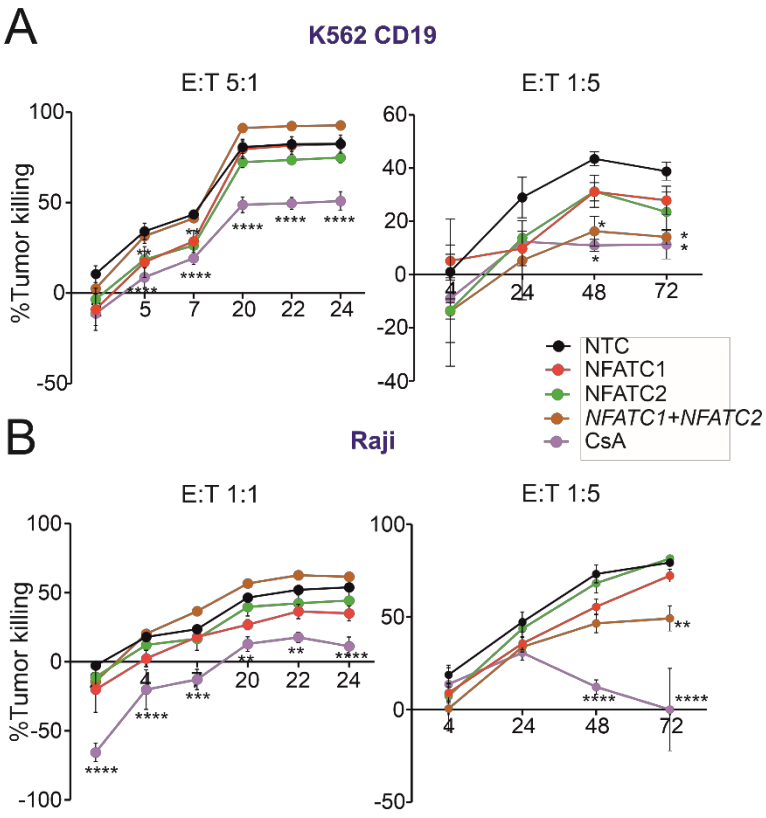

Figure 40. **NFAT single-knockout CD19-CAR T cells can kill tumor cells efficiently *in vitro*.**

Luciferase^{+} **A.** K562-CD19 or **B.** Raji cell lines were co-cultured with CD8^{+}EGFRt^{+} CD19-CAR T cells and luciferin in different E:T ratios up to 72 h. The percentage of tumor-killing was calculated from relative luminescence reduction compared to the tumor alone. Data represent mean ± SD of one out of 3 independent experiments, Two way ANOVA (*p<0.05, **p<0.01, ***p<0.001, ****p<0.0001).

10 Discussions

10.1 Rapid and efficient NFAT ablation by CRISPR/Cas9 in primary mouse T cells to ameliorate aGvHD

10.1.1 Lentiviral mediated CRISPR/Cas9 knockout is inefficient in primary murine T cells.

CRISPR/Cas9 has been extensively used during the last decade in the field of gene therapy due to its high specificity, effectiveness, and simplicity of design. Although mouse T cells are crucial research tools, the effective application of CRISPR/Cas9 gene editing in mouse T cells has shown limited success so far. The retroviral gene delivery method is most commonly used in transducing mouse T cells, to deliver either protein-coding genes or short hairpin RNAs with satisfactory efficiency. However, it requires pre-stimulation of T cells using anti-CD3+anti-CD28. A recent study showed retroviral 'all-in-one' construct expressing both gRNA and Cas9 is ineffective in transduction rates and also yielded low knockout efficiency[91]. On the other hand, lentiviral gene delivery has demonstrated successful gene delivery in mouse tumor cell lines[112] and pre-stimulated human primary T cells[148]. However, no study has shown successful lentiviral CRISPR/Cas9 gene editing in primary mouse T cells. We used a lentiviral system[112], where mouse EL4 and WEHI231 cells were transduced with plasmids encoding Cas9 and gRNAs with high efficiency. However in pre-stimulated primary mouse $CD3^+$ T cells, transduction efficiency was low (Fig. 7) with a very low viability. It has been reported earlier that lentiviral titers and hence transduction efficiency reduces when the plasmid size increases[149]. The large size of our plasmids, FuCas9-mcherry (14Kb) and FgH1tUTG-gRNA (11Kb) could contribute to lower transduction efficiency in primary mouse T cells. Doxycycline-induced gRNA expression led to suboptimal knockout efficiency. Yet, in absence of dox, knockout of the target gene was observed, proving leakiness of the system (Fig. 8B-D). Additionally, viral gene delivery involves cloning of gRNAs, flow-cytometry sorting, or antibiotic selection of transduced cells, making it more tedious and time-consuming. Apart from that, viral backbones could cause immunogenicity and toxicity[124]. This prompted us to study non-viral CRISPR/Cas9 approaches for genetically modifying primary mouse T cells.

10.1.2 Non-viral CRISPR/Cas9 genome editing using *Cd4cre.*Cas9$^+$ transgenic mouse

Researchers have created Cas9 transgenic mice[114, 125] to manipulate the T cells obtained from Cas9$^+$ mice. However, gRNAs are still introduced by retroviral transduction which has disadvantages as described before. Thus, we tried overall transfection of transgenic Cas9$^+$ T cells by electroporation. We present here an effective non-viral CRISPR/Cas9-based method to edit genome in primary murine T cells[68]. We have generated T cell-specific *Cd4cre.*Cas9$^+$ mice (Fig. 9) by breeding the original Cas9$^+$ with *Cd4cre* mice[114, 115]. This mouse also expresses CD90.1 as a congenic marker in all T cells and luciferase ubiquitously. We show that utilizing this mouse, gRNA-only nucleofection in pre-activated and even in naive Cas9$^+$CD3$^+$ T cells is sufficient to achieve high knockout efficiency. We have tested multiple gRNAs for several genes, *Cd90*, *Pdcd1*, *Cd4*, *Cd8*, *Nfatc1*, *Nfatc2,* and *Irf4* by our method. The effectiveness is comparable with another popular method "RNP nucleofection" which was recently described[91, 150] (Fig. 10B, E), except recombinant Cas9 protein usage can be avoided. This eliminates the step of RNP complex preparation before nucleofection, rendering our method more rapid and cost-effective. We like others have shown, more than one gRNA per gene increased the degree of knockout, especially when targeting different exons encoding different domains of a protein (Fig. 12C, Fig. 13E). By nucleofection of multiple gRNAs, it is possible to ablate two genes simultaneously with almost unchanged effectiveness per gene (Fig. 11B, C, Fig. 12F, & Fig. 13E). Using 3 gRNAs per gene in our method, at least 80% knockout efficiency was achieved in mouse T cells. Another finding from our study is, genes can be knocked out efficiently using either the Nucleofector IIb or 4D in pre-stimulated T cells (Fig. 11, Fig. 12C, F, Fig. 13E) but can only be targeted competently in unstimulated/naïve T cells when the Nucleofector 4D was used (Fig. 21A, B). These two nucleofectors are built with different technologies and even the electrode materials are different (Aluminium for IIb and conductive polymer for 4D). Hence, the programs used in this study are not comparable between instruments. While using Nucleofector IIb to deliver gRNA in pre-stimulated and unstimulated mouse CD3$^+$Cas9$^+$ T cells, we have tested the manufacturer's recommended program for plasmid DNA electroporation in the Nucleofector IIb, which is more challenging to deliver compared to gRNA, due to the larger size and toxicity of plasmid DNA. We have also observed constitutively expressed genes (*Cd90*) are easier to target than inducible genes (*Nfatc1, Pdcd1*) in unstimulated T cells (especially while using the Nucleofector IIb) (Fig. 10E, Fig. 21B), suggesting the nuclease activity of *Sp*Cas9 is less efficient when chromatin is

condensed. This is in line with recent studies, where the authors show in a viral-delivery method of Cas9 and gRNA, condensed chromatin affects indel frequencies in rice genome and human cell lines drastically[151, 152]. In summary, both unstimulated/naive and pre-stimulated T cells from our *Cd4cre.*Cas9$^+$ mouse can be efficiently edited using gRNA-only nucleofection resulting in high knockout efficiency simultaneously in all subtypes of T cells (CD4, CD8, and Treg) (Fig. 27A) and high viability (80%) (Fig. 22A, C). The optimized conditions are summarized in Table 3.

Table 3. **Summary of optimized nucleofection programs for CRISPR/Cas9 gene editing in primary mouse T cells**

Cell type	Nucleofector	Buffer	Program
Mouse pre-stimulated T cells	2b/IIb	Mirus Nucleofection solution	X-001
Mouse pre-stimulated T cells	4D	Mirus Nucleofection solution or Lonza P4 buffer	CM-137
Mouse unstimulated T cells	4D	Mirus Nucleofection solution or Lonza P4 buffer	DS-137

10.1.3 CRISPR/Cas9 non-viral genome-edited Cas9$^+$ T cells are metabolically active and can be rapidly transplanted *in vivo*

Importantly, nucleofected resting Cas9$^+$CD3$^+$ T cells could be transferred to the allo-HCT mouse model without any further treatment or rest. The cells acquired their knockout *in vivo* (Fig. 23B), proliferated *in vivo,* and caused acute GvHD in BALB/c recipient mice (Fig. 26). IL-7 pre-incubation was not necessary to achieve high efficiency of knockout using our method in contrast to the previous study[91] (Fig. 21C). Moreover, although IL-7 culture does not activate T cells, it changes the composition of naïve and memory populations (Fig. 22B, E). Electroporation entails other challenges. Effects of electroporation of cells can be irreversible, when it disrupts the plasma membrane, causing loss of cell homeostasis and leading to cell death. On top, applied electric fields, even if they are transient, can reach the mitochondrion, which harbors the electron transport chain and can release cytochrome C, which would affect the metabolic capacities and again induce cell death[153]. Thus, conditions have to be acquired, which allow the cells to fully recover from the transient perturbation. We verified that nucleofection in unstimulated mouse T cells only transiently affected the metabolism of Cas9$^+$CD3$^+$ T cells (Fig. 25). In fact, we did not observe any stress on mitochondria (Fig. 25A), in line with the function and survival of the manipulated T cells. Metabolic competence

including a shift from OXPHOS towards aerobic glycolysis upon stimulation is a prerequisite for proper T-cell function[154]. In addition, although Treg are known to rather utilize OXPHOS to exert their suppressive activity, they also rely on glycolysis for proliferation and migration[155]. Monitoring T-cell bioenergetics after *in vitro* stimulation revealed a preserved full metabolic capacity for all T-cell subtypes three days after nucleofection (Fig. 25B). Induced stress on preferentially glycolytic reserve capacities was apparent only transiently after the intervention (Fig. 25A). Overall, we found conditions with the right nucleofector and program which ensure good survival rates of resting Tcon as well as Treg allowing them to respond with unperturbed proliferation *in vivo* and metabolic reprogramming.

10.1.4 Discrepancy between the behaviour of NFAT-ablated 'unstimulated' and '*in vitro* pre-stimulated' T cells in aGvHD mouse model

We have shown previously and in this study that NFAT-ablated unstimulated T cells ameliorate aGvHD. This was evident when using unstimulated T cells from NFAT-depleted transgenic mice[63] (*Cd4cre.Nfatc1*$^{fl/fl}$ or *Nfatc2*$^{-/-}$) or T cells that have been NFAT-ablated by using our gRNA-only nucleofection mediated CRISPR/Cas9 method[68]. NFAT single-deficient T cells elicited less proliferation *in vivo*, causing less severe aGvHD in recipient mice and prolonged survival (Fig. 26, Fig. 27C, D). However, when T cells were taken from *Cd4cre.Nfatc1*$^{fl/fl}$ or *Nfatc2*$^{-/-}$ mouse and pre-stimulated before transplantation, in long-term, GvHD was aggravated compared to WT T-cell transplantation. This led to the early death of mice receiving NFAT single-knockout T cells (Fig. 18A). The same outcome was also observed when NFAT was depleted in pre-stimulated Cas9$^+$ T cells by gRNA-only nucleofection (Fig. 17B-D). The frequency of Treg, a very important cell type in controlling aGvHD was not changed between genotypes at 30 dpi, eliminating the fact that amplified GvHD is due to loss of Treg (Fig. 19B). Although we observed an induction in Treg frequency *in vivo* upon naïve NFAT-ablated T-cell transfer, it was not noticed in case of pre-stimulated T-cell transfer. The *in vitro* pre-stimulation culture of T cells prior to transplantation involved activation by anti-CD3+anti-CD28+IL-2 for 3 d followed by nucleofection and 3 d culture with IL-2 thereafter. At the end of this 6 d culture period, the CD8$^+$ T cells had expanded more than CD4$^+$ T cells without changing the frequency of Treg (Fig. 18B, C). Overall, the pre-stimulated T cells were mostly CD44$^+$CD62L$^-$ and caused weaker aGvHD symptoms in the recipient mice. This is in line with previous studies which demonstrated that effector memory T cells cause GvHD less

aggressively compared to naïve T cells[156]. The long-term worsening of aGvHD upon loss of a single NFAT member could be due to several reasons. First, the *in vitro* culture changes the transcriptional profile of the T cells. It is worthwhile to find out which activation pathway or its downregulation makes our NFAT single-deficient pre-stimulated T cells more aggressive in the aGvHD model. A whole transcriptome analysis would be necessary to elucidate this. Second, at 30 dpi *ex vivo* analysis of NFATc1 knockout donor T cells from secondary lymphoid organs exhibited reduced CD8 to CD4 ratio due to a dominance of CD4 T cells, increased proinflammatory cytokines (IFN-γ, TNF-α, IL-2), and *Prf1* expression. $CD4^+$ T cells are known to be more prone to cause GvHD compared to $CD8^+$ T cells[157], which could be an explanation for aggravated GvHD in pre-stimulated *Nfatc1*$^{-/-}$ T cell-transplanted mice (Fig. 19A, F). Contradictorily, when unstimulated T cells were transplanted, similar changes in CD8 to CD4 ratio were observed (Fig. 20F) which rules out this being the only reason for increased aGvHD in pre-stimulated NFATc1-deficient T cell-recipient mice. Moreover, NFATc2-deficient T cells had reduced levels of IFN-γ and TNF-α at 35 dpi, but the aggravated disease could be due to increased CCR9 expression (Fig. 19D, F). CCR9 receptor and CCL25 its ligand are known to be important for gut homing of T cells during aGvHD[158]. Third, *Nfatc2*$^{-/-}$ T cells are known to be hyperproliferative and acquired a predominant Th2 phenotype[129]. Indeed, Th2 cells can contribute to hepatic, severe skin, and intestinal GvHD[159]. This could explain our observation of *Nfatc2*$^{-/-}$ T cells showing increased proliferation evident from BLI images (Fig. 17E) at 35 dpi and severe skin GvHD.

To get more insights into the cause of the differential behaviour of unstimulated and pre-stimulated NFAT single-deficient T cells during allo-HCT, we evaluated the degree of exhaustion. Indeed, our data revealed *in vitro* pre-stimulation enhances the $TOX^{hi}PD1^{hi}$ $CD8^+$ T_{EX} population. Previous studies have reported that NFATc2 and especially NFATc1 are crucial for the exhaustion of mouse $CD8^+$ T cells in viral infection and tumor mouse model[133, 160]. This is because members of the transcription factor families TOX and NR4A, essential for T-cell exhaustion are transactivated by NFAT. Here, NFATc1 plays a dominant role as one of its isoforms, i.e. NFATc1/αA, is highly upregulated during chronic stimulation[136, 161]. In absence of classical AP-1, NFAT expresses immune exhaustion-related genes in T cells[24]. In our model, we report NFATc1-deficient pre-stimulated $CD8^+$ T cells present impaired exhaustion (Fig. 20B), which correlates with more proinflammatory functions and early death of recipient mice due to severe GvHD. However, when unstimulated T cells were transplanted, exhaustion was

also prevented upon NFATc1 ablation (Fig. 20C), while mice still benefitted from single NFAT-deficient T cells. However, we demonstrated that $CD8^+$ T_{EX} population is dominant upon pre-stimulation and Tim3, another reliable T_{EX} marker only reduced in NFATc1-deficient pre-stimulated $CD8^+$ T cells (Fig. 20B) and not in unstimulated T cells (Fig. 20C). This indicates exhaustion is more prominent in case of pre-stimulation and the absence of NFATc1 lowered exhaustion and enhanced the effector function of T cells. Again, only a combination of events or their timing can be causative. Likewise, basic leucine zipper ATF-like transcription factor (BATF) and IRF4, induced by TCR signaling, likely in an NFAT-regulated manner, are ambivalent transcription factors contributing to either effector function or exhaustion in T cells[162]. Whether those or other transcription factors and their changed interplay are involved in the increased cytokine production and overall aggravated phenotype of NFATc1 single-deficient pre-stimulated T cells will be further investigated.

Besides, the PD-1/PD-L1 axis plays an important role in the maintenance of immune tolerance after allo-HCT in preclinical studies and patients receiving PD1-blockade therapy for post-transplant relapse, suffer from a high incidence of severe and fatal GvHD[163]. This could point to the missing PD1 upregulation in NFATc1-deficient T cells and their aggressive phenotype when *in vitro* pre-stimulated. Once again, however, beneficial NFATc1-deficient unstimulated T cells in the allo-HCT model also exhibited a failure in PD1 induction as well as less $TOX^{hi}PD1^{hi}$ T_{EX} compared to WT cells. We speculate that here the robustly heightened Treg population (Fig. 20E) contributed to maintaining the immune tolerance, hence lowering cytokine production even at 30 dpi (Fig. 20D) and prolonging the survival of mice. For translation into the clinical application it became clear from our data that only unstimulated NFAT-depleted T cells are safe as a therapy for aGvHD during allo-HCT.

10.1.5 Further application of *Cd4cre.*$Cas9^+$ mouse model

Cd4cre.$Cas9^+$ mice and our protocols are suitable for translational studies. Gene editing by CRISPR/Cas9 and T-cell transfer models highlight attempts like ours, in which $CD3^+$ T cells instead of one T-cell subtype are edited and transplanted for GvHD. In this context, it is noteworthy that $CD4^+$ and $CD8^+$ Tcon, as well as $CD4^+CD25^+Foxp3^+$ Treg, were all efficiently gene-ablated in the mixture of $Cas9^+CD3^+$ T cells (Fig. 27A). Since all T-cell subtypes are edited equally well, this allows the approach to be used in wide-ranging scenarios. For hard to isolate subtypes or subtypes which differentiate *in vivo* after the transfer, Cas9 transgenic mice can

be bred to different Cre lines (for example to *Il21cre* for Tfh cells and FoxP3-IRES-Cre for Treg). Total $CD3^+$ T cells can be nucleofected with gRNA and transplanted in recipient mice. Gene editing, however, will occur exclusively upon subtype-specific Cre expression. This definitely is an important application, which is not possible using the RNP method. Another advantage could be, to study any gene in transfer models when specific gene-floxed transgenic mice are unavailable. Therefore, $Cas9^+$ mice, especially when they are already inbred as B6.Cas9.*Cd4cre*.luc.CD90.1 (or other Cre lines) are a suitable tool for comfortable subsequent studies. Although we avoided a repetition of GvL experiments with NFAT single-ablated mouse T cells[63], successive experiments involving other genes or varying the GvHD model (acute GvHD due to minor mismatch or chronic GvHD) could easily include this aspect. In our context, we might want to knockout further NFAT target genes additionally and in parallel to test if the 'NFAT phenotype' is due to a certain gene's altered expression. One example is demonstrated in this study. The limited study with the ablated NFAT target gene *Irf4* demonstrated already that absence of IRF4, which is dominantly required for Th2, Th17, and Tfh cell differentiation[164], provokes a disadvantageous Th1 phenotype under GvHD inducing conditions (Fig. 28, Fig. 29). This is in contrast to allo-HCT with NFAT-deficient T cells, which can also implement specific T-helper characteristics[165], but restrict the overall cytokine expression irrespective of the individual NFAT family member ablated[63, 68]. Both, NFAT proteins and IRF4 enable proliferation including metabolic reprogramming of naive T cells by a shared pathway[135, 136, 166], a fact that limited T-cell expansion and ameliorated GvHD upon loss of NFATc1, NFATc2, or IRF4. Whether IRF4-deficient Treg are equally able to preserve the GvL effect like NFAT single-deficient Treg has to be tested next.

10.2 Targeting NFAT in primary human T cells by CRISPR/Cas9 to reduce aGvHD and still confer GvL

10.2.1 Efficient non-viral CRISPR/Cas9 genome editing in primary human T cells for clinical application

Encouraged by our observation that ablation of a single NFAT member in co-transplanted T cells protects mice from aGvHD like clinical calcineurin inhibition, while in contrast confers GvL efficacy[63, 68], we wanted to investigate whether this approach can be translated into the clinic. A viral transfer is most commonly used for gene therapy in clinics. Considering the disadvantages of viral delivery of Cas9 and gRNA, we tested the RNP-mediated CRISPR/Cas9

gene editing in primary human T cells[91]. There are pre-existing cell-mediated and humoral immune responses to *Sp*Cas9 in humans as demonstrated in a study where the authors found Cas9-specific T cells and IgG against *Sp*Cas9 to be present in 65% of 34 donors tested[167]. However, the RNP nucleofection method assures gRNA and Cas9 nuclease to be short-lived inside the cells thereby reducing the chance of off-target effects and immunogenicity of Cas9. Similar to mouse T cells, we have observed that the constitutively expressed *CXCR4* could be more efficiently knocked out (Fig. 31C) compared to the inducible gene *NFATC1* (Fig. 32B) using the Nucleofector IIb. In the Nucleofector 4D, two conditions worked equally well, P2 EH-100 and P3 EO-115 achieving a complete loss of NFATC1 and NFATC2 in unstimulated human T cells (Fig. 32E, G). In pre-stimulated human T cells, only P2 EH-100 was tested achieving complete loss of protein (Fig. 32A). For knocking out genes successfully in human T cells, we consistently used a combination of 3 gRNAs targeting multiple exons. Multiplexing, i.e. targeting *NFATC1* and *NFATC2* together was also efficient using our method, attaining high viability and knockout efficiency. The gene-modified T cells obtained by our method can be readily transplanted in *in vivo* humanized GvHD mouse model to study the outcome of the disease upon NFAT ablation. Several other important gene functions can be studied and validation of findings in the mouse can be performed using this method in human T cells which would be much more cumbersome by viral delivery methods. Our optimized conditions for successful CRISPR/Cas9 gene editing in human T cells are mentioned in Table 4. This can also be utilized to knockout genes to improve T-cell effector function for therapeutic applications; for example, knocking out PD1 to enhance tumor killing efficacy of $CD8^+$ T cells in adoptive tumor-infiltrating lymphocyte therapy for solid cancers, such as melanoma[168].

Table 4. **Summary of optimized nucleofection programs for CRISPR/Cas9 gene editing in primary human T cells**

Cell type	**Nucleofector**	**Buffer**	**Program**
Human pre-stimulated T cells	2b/IIb	Mirus Nucleofection solution	T-023
Human pre-stimulated T cells	4D	Lonza P2 buffer	EH-100
Human unstimulated T cells	4D	Lonza P2 buffer	EH-100
Human unstimulated T cells	4D	Lonza P3 buffer	EO-115
Human $CD8^+$ CAR T cells	4D	Lonza P3 buffer	FI-115

10.2.2 NFAT ablation in human T cells affects proinflammatory function but retains the tumor-killing capacity

GvHD pathogenesis has been mostly studied in major or minor mismatch mouse-to-mouse models of allo-HCT. These mouse models, although giving very important initial insights into pathogenicity and treatment of the disease, cannot address the important differences between mouse and human immunity. Apart from this, since the mice are bred in pathogen-free conditions it does not reflect the effect of complex microbiota of patients and donors[169]. It is extremely important to validate the findings of mouse study in human T cells before translation into the clinic. The most common approach for studying human GvHD is to use Xeno-GvHD (xGvHD) mouse models. For this purpose, human PBMCs are transplanted into irradiated (to increase severity) or non-irradiated non-obese diabetic (NOD) Severe combined immunodeficiency (SCID) IL2rγ-null (NSG) mice to develop xGvHD[65]. However, this model is still criticized due to the biological, phenotypic, and genetic differences between mouse and human, and whether they truly add value to the findings in mouse-to-mouse models is a topic of debate. Moreover, also with these models, the pleiotropy of microbes is not allowed. To translate our findings from mouse to human, first, we needed to analyse NFAT knockout human T cells *in vitro*. In this study, we performed *in vitro* analysis of the NFAT-depleted human T cells looking for proinflammatory gene expression, frequencies of T-cell subtypes, and *in vitro* tumor-killing efficiency of these T cells. $CD4^+$ or $CD8^+$ T-cell subtypes did not change upon NFATC1, NFATC2, or NFATC1+NFATC2 knockout, including naïve, effector, memory T cells, and also Treg (Fig. 33C-F). This is in line with the previous studies in mouse T cells[10] that, human Treg can also sustain in absence of NFATC1 and/or NFATC2. A recent study showed that *Nfatc1* but not *Nfatc2* is necessary for mouse memory $CD8^+$ T cell generation in $LCMV^{Arm}$ acute infection mouse model[89]. However, in our study *NFATC1*$^{-/-}$ human T cells did not show changes in frequencies of T_{CM} or T_{EM} cells. Our data verify another published data in mouse $CD8^+$ T cells showing no difference in memory T cell population *in vitro* when *Nfatc1*$^{-/-}$ or *Nfatc2*$^{-/-}$ $CD8^+$ T cells are stimulated with anti-CD3+anti-CD28. However, an upregulation of *Nfatc1*$^{-/-}$ T_{CM} cells was detected in an *in vivo* bacterial infection model[90]. Whether this is really an inter-species difference or a difference between *in vitro* and *in vivo* situations, should be explored more carefully in a long-term (up to 28 d) memory T cell *in vitro* expansion protocol in presence of IL-7 and IL-15[170] or in an *in vivo* NSG mouse models. This is especially important to know because memory T cells are required for the GvL effect and controlling

tumor relapse[171]. Interestingly, expression of GvHD-inducing cytokines IFN-γ and TNF-α both did not change upon NFATC1 knockout but reduced upon NFATC2 or both member knockout in human $CD3^+$ T cells (Fig. 34B, D). In mouse T cells, we and others observed both IFN-γ and TNF-α being downregulated upon either NFATc1 or NFATc2 knockout[89] (Fig. 14). NFATc2 binds to both mouse and human *IFNG* promoter region[172], besides, loss of NFATc2 reduces Th1-specific cytokines in mouse[83]. Furthermore, IL-2 and CD40L being downregulated upon either one or both NFAT members in human T cells are in line with the previous studies which show IL-2 and CD40L both to be NFAT target genes[173, 174] activated upon TCR stimulation (Fig. 34B, D, Fig. 14). Given that, NFATc1 knockout in donor mouse T cells has a stronger effect than NFATc2 in prolonging the survival of recipient mice in an aGvHD model (Fig. 27C, D)[68], a follow-up study on transplantation of NFAT-depleted human T cells in the xGvHD model might give additional insights on prevention of aGvHD in human. Considering the drawbacks of such models, this might be even better investigated in an *in vitro* human GvHD model using intestinal organoids[175]. Our data indicates it is also possible that NFATC1 and NFATC2 has different roles in naïve, effector and memory T cells, which results in different outcomes upon NFAT-ablation in mouse (mostly naïve when unstimulated and mostly effector when pre-stimulated) and human T cells (mostly effector and memory).

Tumor killing efficacy of T cells is another important aspect that needs to be addressed to sustain the GvL efficacy of genetically modified T cells used in allo-HCT. Granule exocytosis is the dominant pathway utilized by effector $CD8^+$ T cells to kill tumor or virus-infected cells. Lytic granules can be described as secretory lysosomes which contain granzymes (e.g. GZMB), perforins (e.g. PRF1), and lysosome-associated membrane protein (e.g. LAMP1 or CD107a) [19, 147]. Our study with human T cells suggests both NFATC1 and NFATC2 have similar effects on cytolytic granule release. NFAT ablated in either pre-stimulated or unstimulated human $CD3^+$ T cells did not show any decline in GZMB or PRF1 expression when restimulated with PMA/ionomycin. Rather *NFATC1*$^{-/-}$ $CD8^+$ T cells showed a slight increased tendency of these proteins (Fig. 34C). These findings were confirmed when $CD3^+$ T cells were cocultured with tumor cells after nucleofection. Coculturing with the tumor cells (RPMI 8226, MV4-11, and MOLM-13) showed an increase in GZMB, PRF1 in *NFATC2*$^{-/-}$ $CD8^+$ T cells in addition to *NFATC1*$^{-/-}$ $CD8^+$ T cells. DKO and CsA treated $CD8^+$ T cells showed no changes in these proteins compared to NTC control (Fig.35B, C). In addition, CD107a expression was also increased upon

NFAT knockout (Fig. 35E). A previous study in *Cd4cre.Nfatc1*$^{fl/fl}$ mouse CD8$^+$ T cells demonstrated a similar increase in GzmB, Prf1, Lamp1 proteins. However, they identified this is due to defective cytoskeleton organization and recruitment of cytosolic organelles to immunological synapses. NFATc1 binds to several sites of the *Gzmb* gene, *Gzmb* mRNA, and protein is reduced in 3 d anti-CD3+anti-CD28-activated *Nfatc1*$^{-/-}$ CD8$^+$ T cells. However, NFATc1 ablation did not cause any defect in *Gzmb, Prf1* transcript level in CTLs, which they differentiated by 3 d anti-CD3+anti-CD28 followed by 5 d IL-2 culture[90]. Interestingly, in this study *Nfatc2*$^{-/-}$ mouse CD8$^+$ T cells did not have any defect in the recruitment of lytic granules or Gzmb, Prf1 expression. An earlier study from our group in mouse T cells revealed no difference in *GzmB* and *Prf1* expression in donor-derived NFAT single-knockout CD8$^+$ T cells 6 d after allo-HCT[63]. NFATC1 and NFATC2 both bind to *GZMB*, *PRF1*, however, other transcription factors might change the expression pattern of these genes in different culture conditions. Moreover, IL-2 added during human T cell culture in our study might be contributing to uninterrupted *GZMB, PRF1* gene expression upon NFAT knockout. Such as, IL-2 induces BLIMP-1 which then induces GZMB, since, BLIMP-1 binds to *GZMB* in CD8$^+$ T cells (CHIP data from earlier studies[24, 90]) and Blimp-1 induces Gzmb in mouse CD8$^+$ T_{EFF}[176]. Besides, IL-2 is known to directly regulate *Prf1* and granzyme gene expression in mouse CD8$^+$ T cells[177]. Of note, NFAT single-deficiency still allows a good amount of IL-2 expression (Fig. 14, Fig. 34C, D) which could be supportive for the expression of cytotoxic molecules and the resulting GvL *in vivo.*

In vitro, tumor-killing efficacy was completely restored in NFATC1 or NFATC2-ablated T cells as shown in coculture assay with two different AML and one multiple myeloma MM cell line (Fig. 36B-E). Whereas, DKO T cells showed a minimal reduction in tumor killing efficacy. It's noteworthy that the significant loss of IFN-γ and TNF-α in *NFATC2*$^{-/-}$ and DKO T cells do not affect the *in vitro* tumor killing efficacy, although both IFN-γ and TNF-α can induce direct killing of certain tumor cells. IFN-γ induces apoptosis of NSCLC cell lines by activating JAK-STAT1-caspase signaling and approximately 28% of cancers are susceptible to direct killing by soluble TNF-α[178, 179]. However, this is not well known in any of the cell lines we have tested for cytotoxicity assay. Nevertheless, a reduction in tumor-killing efficacy of CsA-treated T cells confirmed the earlier finding that CsA diminishes GvL efficacy in patients undergoing allo-HCT[180]. These results seem to contradict published data on mouse CD8$^+$ T cells, where the

authors showed *in vitro* tumor-killing activity defect of NFATc1-deficient $CD8^+$ T cells[90]. In contrast to them, in our human T cell culture, we have added IL-2 during T cell activation and culture until a cytotoxicity assay was performed. In contrast, IL-2 was not added during the activation of $CD8^+$ T cells in the published mouse study. Another difference is that we have performed cytotoxicity assays with total $CD3^+$ T cells instead of only $CD8^+$ T cells to maintain the condition similar to the clinic or *in vivo* situation. Both mouse and human $CD4^+$ T cells not only have direct anti-tumor activity but also help in $CD8^+$ T cell proliferation and effector function during tumor killing[181], while, Treg are also known to be essential for maintaining GvL during allo-HCT[60]. However, in our study NFATC1 or NFATC2-deficient $CD8^+$ T cells could kill tumor cells as efficiently as WT $CD8^+$ T cells (data not shown) making the influence of $CD4^+$ Tcon and Treg unlikely as a reason between their and our data, at least when enough exogenous IL-2 is provided.

Our *in vitro* study of NFAT knockout by CRISPR/Cas9 in human $CD3^+$ T cells has given insights on NFATC2 majorly driving effector gene expression in human T cells whereas the effect upon NFATC1 ablation was not strong on effector gene expression *in vitro*. This strengthens the need to examine human lymphocytes in addition to murine models since this NFATC2 dominance in human T cells had not been observed in mouse T cells. In general, this study validates our hypothesis and previous findings with murine cells that NFATC1 or NFATC2 single-deficiency does not affect the cytotoxicity of T cells against tumor cells[63].

10.3 Functional analysis of NFAT-depleted human CD19-CAR T cells

10.3.1 Non-viral method-generated NFAT-ablated anti-CD19-CAR T cells retain cytotoxicity *in vitro*

A few clinical trials in the allogeneic and autologous setup are ongoing with sleeping beauty transposition generated anti-CD19-CAR T cells. Initial data suggest that SB engineering is safe and allows stable engraftment of modified T cells with comparable efficiencies to viral vectors[182]. We have adapted the SB transposition-mediated CAR T-cell generation method from an earlier publication of our collaborator[102]. These anti-CD19-CAR T cells showed tumor-killing efficiency *in vitro* and *in vivo*, equivalent to lentiviral-transduced anti-CD19-CAR T cells. We have modified this method to incorporate our standardized RNP nucleofection system to ablate single or two NFAT members in CAR T cells (Fig. 37). We have achieved an almost

complete loss of NFAT proteins in the cells that received CAR construct (Fig. 38) and the anti-CD19-CAR T cells exerted high cytotoxicity *in vitro*. This method is unique and achieves NFAT knockout and CAR delivery in a 'one-step nucleofection'. Utilizing this, we could study the role of individual NFAT members in human CAR T cells which is not evaluated so far. Currently, the role of the NFAT signaling pathway in CD19-CAR T cell exhaustion is beginning to emerge[162, 183]. Whereas, it is still unexplored whether individual NFAT members have a redundant or specific function in CAR T-cell effector function, proliferation, memory generation, and exhaustion. Our data demonstrate that NFATC2 strongly regulates cytokine secretion, CD40L, GZMB, and PRF1 expression of $CD8^+$ anti-CD19-CAR T cells *in vitro* which is similar to our finding in the human $CD3^+$ T cell study. NFATC1 ablation alone did not affect greatly any of these genes necessary for CAR T-cell function. Ablation of NFATC1 and NFATC2 together had a slight additional decline of IFN-γ, TNF-α, and PRF1 in comparison to *NFATC2*$^{-/-}$ CAR T cells (Fig. 39). However, the loss of these proteins did not affect *in vitro* cytotoxicity of NFATC1 or NFATC2-deficient CAR T cells. Only DKO CAR T cells had a minor reduction in cytotoxicity against CD19-expressing tumor cells whereas CsA treatment majorly affected the cytotoxicity of CAR T cells (Fig. 40). We are interested in further studying other aspects of NFAT-depleted CAR T cells *in vitro* and *in vivo,* such as exhaustion, which will add value to the current understanding in this field. Our data so far suggest yet again NFATC1 or NFATC2 single-depletion does not reduce cytotoxicity of human $CD8^+$ T cells or $CD8^+$ anti-CD19-CAR T cells which encourages us to consider single NFAT member depletion in T cells as a therapy for allo-HCT patients to reduce GvHD and still keeping GvL effect undisturbed. Furthermore, our non-viral 'one-step nucleofection' CAR delivery method can also be applied to knockout endogenous TCR to generate 'allogenic CAR T cells' or 'off the shelf' CAR T cells[184].

11 Conclusion and perspective

In this study, we successfully developed a non-viral CRISPR/Cas9 gene engineering strategy in unstimulated and pre-stimulated mouse T cells using *Cd4cre.*Cas9$^+$ mouse. This one-step gRNA-only nucleofection resulted in high knockout efficiency of several genes tested, targeting all T-cell subtypes equally, while multiplexing was also possible. Unstimulated T cells were metabolically active and proliferated *in vivo* when rapidly transplanted in an aGvHD mouse model. NFATc1 or NFATc2 knockout unstimulated T cells ameliorated aGvHD, whereas NFATc1 or NFATc2-ablated pre-stimulated T cells aggravated aGvHD compared to NTC T cells. Our simple and cost-effective non-viral method of CRISPR/Cas9 gene editing in Cas9$^+$ T cells would be useful to study any other gene in T cells for aGvHD pre-clinical research. We believe, this method can be easily translated into GvL mouse models or any other widely used adoptive T-cell transfer model. This will help in avoiding several transgenic mouse generations harboring the absence of functional proteins and also crossing the Cas9$^+$ mouse with other *Cre* mice can help in specifically editing hard to isolate cell types.

Next, we effectively established non-viral RNP-mediated CRISPR/Cas9 gene-editing in human T cells and a one-step non-viral anti-CD19-CAR CD8$^+$ T cells generation method in combination with RNP-mediated gene editing. Our study shows predominantly *NFATC2* but not *NFATC1* knockout significantly reduces GvHD-causing proinflammatory cytokines *in vitro* in human T cells. However, *in vitro* GvL efficacy is maintained by CD3$^+$ T cells or anti-CD19 CAR CD8$^+$ T cells upon single NFAT omission. This strengthens our earlier finding in the mouse study and proves our hypothesis that NFAT single-ablation ameliorates aGvHD while retaining GvL. This turns out to have the potential to be a better therapy compared to calcineurin inhibitors. Lastly, we realize from our mouse studies, we have to take enormous care while ablating NFAT in human T cells, as NFAT single-deficient T_{EFF} (similar to mouse pre-stimulated T cells) might harm the allo-HCT receiving patient even more than non-manipulated effector T cells would. This can be further validated with *in vivo* models or organoids to bring this therapy into the clinic. Finally, we expect our findings will help to improve life expectancy and quality of life of patients undergoing allo-HCT as a therapy for hematological malignancies.

12 List of Abbreviations

µl, µM, µg	Microliter, Micromolar, Microgram
Ab	Antibody
Ag	Antigen
aGvHD	Acute graft-versus-host disease
Allo	Allogenic
AP-1	Adaptor protein 1
APC	Antigen-presenting cells
ATP	Adenosine triphosphate
BALB	Bagg Albino
B-ALL	B cell acute lymphoblastic leukemia
BFP	Blue fluorescent protein
BLI	Bioluminescence imaging
BM	Bone marrow
BSS/BSA	Basal salt solution/Bovine serum albumin
C57BL/6	C57 black 6
CAR	Chimeric antigen receptor
CD	Cluster of differentiation
CD40L	CD40 ligand
cDNA	complementary DANN
CFP	Cyan fluorescent protein
cLN	Cervical lymph node
CLP	Common lymphoid progenitor
Cm	Centimeter
CNI	Calcineurin inhibitors
CNS	Conserved Non-coding Sequence
ConA	Concavalin-A
CRAC	Ca^{2+} release-activated Ca^{2+}
CRISPR/Cas9	Clustered regularly interspaced short palindromic repeats/CRISPR-associated nuclease 9
crRNA	CRISPR RNA
CTL	Cytotoxic T lymphocytes
CTLA4	Cytotoxic T-lymphocyte associated protein 4
CsA	Cyclosporin-A
d	Day
DAG	Diacyl-glycerol
DAMP	Damage-associated molecular patterns
DC	Dendritic cells
DKO	NFATc1 and NFATc2 double-knockout
DMEM	DMEM - Dulbecco's Modified Eagle Medium
DN	Double-negative
Dox	Doxycycline
DP	Double-positive
Dpi	Days post-irradiation/ days post-transplantation
dsDNA	Double-stranded DNA
EAE	Experimental autoimmune encephalomyelitis
ECAR	Extracellular acidification rate
EGFRt	Epidermal growth factor-receptor truncated
ER	Endoplasmic reticulum

E:T	Effector:Target/tumor ratio
FBS/FCS	Fetal bovine serum/ Fetal calf serum
FMO	Fluorescence minus one
FoxP3	Forkhead box protein 3
GFP	Green fluorescent protein
GIT	Gastrointestinal tract
GM-CSF	Granulocyte/macrophage colony stimulation factor
gRNA	Guide RNA
GST	Glycolysis stress test
GvL	Graft versus leukemia
h	Hours
HDAC	Histone deacetylase
HDR	Homology directed repair
HEPES	4-(2-hydroxyethyl)-1-piperazineethanesulfonic acid
HCT/HCT	Hematopoietic stem cell transplantation/ Hematopoietic cell transplantation
IFN	Interferon
Ig	Immunoglobulin
ILC	Innate lymphoid cells
IL	Interleukin
inLN	Inguinal lymph node
Indel	Insertion/deletion
IP3	Inositol triphosphate
IRF4	Interferon regulatory factor-4
ITAM	Immunoreceptor tyrosine-based activation motifs
ITK	IL-2 Inducible T Cell Kinase
iTreg	Induced Treg
JAK	Janus kinases
Kb	Kilobase
LAG3	Lymphocyte-activation gene 3
LAT	Linker for activation of T cells
LB	Luria Broth
LN	Lymph node
LPS	Lipopolysaccharide
Luc	Luciferase
mAb	Monoclonal antibody
MAdCAM-1	Mucosal vascular addressin cell adhesion molecule 1
MC	Minicircle
MEK	MAPK/ERK kinase
MHC	Major histocompatibility complex
miHAgs	Minor histocompatibility complex
mins	Minutes
mm, ml, mg	Milimeter, mililiter, miligram
mLN	Mesenteric lymph node
MOPC	Mineral oil plasmacytoma cells
MRD	Matched related donor
MST	Mitochondrial stress test
mTOR	Mammalian target of rapamycin
MUD	Matched unrelated donor
NFAT	Nuclear factor of activated T cells
NFκB	nuclear factor 'kappa-light-chain-enhancer' of activated B-cells
ng	Nanogram

NHEJ	Non-homologous end-joining
NHR	NFAT homologous region
NK	Natural killer cells
NLS	Nuclear localization signal
nTreg or tTreg	Natural Treg or thymus-derived Treg
nt	Nucleotide
NTC	Non-targeting crRNA
OCR	Oxygen consumption rate
OXPHOS	Oxidative phosphorylation
PAM	Protospacer adjacent motif
PAMP	Pathogen-associated molecular patterns
PBMC	Peripheral blood mononuclear cell
PBS	Phosphate buffer saline
PCR	Polymerase chain reaction
PD1	Programmed cell death protein 1
PI 3-kinase	Phosphoinositide 3-kinase
PKC	Protein kinase C
PLC	Phospholipase
PM	Plasma membrane
PMA/TPA	Phorbol 12-myristate 13-acetate
Pmol	Picomole
qRT-PCR	Quantitative real-time PCR
RAG	Recombination activating gene
RHD	Rel-homology domain
RNP	Ribonucleoprotein
RORγt	RAR-related orphan receptor gamma isoform t
ROS	Reactive oxygen species
RPMI	Roswell Park Memorial Institute
RSD	Rel-similarity domain
RT	Room temperature
SB	Sleeping beauty
scFv	Single-chain variable fragment
SCID	Severe combined immunodeficiency
SDS-PAGE	Sodium dodecyl sulfate–polyacrylamide gel electrophoresis
SLO	Secondary lymphoid organ
SOCE	Store-operated calcium entry
SP	Single positive
SRD	Serine rich domain
STAT	Signal transducer and activator of transcription
STIM	Stromal interaction molecule
Stim	Stimulated
Sp	*Streptococcus pyogenes*
SUMO	Small ubiquitin-like modifier
T4 PNK	T4 Polynucleotide kinase
TAD	Transactivating domain
T-bet	T-box expressed in T cells
TBI	Total body irradiation
TBS	Tris-buffered saline
Tc	Cytotoxic T cells
T_{CM}	Central memory T cells
Tcon	Conventional T cells

TCR	T-cell receptor
T_{EFF}	Effector T cells
T_{EM}	Effector memory T cells
T_{EX}	Exhausted T cells
Tfh	T follicular helper cell
Tfr	T follicular regulatory cells
TGF-β	Transforming growth factor-beta
Th	T helper
TIDE	Tracking of indels by decomposition
TIGIT	T cell immunoreceptor with Ig and ITIM domains
TIM3	T-cell immunoglobulin domain and mucin domain 3
T_M	Memory T cells
TNF	Tumor necrosis factor
tracrRNA	Transactivating crRNA
Treg	Regulatory T cells
T_{SCM}	Stem cell memory T cells
Unstim	Unstimulated
UV	Ultraviolet
V(D)J	Variable diversity joining recombination
WT	Wildtype
ZAP-70	Zeta-chain-associated protein kinase 70

13 References

1. Weaver, K.M.a.C. *Janeway's Immunobiology*, 9th edn, 2017.
2. Wang, X., Peng, H. & Tian, Z. Innate lymphoid cell memory. *Cell Mol Immunol* **16**, 423-429 (2019).
3. Abbas, A. *Cellular and Molecular Immunology*, 9th edn, 2017.
4. Shah, D.K. T-cell development in the thymus. British Society for Immunology.
5. Germain, R.N. T-cell development and the CD4-CD8 lineage decision. *Nat Rev Immunol* **2**, 309-322 (2002).
6. Gaud, G., Lesourne, R. & Love, P.E. Regulatory mechanisms in T cell receptor signalling. *Nat Rev Immunol* **18**, 485-497 (2018).
7. Kaiko, G.E., Horvat, J.C., Beagley, K.W. & Hansbro, P.M. Immunological decision-making: how does the immune system decide to mount a helper T-cell response? *Immunology* **123**, 326-338 (2008).
8. Maitra, U., Davis, S., Reilly, C.M. & Li, L. Differential regulation of Foxp3 and IL-17 expression in CD4 T helper cells by IRAK-1. *J Immunol* **182**, 5763-5769 (2009).
9. Takimoto, T. *et al.* Smad2 and Smad3 are redundantly essential for the TGF-beta-mediated regulation of regulatory T plasticity and Th1 development. *J Immunol* **185**, 842-855 (2010).
10. Vaeth, M. *et al.* Dependence on nuclear factor of activated T-cells (NFAT) levels discriminates conventional T cells from Foxp3+ regulatory T cells. *Proc Natl Acad Sci U S A* **109**, 16258-16263 (2012).
11. Hori, S., Nomura, T. & Sakaguchi, S. Control of regulatory T cell development by the transcription factor Foxp3. *Science* **299**, 1057-1061 (2003).
12. Sakaguchi, S., Wing, K., Onishi, Y., Prieto-Martin, P. & Yamaguchi, T. Regulatory T cells: how do they suppress immune responses? *Int Immunol* **21**, 1105-1111 (2009).
13. Andre, S., Tough, D.F., Lacroix-Desmazes, S., Kaveri, S.V. & Bayry, J. Surveillance of antigen-presenting cells by CD4+ CD25+ regulatory T cells in autoimmunity: immunopathogenesis and therapeutic implications. *Am J Pathol* **174**, 1575-1587 (2009).
14. Zhao, D.M., Thornton, A.M., DiPaolo, R.J. & Shevach, E.M. Activated CD4+CD25+ T cells selectively kill B lymphocytes. *Blood* **107**, 3925-3932 (2006).
15. Scheffold, A., Murphy, K.M. & Hofer, T. Competition for cytokines: T(reg) cells take all. *Nat Immunol* **8**, 1285-1287 (2007).
16. Pandiyan, P., Zheng, L., Ishihara, S., Reed, J. & Lenardo, M.J. CD4+CD25+Foxp3+ regulatory T cells induce cytokine deprivation-mediated apoptosis of effector CD4+ T cells. *Nat Immunol* **8**, 1353-1362 (2007).
17. Mittrucker, H.W., Visekruna, A. & Huber, M. Heterogeneity in the differentiation and function of CD8(+) T cells. *Arch Immunol Ther Exp (Warsz)* **62**, 449-458 (2014).
18. Berke, G. The CTL's kiss of death. *Cell* **81**, 9-12 (1995).
19. Barry, M. & Bleackley, R.C. Cytotoxic T lymphocytes: all roads lead to death. *Nat Rev Immunol* **2**, 401-409 (2002).
20. Janeway CA Jr, T.P., Walport M. *Immunobiology: The Immune System in Health and Disease*. Garland Science: New York, 2001.
21. Golubovskaya, V. & Wu, L. Different Subsets of T Cells, Memory, Effector Functions, and CAR-T Immunotherapy. *Cancers (Basel)* **8** (2016).

22. Farber, D.L., Yudanin, N.A. & Restifo, N.P. Human memory T cells: generation, compartmentalization and homeostasis. *Nat Rev Immunol* **14**, 24-35 (2014).

23. Hong, H. *et al.* The Distribution of Human Stem Cell-like Memory T Cell in Lung Cancer. *J Immunother* **39**, 233-240 (2016).

24. Martinez, G.J. *et al.* The transcription factor NFAT promotes exhaustion of activated CD8(+) T cells. *Immunity* **42**, 265-278 (2015).

25. Schietinger, A. & Greenberg, P.D. Tolerance and exhaustion: defining mechanisms of T cell dysfunction. *Trends Immunol* **35**, 51-60 (2014).

26. Kallies, A., Zehn, D. & Utzschneider, D.T. Precursor exhausted T cells: key to successful immunotherapy? *Nat Rev Immunol* **20**, 128-136 (2020).

27. Hall, B.M. T Cells: Soldiers and Spies--The Surveillance and Control of Effector T Cells by Regulatory T Cells. *Clin J Am Soc Nephrol* **10**, 2050-2064 (2015).

28. Guisier, F. *et al.* Janus or Hydra: The Many Faces of T Helper Cells in the Human Tumour Microenvironment. *Adv Exp Med Biol* **1224**, 35-51 (2020).

29. Bryder, D., Rossi, D.J. & Weissman, I.L. Hematopoietic stem cells: the paradigmatic tissue-specific stem cell. *Am J Pathol* **169**, 338-346 (2006).

30. Urbano-Ispizua, A. *et al.* Allogeneic and autologous transplantation for haematological diseases, solid tumours and immune disorders: definitions and current practice in Europe. *Bone Marrow Transplant* **29**, 639-646 (2002).

31. Wildes, T.M., Stirewalt, D.L., Medeiros, B. & Hurria, A. Hematopoietic stem cell transplantation for hematologic malignancies in older adults: geriatric principles in the transplant clinic. *J Natl Compr Canc Netw* **12**, 128-136 (2014).

32. Copelan, E.A. Hematopoietic stem-cell transplantation. *N Engl J Med* **354**, 1813-1826 (2006).

33. Thomas, E.D., Lochte, H.L., Jr., Cannon, J.H., Sahler, O.D. & Ferrebee, J.W. Supralethal whole body irradiation and isologous marrow transplantation in man. *J Clin Invest* **38**, 1709-1716 (1959).

34. Thomas, E.D., Lochte, H.L., Jr., Lu, W.C. & Ferrebee, J.W. Intravenous infusion of bone marrow in patients receiving radiation and chemotherapy. *N Engl J Med* **257**, 491-496 (1957).

35. Juric, M.K. *et al.* Milestones of Hematopoietic Stem Cell Transplantation - From First Human Studies to Current Developments. *Front Immunol* **7**, 470 (2016).

36. Jenq, R.R. & van den Brink, M.R. Allogeneic haematopoietic stem cell transplantation: individualized stem cell and immune therapy of cancer. *Nat Rev Cancer* **10**, 213-221 (2010).

37. EBMT Annual Report 2019. (2019).

38. Horowitz, M.M. *Uses and Growth of Hematopoietic Cell Transplantation. Thomas' Hematopoietic Cell Transplantation: Stem Cell Transplantation, I, Fifth Edition*, 2015.

39. Kenyon, S.Z.a.M. Principles of Conditioning Therapy and Cell Infusion. In: A, K.M.a.B. (ed). *The European Blood and Marrow Transplantation Textbook for Nurses: Under the Auspices of EBMT*. Springer, 2017.

40. Kolb, H.J. Graft-versus-leukemia effects of transplantation and donor lymphocytes. *Blood* **112**, 4371-4383 (2008).

41. Choo, S.Y. The HLA system: genetics, immunology, clinical testing, and clinical implications. *Yonsei Med J* **48**, 11-23 (2007).

42. Kanda, J. *et al.* Reduced-intensity allogeneic transplantation using alemtuzumab from HLA-matched related, unrelated, or haploidentical related donors for patients with hematologic malignancies. *Biol Blood Marrow Transplant* **20**, 257-263 (2014).

43. Gooptu, M. & Antin, J.H. GVHD Prophylaxis 2020. *Front Immunol* **12**, 605726 (2021).

44. Ferrara, J.L. & Reddy, P. Pathophysiology of graft-versus-host disease. *Semin Hematol* **43**, 3-10 (2006).

45. Ferrara, J.L., Levine, J.E., Reddy, P. & Holler, E. Graft-versus-host disease. *Lancet* **373**, 1550-1561 (2009).

46. Jagasia, M. *et al.* Risk factors for acute GVHD and survival after hematopoietic cell transplantation. *Blood* **119**, 296-307 (2012).

47. Atkinson, K. *et al.* Risk factors for chronic graft-versus-host disease after HLA-identical sibling bone marrow transplantation. *Blood* **75**, 2459-2464 (1990).

48. Ramachandran, V., Kolli, S.S. & Strowd, L.C. Review of Graft-Versus-Host Disease. *Dermatol Clin* **37**, 569-582 (2019).

49. Ball, L.M., Egeler, R.M. & Party, E.P.W. Acute GvHD: pathogenesis and classification. *Bone Marrow Transplant* **41 Suppl 2**, S58-64 (2008).

50. Waldman, E. *et al.* Absence of beta7 integrin results in less graft-versus-host disease because of decreased homing of alloreactive T cells to intestine. *Blood* **107**, 1703-1711 (2006).

51. Nassereddine, S., Rafei, H., Elbahesh, E. & Tabbara, I. Acute Graft Versus Host Disease: A Comprehensive Review. *Anticancer Res* **37**, 1547-1555 (2017).

52. Gooley, T.A. *et al.* Reduced mortality after allogeneic hematopoietic-cell transplantation. *N Engl J Med* **363**, 2091-2101 (2010).

53. Hogan, W.J. & Storb, R. Use of cyclosporine in hematopoietic cell transplantation. *Transplant Proc* **36**, 367S-371S (2004).

54. Martin, P.J. *et al.* First- and second-line systemic treatment of acute graft-versus-host disease: recommendations of the American Society of Blood and Marrow Transplantation. *Biol Blood Marrow Transplant* **18**, 1150-1163 (2012).

55. Zahid, M.F. *et al.* Can we prevent or treat graft-versus-host disease with cellular-therapy? *Blood Rev* **43**, 100669 (2020).

56. Ghimire, S. *et al.* Pathophysiology of GvHD and Other HSCT-Related Major Complications. *Front Immunol* **8**, 79 (2017).

57. Mavin, E. *et al.* Human Regulatory T Cells Mediate Transcriptional Modulation of Dendritic Cell Function. *J Immunol* **198**, 138-146 (2017).

58. Riegel, C. *et al.* Efficient treatment of murine acute GvHD by in vitro expanded donor regulatory T cells. *Leukemia* **34**, 895-908 (2020).

59. Di Ianni, M. *et al.* Tregs prevent GVHD and promote immune reconstitution in HLA-haploidentical transplantation. *Blood* **117**, 3921-3928 (2011).

60. Edinger, M. *et al.* CD4+CD25+ regulatory T cells preserve graft-versus-tumor activity while inhibiting graft-versus-host disease after bone marrow transplantation. *Nat Med* **9**, 1144-1150 (2003).

61. Heinrichs, J. *et al.* Regulatory T-Cell Therapy for Graft-versus-host Disease. *J Immunol Res Ther* **1**, 1-14 (2016).

62. Chang, Y.J., Zhao, X.Y. & Huang, X.J. Strategies for Enhancing and Preserving Anti-leukemia Effects Without Aggravating Graft-Versus-Host Disease. *Front Immunol* **9**, 3041 (2018).

63. Vaeth, M. *et al.* Selective NFAT targeting in T cells ameliorates GvHD while maintaining antitumor activity. *Proc Natl Acad Sci U S A* **112**, 1125-1130 (2015).

64. Mammadli, M. *et al.* Targeting Interleukin-2-Inducible T-Cell Kinase (ITK) Differentiates GVL and GVHD in Allo-HSCT. *Front Immunol* **11**, 593863 (2020).

65. Schroeder, M.A. & DiPersio, J.F. Mouse models of graft-versus-host disease: advances and limitations. *Dis Model Mech* **4**, 318-333 (2011).

66. Beilhack, A. *et al.* In vivo analyses of early events in acute graft-versus-host disease reveal sequential infiltration of T-cell subsets. *Blood* **106**, 1113-1122 (2005).

67. Xiao, Y. *et al.* Lack of NFATc1 SUMOylation prevents autoimmunity and alloreactivity. *J Exp Med* **218** (2021).

68. Majumder, S. *et al.* Rapid and Efficient Gene Editing for Direct Transplantation of Naive Murine Cas9(+) T Cells. *Front Immunol* **12**, 683631 (2021).

69. Edinger, M. *et al.* Revealing lymphoma growth and the efficacy of immune cell therapies using in vivo bioluminescence imaging. *Blood* **101**, 640-648 (2003).

70. Chopra, M. *et al.* Non-invasive bioluminescence imaging to monitor the immunological control of a plasmablastic lymphoma-like B cell neoplasia after hematopoietic cell transplantation. *PLoS One* **8**, e81320 (2013).

71. Huai, Q. *et al.* Crystal structure of calcineurin-cyclophilin-cyclosporin shows common but distinct recognition of immunophilin-drug complexes. *Proc Natl Acad Sci U S A* **99**, 12037-12042 (2002).

72. Muller, M.R. & Rao, A. NFAT, immunity and cancer: a transcription factor comes of age. *Nat Rev Immunol* **10**, 645-656 (2010).

73. Vaeth, M. & Feske, S. NFAT control of immune function: New Frontiers for an Abiding Trooper. *F1000Res* **7**, 260 (2018).

74. Mognol, G.P., Carneiro, F.R., Robbs, B.K., Faget, D.V. & Viola, J.P. Cell cycle and apoptosis regulation by NFAT transcription factors: new roles for an old player. *Cell Death Dis* **7**, e2199 (2016).

75. Aramburu, J., Azzoni, L., Rao, A. & Perussia, B. Activation and expression of the nuclear factors of activated T cells, NFATp and NFATc, in human natural killer cells: regulation upon CD16 ligand binding. *J Exp Med* **182**, 801-810 (1995).

76. Fric, J. *et al.* NFAT control of innate immunity. *Blood* **120**, 1380-1389 (2012).

77. Shukla, U., Hatani, T., Nakashima, K., Ogi, K. & Sada, K. Tyrosine phosphorylation of 3BP2 regulates B cell receptor-mediated activation of NFAT. *J Biol Chem* **284**, 33719-33728 (2009).

78. Zanoni, I. *et al.* CD14 regulates the dendritic cell life cycle after LPS exposure through NFAT activation. *Nature* **460**, 264-268 (2009).

79. Serfling, E. *et al.* The role of NF-AT transcription factors in T cell activation and differentiation. *Biochim Biophys Acta* **1498**, 1-18 (2000).

80. Nayak, A. *et al.* Sumoylation of the transcription factor NFATc1 leads to its subnuclear relocalization and interleukin-2 repression by histone deacetylase. *J Biol Chem* **284**, 10935-10946 (2009).

81. Chuvpilo, S. *et al.* Autoregulation of NFATc1/A expression facilitates effector T cells to escape from rapid apoptosis. *Immunity* **16**, 881-895 (2002).

82. Macian, F. NFAT proteins: key regulators of T-cell development and function. *Nat Rev Immunol* **5**, 472-484 (2005).

83. Lee, J.U., Kim, L.K. & Choi, J.M. Revisiting the Concept of Targeting NFAT to Control T Cell Immunity and Autoimmune Diseases. *Front Immunol* **9**, 2747 (2018).

84. Dietz, L. *et al.* NFAT1 deficit and NFAT2 deficit attenuate EAE via different mechanisms. *Eur J Immunol* **45**, 1377-1389 (2015).

85. Reppert, S. *et al.* NFATc1 deficiency in T cells protects mice from experimental autoimmune encephalomyelitis. *Eur J Immunol* **45**, 1426-1440 (2015).

86. Zheng, Y. *et al.* Role of conserved non-coding DNA elements in the Foxp3 gene in regulatory T-cell fate. *Nature* **463**, 808-812 (2010).

87. Tone, Y. *et al.* Smad3 and NFAT cooperate to induce Foxp3 expression through its enhancer. *Nat Immunol* **9**, 194-202 (2008).

88. Vaeth, M. *et al.* Follicular regulatory T cells control humoral autoimmunity via NFAT2-regulated CXCR5 expression. *J Exp Med* **211**, 545-561 (2014).

89. Xu, T., Keller, A. & Martinez, G.J. NFAT1 and NFAT2 Differentially Regulate CTL Differentiation Upon Acute Viral Infection. *Front Immunol* **10**, 184 (2019).

90. Klein-Hessling, S. *et al.* NFATc1 controls the cytotoxicity of CD8(+) T cells. *Nat Commun* **8**, 511 (2017).

91. Seki, A. & Rutz, S. Optimized RNP transfection for highly efficient CRISPR/Cas9-mediated gene knockout in primary T cells. *J Exp Med* **215**, 985-997 (2018).

92. Ran, F.A. *et al.* Genome engineering using the CRISPR-Cas9 system. *Nat Protoc* **8**, 2281-2308 (2013).

93. Ren, J. *et al.* Multiplex Genome Editing to Generate Universal CAR T Cells Resistant to PD1 Inhibition. *Clin Cancer Res* **23**, 2255-2266 (2017).

94. Hultquist, J.F. *et al.* CRISPR-Cas9 genome engineering of primary CD4(+) T cells for the interrogation of HIV-host factor interactions. *Nat Protoc* **14**, 1-27 (2019).

95. Hudecek, M. *et al.* The nonsignaling extracellular spacer domain of chimeric antigen receptors is decisive for in vivo antitumor activity. *Cancer Immunol Res* **3**, 125-135 (2015).

96. Hirayama, A.V. *et al.* High rate of durable complete remission in follicular lymphoma after CD19 CAR-T cell immunotherapy. *Blood* **134**, 636-640 (2019).

97. Hirayama, A.V. *et al.* The response to lymphodepletion impacts PFS in patients with aggressive non-Hodgkin lymphoma treated with CD19 CAR T cells. *Blood* **133**, 1876-1887 (2019).

98. Turtle, C.J. *et al.* CD19 CAR-T cells of defined CD4+:CD8+ composition in adult B cell ALL patients. *J Clin Invest* **126**, 2123-2138 (2016).

99. Phase I/II Study of Immunotherapy for Advanced CD19+ Chronic Lymphocytic Leukemia, Acute Lymphoblastic Leukemia/Lymphoma and Non-Hodgkin Lymphoma With Defined Subsets of Autologous T Cells Engineered to Express a CD19-Specific Chimeric Antigen Receptor. 2013-2021.

100. Wang, X. *et al.* A transgene-encoded cell surface polypeptide for selection, in vivo tracking, and ablation of engineered cells. *Blood* **118**, 1255-1263 (2011).

101. Paszkiewicz, P.J. *et al.* Targeted antibody-mediated depletion of murine CD19 CAR T cells permanently reverses B cell aplasia. *J Clin Invest* **126**, 4262-4272 (2016).

102. Monjezi, R. Engineering of chimeric antigen receptor T cells with enhanced therapeutic index in cancer immunotherapy using non-viral gene transfer and genome editing Doctoral degree thesis, Universität Würzburg, Würzburg, 2017.

103. Croft, M. The role of TNF superfamily members in T-cell function and diseases. *Nat Rev Immunol* **9**, 271-285 (2009).

104. Chen, L. & Flies, D.B. Molecular mechanisms of T cell co-stimulation and co-inhibition. *Nat Rev Immunol* **13**, 227-242 (2013).

105. Zhao, X. *et al.* Efficacy and Safety of CD28- or 4-1BB-Based CD19 CAR-T Cells in B Cell Acute Lymphoblastic Leukemia. *Mol Ther Oncolytics* **18**, 272-281 (2020).

106. Long, A.H. *et al.* 4-1BB costimulation ameliorates T cell exhaustion induced by tonic signaling of chimeric antigen receptors. *Nat Med* **21**, 581-590 (2015).

107. Cappell, K.M. & Kochenderfer, J.N. A comparison of chimeric antigen receptors containing CD28 versus 4-1BB costimulatory domains. *Nat Rev Clin Oncol* **18**, 715-727 (2021).

108. Institute, N.C. T-cell Transfer Therapy. Available from: https://www.cancer.gov/about-cancer/treatment/types/immunotherapy/t-cell-transfer-therapy

109. Liu, J., Zhou, G., Zhang, L. & Zhao, Q. Building Potent Chimeric Antigen Receptor T Cells With CRISPR Genome Editing. *Front Immunol* **10**, 456 (2019).

110. Vafadari, R., Kraaijeveld, R., Weimar, W. & Baan, C.C. Tacrolimus inhibits NF-kappaB activation in peripheral human T cells. *PLoS One* **8**, e60784 (2013).

111. Du, S. *et al.* Suppression of NF-kappaB by cyclosporin a and tacrolimus (FK506) via induction of the C/EBP family: implication for unfolded protein response. *J Immunol* **182**, 7201-7211 (2009).

112. Aubrey, B.J. *et al.* An inducible lentiviral guide RNA platform enables the identification of tumor-essential genes and tumor-promoting mutations in vivo. *Cell Rep* **10**, 1422-1432 (2015).

113. Okamura, H. *et al.* Concerted dephosphorylation of the transcription factor NFAT1 induces a conformational switch that regulates transcriptional activity. *Mol Cell* **6**, 539-550 (2000).

114. Platt, R.J. *et al.* CRISPR-Cas9 knockin mice for genome editing and cancer modeling. *Cell* **159**, 440-455 (2014).

115. Lee, P.P. *et al.* A critical role for Dnmt1 and DNA methylation in T cell development, function, and survival. *Immunity* **15**, 763-774 (2001).

116. Baumgart, S. *et al.* Inflammation-induced NFATc1-STAT3 transcription complex promotes pancreatic cancer initiation by KrasG12D. *Cancer Discov* **4**, 688-701 (2014).

117. Zhang, D.J. *et al.* Selective expression of the Cre recombinase in late-stage thymocytes using the distal promoter of the Lck gene. *J Immunol* **174**, 6725-6731 (2005).

118. Cooke, K.R. *et al.* An experimental model of idiopathic pneumonia syndrome after bone marrow transplantation: I. The roles of minor H antigens and endotoxin. *Blood* **88**, 3230-3239 (1996).

119. Bottcher, M. *et al.* D-2-hydroxyglutarate interferes with HIF-1alpha stability skewing T-cell metabolism towards oxidative phosphorylation and impairing Th17 polarization. *Oncoimmunology* **7**, e1445454 (2018).

120. Hock, M. *et al.* NFATc1 induction in peripheral T and B lymphocytes. *J Immunol* **190**, 2345-2353 (2013).

121. Nanbakhsh, A. *et al.* Dextran Enhances the Lentiviral Transduction Efficiency of Murine and Human Primary NK Cells. *J Vis Exp* (2018).

122. Denning, W. *et al.* Optimization of the transductional efficiency of lentiviral vectors: effect of sera and polycations. *Mol Biotechnol* **53**, 308-314 (2013).

123. Rao, A., Luo, C. & Hogan, P.G. Transcription factors of the NFAT family: regulation and function. *Annu Rev Immunol* **15**, 707-747 (1997).

124. Kondo, E. *et al.* Retroviral vector backbone immunogenicity: identification of cytotoxic T-cell epitopes in retroviral vector-packaging sequences. *Gene Ther* **12**, 252-258 (2005).

125. Chu, V.T. *et al.* Efficient CRISPR-mediated mutagenesis in primary immune cells using CrispRGold and a C57BL/6 Cas9 transgenic mouse line. *Proc Natl Acad Sci U S A* **113**, 12514-12519 (2016).

126. Huang, B., Johansen, K.H. & Schwartzberg, P.L. Efficient CRISPR/Cas9-Mediated Mutagenesis in Primary Murine T Lymphocytes. *Curr Protoc Immunol* **124**, e62 (2019).

127. Oh, S.A., Seki, A. & Rutz, S. Ribonucleoprotein Transfection for CRISPR/Cas9-Mediated Gene Knockout in Primary T Cells. *Curr Protoc Immunol* **124**, e69 (2019).

128. Hendel, A. *et al.* Chemically modified guide RNAs enhance CRISPR-Cas genome editing in human primary cells. *Nat Biotechnol* **33**, 985-989 (2015).

129. Hodge, M.R. *et al.* Hyperproliferation and dysregulation of IL-4 expression in NF-ATp-deficient mice. *Immunity* **4**, 397-405 (1996).

130. Castor, M.G., Pinho, V. & Teixeira, M.M. The role of chemokines in mediating graft versus host disease: opportunities for novel therapeutics. *Front Pharmacol* **3**, 23 (2012).

131. Bauerlein, C.A. *et al.* A T-Cell Surface Marker Panel Predicts Murine Acute Graft-Versus-Host Disease. *Front Immunol* **11**, 593321 (2020).

132. Sckisel, G.D. *et al.* Differential phenotypes of memory CD4 and CD8 T cells in the spleen and peripheral tissues following immunostimulatory therapy. *J Immunother Cancer* **5**, 33 (2017).

133. Khan, O. *et al.* TOX transcriptionally and epigenetically programs CD8(+) T cell exhaustion. *Nature* **571**, 211-218 (2019).

134. Kurachi, M. CD8(+) T cell exhaustion. *Semin Immunopathol* **41**, 327-337 (2019).

135. Vaeth, M. *et al.* Store-Operated Ca(2+) Entry Controls Clonal Expansion of T Cells through Metabolic Reprogramming. *Immunity* **47**, 664-679 e666 (2017).

136. Man, K. *et al.* Transcription Factor IRF4 Promotes CD8(+) T Cell Exhaustion and Limits the Development of Memory-like T Cells during Chronic Infection. *Immunity* **47**, 1129-1141 e1125 (2017).

137. Wang, W. *et al.* CCR5 gene disruption via lentiviral vectors expressing Cas9 and single guided RNA renders cells resistant to HIV-1 infection. *PLoS One* **9**, e115987 (2014).

138. Li, C. *et al.* Inhibition of HIV-1 infection of primary CD4+ T-cells by gene editing of CCR5 using adenovirus-delivered CRISPR/Cas9. *J Gen Virol* **96**, 2381-2393 (2015).

139. Eyquem, J. *et al.* Targeting a CAR to the TRAC locus with CRISPR/Cas9 enhances tumour rejection. *Nature* **543**, 113-117 (2017).

140. Baum, C. *et al.* Side effects of retroviral gene transfer into hematopoietic stem cells. *Blood* **101**, 2099-2114 (2003).

141. McCormack, J.E. *et al.* Anti-vector immunoglobulin induced by retroviral vectors. *Hum Gene Ther* **8**, 1263-1273 (1997).

142. Aubert, D. *et al.* Cytotoxic immune response blunts long-term transgene expression after efficient retroviral-mediated hepatic gene transfer in rat. *Mol Ther* **5**, 388-396 (2002).

143. Kang, E. *et al.* In vivo persistence of retrovirally transduced murine long-term repopulating cells is not limited by expression of foreign gene products in the fully or minimally myeloablated setting. *Hum Gene Ther* **12**, 1663-1672 (2001).

144. Lutzko, C. *et al.* Genetically corrected autologous stem cells engraft, but host immune responses limit their utility in canine alpha-L-iduronidase deficiency. *Blood* **93**, 1895-1905 (1999).

145. Shifrut, E. *et al.* Genome-wide CRISPR Screens in Primary Human T Cells Reveal Key Regulators of Immune Function. *Cell* **175**, 1958-1971 e1915 (2018).

146. Wienert, B. *et al.* Timed inhibition of CDC7 increases CRISPR-Cas9 mediated templated repair. *Nat Commun* **11**, 2109 (2020).

147. Shen, D.T., Ma, J.S., Mather, J., Vukmanovic, S. & Radoja, S. Activation of primary T lymphocytes results in lysosome development and polarized granule exocytosis in CD4+ and CD8+ subsets, whereas expression of lytic molecules confers cytotoxicity to CD8+ T cells. *J Leukoc Biol* **80**, 827-837 (2006).

148. Chen, X. *et al.* Functional Interrogation of Primary Human T Cells via CRISPR Genetic Editing. *J Immunol* **201**, 1586-1598 (2018).

149. Sweeney, N.P. & Vink, C.A. The impact of lentiviral vector genome size and producer cell genomic to gag-pol mRNA ratios on packaging efficiency and titre. *Mol Ther Methods Clin Dev* **21**, 574-584 (2021).

150. Nussing, S. *et al.* Efficient CRISPR/Cas9 Gene Editing in Uncultured Naive Mouse T Cells for In Vivo Studies. *J Immunol* **204**, 2308-2315 (2020).

151. Liu, G., Yin, K., Zhang, Q., Gao, C. & Qiu, J.L. Modulating chromatin accessibility by transactivation and targeting proximal dsgRNAs enhances Cas9 editing efficiency in vivo. *Genome Biol* **20**, 145 (2019).

152. Jensen, K.T. *et al.* Chromatin accessibility and guide sequence secondary structure affect CRISPR-Cas9 gene editing efficiency. *FEBS Lett* **591**, 1892-1901 (2017).

153. Goswami, I. *et al.* Influence of Pulsed Electric Fields and Mitochondria-Cytoskeleton Interactions on Cell Respiration. *Biophys J* **114**, 2951-2964 (2018).

154. Buck, M.D., Sowell, R.T., Kaech, S.M. & Pearce, E.L. Metabolic Instruction of Immunity. *Cell* **169**, 570-586 (2017).

155. Kempkes, R.W.M., Joosten, I., Koenen, H. & He, X. Metabolic Pathways Involved in Regulatory T Cell Functionality. *Front Immunol* **10**, 2839 (2019).

156. Dutt, S. *et al.* Naive and memory T cells induce different types of graft-versus-host disease. *J Immunol* **179**, 6547-6554 (2007).

157. Truitt, R.L. & Atasoylu, A.A. Contribution of CD4+ and CD8+ T cells to graft-versus-host disease and graft-versus-leukemia reactivity after transplantation of MHC-compatible bone marrow. *Bone Marrow Transplant* **8**, 51-58 (1991).

158. Wurbel, M.A., Malissen, M., Guy-Grand, D., Malissen, B. & Campbell, J.J. Impaired accumulation of antigen-specific CD8 lymphocytes in chemokine CCL25-deficient intestinal epithelium and lamina propria. *J Immunol* **178**, 7598-7606 (2007).

159. Nikolic, B., Lee, S., Bronson, R.T., Grusby, M.J. & Sykes, M. Th1 and Th2 mediate acute graft-versus-host disease, each with distinct end-organ targets. *J Clin Invest* **105**, 1289-1298 (2000).

160. Seo, H. *et al.* TOX and TOX2 transcription factors cooperate with NR4A transcription factors to impose CD8(+) T cell exhaustion. *Proc Natl Acad Sci U S A* **116**, 12410-12415 (2019).

161. Serfling, E. *et al.* NFATc1/alphaA: The other Face of NFAT Factors in Lymphocytes. *Cell Commun Signal* **10**, 16 (2012).

162. Seo, H. *et al.* BATF and IRF4 cooperate to counter exhaustion in tumor-infiltrating CAR T cells. *Nat Immunol* **22**, 983-995 (2021).

163. Simonetta, F. *et al.* Dynamics of Expression of Programmed Cell Death Protein-1 (PD-1) on T Cells After Allogeneic Hematopoietic Stem Cell Transplantation. *Front Immunol* **10**, 1034 (2019).

164. Huber, M. & Lohoff, M. IRF4 at the crossroads of effector T-cell fate decision. *Eur J Immunol* **44**, 1886-1895 (2014).

165. Hermann-Kleiter, N. & Baier, G. NFAT pulls the strings during CD4+ T helper cell effector functions. *Blood* **115**, 2989-2997 (2010).

166. Miyakoda, M. *et al.* Differential requirements for IRF4 in the clonal expansion and homeostatic proliferation of naive and memory murine CD8(+) T cells. *Eur J Immunol* **48**, 1319-1328 (2018).

167. Charlesworth, C.T. *et al.* Identification of preexisting adaptive immunity to Cas9 proteins in humans. *Nat Med* **25**, 249-254 (2019).

168. Freen-van Heeren, J.J. Using CRISPR to enhance T cell effector function for therapeutic applications. *Cytokine X* **3**, 100049 (2021).

169. Ehx, G. *et al.* Xenogeneic Graft-Versus-Host Disease in Humanized NSG and NSG-HLA-A2/HHD Mice. *Front Immunol* **9**, 1943 (2018).

170. Herda, S. *et al.* Long-term in vitro expansion ensures increased yield of central memory T cells as perspective for manufacturing challenges. *Int J Cancer* **148**, 3097-3110 (2021).

171. Huang, W. & Chao, N.J. Memory T cells: A helpful guard for allogeneic hematopoietic stem cell transplantation without causing graft-versus-host disease. *Hematol Oncol Stem Cell Ther* **10**, 211-219 (2017).

172. Lee, D.U., Avni, O., Chen, L. & Rao, A. A distal enhancer in the interferon-gamma (IFN-gamma) locus revealed by genome sequence comparison. *J Biol Chem* **279**, 4802-4810 (2004).

173. Serfling, E., Avots, A. & Neumann, M. The architecture of the interleukin-2 promoter: a reflection of T lymphocyte activation. *Biochim Biophys Acta* **1263**, 181-200 (1995).

174. Schubert, L.A. *et al.* The human gp39 promoter. Two distinct nuclear factors of activated T cell protein-binding elements contribute independently to transcriptional activation. *J Biol Chem* **270**, 29624-29627 (1995).

175. Schreurs, R., Baumdick, M.E., Drewniak, A. & Bunders, M.J. In vitro co-culture of human intestinal organoids and lamina propria-derived CD4(+) T cells. *STAR Protoc* **2**, 100519 (2021).

176. Kragten, N.A.M. *et al.* Blimp-1 induces and Hobit maintains the cytotoxic mediator granzyme B in CD8 T cells. *Eur J Immunol* **48**, 1644-1662 (2018).

177. Janas, M.L., Groves, P., Kienzle, N. & Kelso, A. IL-2 regulates perforin and granzyme gene expression in CD8+ T cells independently of its effects on survival and proliferation. *J Immunol* **175**, 8003-8010 (2005).

178. Josephs, S.F. *et al.* Unleashing endogenous TNF-alpha as a cancer immunotherapeutic. *J Transl Med* **16**, 242 (2018).

179. Jorgovanovic, D., Song, M., Wang, L. & Zhang, Y. Roles of IFN-gamma in tumor progression and regression: a review. *Biomark Res* **8**, 49 (2020).

180. Michallet, M. *et al.* Impact of cyclosporine and methylprednisolone dose used for prophylaxis and therapy of graft-versus-host disease on survival and relapse after allogeneic bone marrow transplantation. *Bone Marrow Transplant* **23**, 145-150 (1999).

181. Tay, R.E., Richardson, E.K. & Toh, H.C. Revisiting the role of CD4(+) T cells in cancer immunotherapy-new insights into old paradigms. *Cancer Gene Ther* **28**, 5-17 (2021).

182. Magnani, C.F. *et al.* Transposon-Based CAR T Cells in Acute Leukemias: Where are We Going? *Cells* **9** (2020).

183. Chen, J. *et al.* NR4A transcription factors limit CAR T cell function in solid tumours. *Nature* **567**, 530-534 (2019).

184. Depil, S., Duchateau, P., Grupp, S.A., Mufti, G. & Poirot, L. 'Off-the-shelf' allogeneic CAR T cells: development and challenges. *Nat Rev Drug Discov* **19**, 185-199 (2020).